

University of Naples Federico II
School of Polytechnic and Basic Sciences

Department of Structures
for Engineering and Architecture



Ph.D. Programme in
Industrial Product and Process Engineering
XXXII Cycle



Stefano Belliazzi

Ph.D. Thesis

VULNERABILITY OF COASTAL
ITALIAN RESIDENTIAL MASONRY BUILDINGS
UNDER TSUNAMI LOADS

Tutors:

Prof. Eng. Andrea Prota

Prof. Eng. Gian Piero Lignola

2020

Acknowledgements

I want to express all my gratitude to Prof. Gian Piero Lignola for his encouragement, interest and unwavering guidance and he will be an example for me in the future. It was because of his intuition and constant support that the development of my work has been possible.

Special thanks go to Prof. Andrea Prota for his thoughtful support of my work and precious advices during these three years.

I would like to express my very great appreciation to Dr. Palermo for his constructive suggestions to the development of an important field of this research work during my experience abroad at *York University* in Toronto.

I am also particularly grateful to the *SPOT* project (*Potentially Triggerable Offshore Seismicity and Tsunamis*) sponsored by the Italian Ministry of Economic Development, Directorate-General for Safety of mining and energy activities (*MiSE-DGS*), with the technical support of the National Department of Civil Protection (*DCP*). I want to express my thanks to all project partners for their contribution in these years.

I want to thank past and present colleagues, in particular: Anna Bozza, Fabrizia Cilento, Vittoria Ciotta, Francesco Colella, Claudio D'Ambra, Raffaele Frascadore, Rosanna Napolitano, Iolanda Nuzzo, Giancarlo Ramaglia and Umberto Vitiello.

Finally, last but not least, I would express my thanks to my family for their constant presence. Special thank go to Daria for her sacrifice and constant encouragement.

Without these people, my Ph.D. thesis would not have been completed.

Naples, 10/03/2020

Stefano Belliazzi

Abstract

In the last years, several tsunami events caused great damages in terms of buildings collapse and casualties; research work has been done to analyse and to clarify causes and effects of tsunamis due to “*The Indian Ocean Tsunami*” of Sumatra (2004) and “*The great east Japan Tsunami*” of Tohoku (2011).

The thesis focuses on the vulnerability of existing coastal Italian residential masonry buildings along Italian coast, the overall outputs of the project require a large scale approach due to wide interested areas. Furthermore, damage scenarios are provided in terms of number of damaged buildings, reconstruction costs and humans involved by means of a tool developed in *GIS* system and *Mathworks MATLAB* using scripts to assume generic tsunami events.

In general, a masonry wall under tsunami loads could reach failure for out of plane collapse mechanism (bending and overturning) or in plane collapse mechanism (sliding, cracking by diagonal tension and crushing by diagonal compression), depending on the direction of the flow, if it is parallel or perpendicular to the masonry wall plane. After the tsunami event in Sumatra 2004 and Japan 2011, field investigations showed a high vulnerability of masonry structures subjected to tsunami load, especially against out of plane mechanism.

Most of the major scientific works are based on earthquake loads and their conclusions are not comparable in case of tsunami loads. In particular, seismic forces are inertia forces depending on the mass of structure, while tsunami forces are superficial forces that depend on

exposed surface of the structure to the tsunami wave. In addition, seismic forces involve the entire structure while tsunami forces are applied only on the part of the structure that is below the inundation depth. Generally, structures with a large number of stories exhibit a better behaviour against tsunami forces as shown in post-tsunami surveys in Tohoku region after “*The 2011 Great East Japan Tsunami*”. There are several differences in modelling tsunami loads on structures than earthquake loads; furthermore, the behaviour of masonry walls and local mechanisms activation are different during a tsunami or an earthquake event. For these reasons, specific mechanical fragility curves are retrieved in order to clarify the structural behaviour of masonry structures under tsunami loads.

The first step of the research has required a deep analysis of the state of the art based on existing international reports on the behaviour of structures under tsunami loads. Empirical outcomes represent the basis of this research and, in particular, post-tsunami event surveys show that damage and collapse mechanisms of masonry buildings are particularly dependent on some critical parameters involving local mechanisms activation on principal structural elements.

Empirical fragility curves are analysed and compared for several tsunami events in the last decades as preliminary study of masonry buildings behaviour under tsunami loads. It is important to note that empirical fragility curves are strictly related to local buildings typologies as shown in following chapter. In addition, there is a lack of analytical fragility curves due to the absence of empirical and experimental data in the literature while main empirical fragility curves are related to few tsunami events.

Another important aspect is related to the modelling of the tsunami effects on structures and it represents a hard challenge due to the high degree of anomaly of the problem and many other studies are needed to

improve current codes. Nowadays, the main international building codes and guidelines provide two different approaches based on U.S. codes and Japanese guidelines. The latter provides a conservative and simplified approach assuming one equivalent distribution depending on the inundation depth of wave. Japanese guidelines have been assumed to model tsunami loads on structures according to low knowledge level of the project.

In fact, a regional scale approach is characterized by an inevitable low knowledge level of buildings characteristics and the masonry structures are characterized by a large number of uncertainties (construction techniques, regularity, mechanical properties, etc.) which are complex to simulate and predict in numerical analyses.

Several *Monte Carlo* simulations are performed in order to simulate the behaviour of Italian masonry buildings assuming different building classes based on a regional scale approach.

The buildings models are generated considering a range of parameters based on available data in public repositories provided by “*National Institute of Statistics*” (*ISTAT*) database and “*National Earthquake Defense Group*” (*GNDT*) database. In situ-surveys were performed in Calabria region in several cities depending on geographic position and number of buildings in order to validate information about structures based on *ISTAT*.

For each model, the structural elements are defined according to simulated design, based on codes, guidelines, empirical equations and historical usual practices of the different construction ages.

For masonry buildings it is complicated to predict global mechanism due to high material inhomogeneity especially in the case of large scale analysis; a critical review on local mechanisms activation of walls under tsunami loads is taken into account in structural analyses. Therefore, local mechanisms activation on masonry walls is investigated

related to out-of-plane mechanisms and in-plane mechanisms assuming both flexural and shear failure.

The structural analyses are performed assuming safety criteria according to the low knowledge level reached as for example linear analysis and simple supported beam instead the real bi-dimensional behaviour of masonry walls for out-of-plane vertical bending mechanisms.

In addition, a critical review is provided by means of several parametric analyses in order to assess the impact of some mechanical and geometrical parameters that influence most the structural behaviour of masonry buildings under tsunami loads.

For each representative building class, the structural analyses provide fragility curves that are the main step to make damage scenarios in terms of number of damaged buildings, reconstruction costs and potential casualties. Furthermore, mechanical fragility curves are developed for groups of buildings depending on the number of storeys, design criterion and age of construction, to clarify the main aspects that influence the structural behaviour of masonry buildings under tsunami loads.

Fragility curves allow to estimate complete damage scenario in terms of inundation maps, number of damaged buildings, reconstruction costs and potential casualties by means of thematic maps managed in a *GIS* system. Potentially inundated areas are defined according to New Zealand guidelines *DGL 08-16* and a grid subdivision is defined with a variable spacing depending on census area type: urban or rural area.

The last part of the work focuses on prevention systems in the case of tsunami events, like as evacuation buildings, seawalls, early-warning systems and strengthening systems with innovative materials.

The adopted strengthening techniques are mainly based on *Fiber Reinforced Cementitious Matrix (FRCM)* system and the performance

of the strengthened masonry walls is assessed by means of several parametric analyses assuming different mechanical parameters for the strengthening system like as ultimate strain or composite mechanical percentage.

Furthermore, it is not obvious that seismic retrofitting solutions are cross applicable to tsunami risk prevention and the effects of the strengthening system on the local out-of-plane mechanisms activation is analysed in terms of vertical and horizontal bending mechanisms. In particular, a tool is provided to design strengthening system for masonry wall considering vertical bending mechanisms activation.

The main aim of this thesis is to assess the vulnerability of coastal Italian residential masonry buildings under tsunami loads and it represents an important contribution in the tsunami risk assessment. Damage scenarios are developed by means of a fast tool and it aims to provide a preliminary approach in the case of tsunami event to estimate inundation maps, number of damaged buildings, reconstruction costs and potential casualties.

KEYWORDS: *Vulnerability, Large scale analysis, Tsunami, Masonry walls, Risk assessment, Damage states, Cultural heritage, Local mechanisms, Strengthening systems, Interaction chart.*

Summary

ACKNOWLEDGEMENTS.....	III
ABSTRACT.....	V
SUMMARY	X
LIST OF TABLES	XIII
LIST OF FIGURES	XV
CHAPTER 1 INTRODUCTION: OVERVIEW OF TSUNAMI EVENTS.....	26
1.1. PHYSICAL PHENOMENON	27
1.2. HISTORICAL EVENT.....	30
1.3. INTENSITY SCALE.....	33
CHAPTER 2 STATE OF ART ANALYSIS.....	38
2.1. INTERNATIONAL BUILDING CODES	38
2.1.1. <i>Historical building codes evolution</i>	40
2.1.2. <i>Structural Design Requirements for Tsunami Evacuation Buildings (SDRTEB)</i>	43
2.1.3. <i>Federal Emergency Management Agency – FEMA P-646</i> 47	
2.1.3.1. Hydrostatic forces	48
2.1.3.2. Buoyant forces	49
2.1.3.3. Hydrodynamic forces.....	50
2.1.3.4. Impulsive Forces.....	51
2.1.3.5. Floating debris impact forces.....	52
2.1.3.6. Damming of accumulated waterborne debris.....	53
2.1.3.7. Load combinations.....	54

2.1.4.	<i>American Society of Civil Engineering – ASCE 7-16</i>	56
2.1.5.	<i>Comparison and discussion</i>	59
2.2.	STRUCTURAL BEHAVIOUR UNDER TSUNAMI LOADS.....	60
2.2.1.	<i>Masonry structures</i>	60
2.2.2.	<i>Reinforced concrete (RC) structures</i>	62
2.2.3.	<i>Steel structures</i>	63
2.2.4.	<i>Wooden structures</i>	64
2.3.	EMPIRICAL FRAGILITY CURVES.....	65
2.3.1.	<i>“The 2004 Indian Ocean Tsunami”</i>	67
2.3.2.	<i>“The 2009 South Pacific Tsunami”</i>	69
2.3.3.	<i>“The 2011 Great East Japan Tsunami”</i>	73
2.3.4.	<i>Comparison and discussion</i>	80
CHAPTER 3 BASIS OF FRAGILITY EVALUATION.....		85
3.1.	MASONRY BUILDING BEHAVIOUR UNDER TSUNAMI LOADS....	85
3.2.	BUILDING CLASSES DEFINITION.....	87
3.3.	STRUCTURAL MODELS GENERATION.....	92
3.4.	STRUCTURAL ANALYSIS.....	103
3.4.1.	<i>In-plane mechanisms</i>	107
3.4.1.1.	Wall model I.....	111
3.4.1.2.	Wall model II.....	111
3.4.1.3.	Wall model III.....	113
3.4.1.4.	Capacity model.....	114
3.4.2.	<i>Out-of-plane mechanisms</i>	119
3.4.2.1.	Vertical bending mechanism.....	121
3.4.2.2.	Horizontal bending mechanism.....	123
3.5.	INFLUENCE OF PARAMETERS.....	127
3.5.1.	<i>Out-of-plane mechanisms</i>	127
3.5.1.1.	Vertical bending mechanism.....	127
3.5.1.2.	Horizontal bending mechanism.....	132
3.5.2.	<i>In-plane mechanisms</i>	136

CHAPTER 4	FRAGILITY CURVES AND DAMAGE SCENARIOS.....	143
4.1.	FRAGILITY FUNCTION	144
4.1.1.	<i>Damage state definition</i>	145
4.1.2.	<i>Results and discussion</i>	147
4.2.	ALGORITHM ORGANIZATION	154
4.2.1.	<i>GIS system and census database</i>	156
4.2.2.	<i>Potentially inundated area definition</i>	158
4.2.3.	<i>In situ-surveys</i>	163
4.3.	INPUT DATA	165
4.4.	INUNDATION SIMULATION	166
4.5.	DAMAGE PREDICTION AND OUTPUT	169
CHAPTER 5	PREVENTION SYSTEMS.....	174
5.1.	STRENGTHENING SYSTEM WITH INNOVATIVE MATERIAL.....	178
5.1.1.	<i>Materials behaviour</i>	179
5.1.1.1.	Masonry	180
5.1.1.2.	Strengthening system	182
5.1.2.	<i>P-M interaction diagrams</i>	184
5.1.3.	<i>Parametric analysis</i>	188
5.1.4.	<i>Retrofit system effects on out-of-plane mechanisms</i>	192
5.1.4.1.	Vertical bending mechanism.....	193
5.1.4.2.	Horizontal bending mechanism.....	200
CHAPTER 6	CONCLUSIONS: RESULTS AND DISCUSSION.....	203
REFERENCES.....	210	
CHAPTER 7	APPENDIX A: FRAGILITY CURVES	222
CHAPTER 8	APPENDIX B: APPLICATION EXAMPLE	231

List of tables

Table 2.1: Damage state definition (Peiris et al. 2005).....	67
Table 2.2: Damage state definition (Suppasri et al. 2011).....	68
Table 2.3: Damage state definition (Reese et al. 2011)	69
Table 2.4: Damage state definition (Suppasri et al. 2013).....	74
Table 3.1: Summary of the coefficient ranges depending on the design approach	94
Table 3.2: Summary of the compressive tensile strength ranges depending on the age of construction	95
Table 3.3: Summary of the buildings distribution depending on the gravitational building class and the masonry substrates	95
Table 3.4: Summary of the buildings distribution depending on the seismic building class and the masonry substrates.....	96
Table 3.5: Minimum wall thickness for masonry structures in metres proposed by Marullier	101
Table 3.6: ρ parameter depending on the ratio h/a according to NTC 2008	102
Table 3.7: Critical inundation depth equation for wall model I in terms of shear and flexural failure depending on triangular and trapezoidal pressure distribution	111
Table 3.8: β coefficient values for different material types	117
Table 3.9: Critical inundation depth equation for horizontal bending mechanism in ultimate limit state condition.....	126

List of tables

Table 3.10: Critical inundation depth equation for horizontal bending mechanism in elastic conditions.....	126
Table 3.11: Masonry building model parameters	137
Table 3.12: Analysis results in terms of shear and bending moment demand	138
Table 7.1: Number of buildings for each buildings group	230

List of figures

Figure 1.1: Tsunami genesis (image provided by United States Geological Survey agency).....	26
Figure 1.2: The main wave parameters	28
Figure 1.3: Wave propagation offshore and near coastline.....	29
Figure 1.4: An aerial photography post and pre tsunami event on Sumatra coast (2004).....	30
Figure 1.5: An aerial photography post and pre tsunami event on Japanese coast (2011).....	31
Figure 2.1: Design tsunami pressure distribution	44
Figure 2.2: Inundation depth coefficient η depending on energy dissipation structures and distance from shoreline or riverbank (Nakano et al. 2011)	45
Figure 2.3: Horizontal load combination (Nakano et al. 2011)	46
Figure 2.4: Hydrostatic force model	48
Figure 2.5: Buoyant forces model.....	49
Figure 2.6: Hydrodynamic forces model	50
Figure 2.7: Impulsive forces model	51
Figure 2.8: Floating debris impact forces model	53
Figure 2.9: Load combinations (FEMA P-646)	55
Figure 2.10: Emery grade line parameters (ASCE 7-16).....	57
Figure 2.11: Out-of-plane mechanisms, liquefaction event and global collapse mechanisms of masonry buildings affected by the 2004 Indian Ocean Tsunami (a,b,c, Mallawaarachch et al. 2008; d, e, Peiris et al. 2005).....	61

Figure 2.12: Main RC structures collapse mechanisms observed in Tohoku region, Japan, 2011 (a, b, c, Chock 2011; d, Hayashi,et al. 2012)	62
Figure 2.13: Circular openings due to infill walls collapse in Chile (2010) and Thailand (2004) (a, Al-Faesly et al. 2012; b, Foytong,et al. 2006)	63
Figure 2.14: Effects of the Tohoku tsunami (2011) on steel structures (Lignos 2011)	64
Figure 2.15: Effects of Tohoku Tsunami (2011) on wooden structures (Cuada et al. 2012)	65
Figure 2.16: Fire in wooden buildings related to Tohoku tsunami in 2011	65
Figure 2.17: Fragility curves for masonry structures at a distance of 300 metres or more from the coast (a) and at a distance of 100 metres or more from the coast (b) (Periris et al. 2005)	68
Figure 2.18: Fragility curves for RC buildings (Suppasri et al. 2011) ..	69
Figure 2.19: Fragility curves related to DS3 for American Samoa and Samoa buildings (Reese et al. 2011)	70
Figure 2.20: Fragility curves for masonry buildings (Reese et al. 2011)	70
Figure 2.21: Effect of shielding on building fragilities: DS ₃ (a), DS ₄ (b) and DS ₅ (c) (Reese et al. 2011)	71
Figure 2.22: Effect of debris impact on building fragilities: DS ₃ (a) and DS ₄ (b) (Reese et al. 2011)	72
Figure 2.23: Fragility curves for masonry and RC residential buildings (Reese et al. 2011)	72
Figure 2.24: Fragility curves for masonry and timber residential buildings (Reese et al. 2011)	73
Figure 2.25: Fragility curves for different buildings structural material: RC (a), steel (b), wood (c) and masonry (d) residential buildings (Suppasri et al. 2013)	75

List of figures

Figure 2.26: Fragility curves for different buildings structural material and number of storeys: RC single storey (a), wood single storey (b), RC two storeys (c), wood two storeys (d), RC three or more storeys (e) and wood (three or more storeys (f) residential buildings (Suppasri et al. 2013)	76
Figure 2.27: Fragility curves for different buildings structural material: RC (a), steel (b), wood (c) and masonry (d) residential buildings (Suppasri et al. 2013).....	78
Figure 2.28: Fragility curves for different buildings structural material: RC (a), steel (b), wood (c) and masonry (d) residential buildings (Suppasri et al. 2013).....	79
Figure 2.29: Comparison between fragility curves of masonry and RC buildings related to 2001 Great East Japan tsunami.....	82
Figure 2.30: Comparison between fragility curves for masonry buildings based on The 2011 Great East Japan Tsunami and The 2009 South Pacific Tsunami.....	83
Figure 2.31: Comparison between fragility curves for RC buildings related to the 2011 Great East Japan Tsunami and the 2004 Indian Ocean Tsunami	83
Figure 3.1: Masonry walls structural model adopted for in-plane (a) and out-of-plane (b) mechanisms analyses	86
Figure 3.2: Stress distribution in a frame structure under triangular pressure distribution.....	87
Figure 3.3: Evolution of the seismic areas in Italy: Decree-Law No. 193-1909 (a), Decree-Law No. 640-1935 (b), Ministerial Decree No. 9/10/1981 (c), O.P.C.M. No. 3274-2003 (d).....	89
Figure 3.4: Masonry buildings distribution depending on number of floors (a) and age of construction (b) (ISTAT 2001 and ISTAT 2011 data).....	91
Figure 3.5: Building classes for masonry buildings and acronyms.....	92
Figure 3.6: Monte Carlo simulation parameters based on the National Group for Earthquake Defence (GNDT) database	93
Figure 3.7: Macro elements in typical masonry frame	96

List of figures

Figure 3.8: Wall model I.....	97
Figure 3.9: Wall model II.....	97
Figure 3.10: Wall model III	98
Figure 3.11: Structural parameters required to evaluate the wall thickness of a generic floor n according to Breymann equation	100
Figure 3.12: Tsunami load model according to Japanese guideline (a) and exposed surface to wave flow (b).....	104
Figure 3.13: Local mechanisms activation model.....	105
Figure 3.14: Masonry wall analysis: triangular (a) or trapezoidal (b) pressure distribution	107
Figure 3.15: Flexural failure	108
Figure 3.16: Sliding shear failure.....	108
Figure 3.17: Diagonal shear failure.....	109
Figure 3.18: Wall models: case I (a), case II (b) and case III (c).....	110
Figure 3.19: Wall model II and force method application for three storeys building model	112
Figure 3.20: Structural models for wall model III	114
Figure 3.21: Distribution coefficient of tangential stress acting on wall cross section	116
Figure 3.22: PM domains for elastic, cracking and ultimate states.....	117
Figure 3.23: Out-of-plane mechanisms model proposed by Rondelet (1802).....	119
Figure 3.24: Vertical bending mechanism	121
Figure 3.25: Vertical bending mechanism static model.....	122
Figure 3.26: Horizontal bending mechanism	123
Figure 3.27: Horizontal bending mechanism static model for gravitational buildings.....	125

Figure 3.28: Vertical bending mechanism sensitivity to wall length L for gravitational (a) and seismic (b) buildings	129
Figure 3.29: Vertical bending mechanism sensitivity to wall thickness s for gravitational (a) and seismic (b) buildings	130
Figure 3.30: Vertical bending mechanism sensitivity to interstorey height H_i for gravitational (a) and seismic (b) buildings.....	131
Figure 3.31: Horizontal bending mechanism sensitivity to wall length L for gravitational (a) and seismic (b) buildings	133
Figure 3.32: Horizontal bending mechanism sensitivity to wall thickness s for gravitational (a) and seismic (b) buildings.....	134
Figure 3.33: Horizontal bending mechanism sensitivity to interstorey height H_i for gravitational (a) and seismic (b) buildings.....	135
Figure 3.34: Masonry wall panels analysed for in-plane mechanisms	138
Figure 3.35: PV domain envelops depending on shear and flexural failure modes and wall models	139
Figure 3.36: Comparison between external demand and cross section capacity in terms of shear stresses depending on wall model	140
Figure 3.37: Minimum admissible external axial loads for wall model III for an inundation depth of 12 meters	141
Figure 3.38: Design chart that provides the minimum admissible axial load for a masonry wall panel depending on expected inundation depth	141
Figure 4.1: Damage states definition according to MLIT (Japan)	145
Figure 4.2: Discrete and continue fragility curves derived with least square estimation method	147
Figure 4.3: Fragility curves for generic masonry buildings.....	148
Figure 4.4: Fragility curves for gravitational buildings	149
Figure 4.5: Fragility curves for seismic buildings	149
Figure 4.6: Fragility curves comparison between gravitational and seismic masonry buildings	150

Figure 4.7: Fragility curves for low rise masonry buildings	151
Figure 4.8: Fragility curves for medium-high rise masonry buildings	151
Figure 4.9: Fragility curves comparison between low and high rise masonry buildings	151
Figure 4.10: Fragility curves comparison between ages of construction for DS ₅	152
Figure 4.11: Comparison between empirical and mechanical fragility curves	153
Figure 4.12: Algorithm flow chart	155
Figure 4.13: Building data provided by ISTAT censuses for Sicily region	157
Figure 4.14: Wave attenuation law for the identification of areas potentially subjected to flooding	158
Figure 4.15: Example of a hazard map produced by the TSUMAPS-NEAM project	159
Figure 4.16: Application example of the proposed method for the Sicily region according to DGL 08-16	159
Figure 4.17: Example census areas (in green) and grids (in grey) for Gela city in Sicily region	160
Figure 4.18: Grids altimetric trend represented by a colour gradient for Gela city in Sicily region	161
Figure 4.19: Example of grid filter based on altimetric trend for Gela city in Sicily region. The total number of grids in Sicily region is approximately equal to 230 000 grids	161
Figure 4.20: Example of minimum distances between grid centres and coastline for each grid for Gela city in Sicily region	162
Figure 4.21: Potentially inundated areas discretized in 1 400 000 grids	163
Figure 4.22: Cities inspected during in-situ surveys	164

Figure 4.23: Example of constant attenuation laws: incompatible (a) and compatible (b) inundation	168
Figure 4.24: Example of EGL analysis compared to constant attenuation law (CAL)	169
Figure 4.25: Example of inundation simulation in Ispica city (Ragusa, Sicily).....	171
Figure 4.26: Example damage scenarios output in terms of thematic maps: city (a), provincial (b) and regional (c) scale assuming an inundation depth of 5 meters along the coast based on hazard maps provided by TSUMAPS-NEAM project. Figure (b) shows reconstruction costs related to DS ₂ while Figure (a) and (c) show number of damaged buildings by histograms representation.	173
Figure 5.1: Example of tsunami evacuation building in Sendai City (Japan).....	175
Figure 5.2: Examples of concrete (a), grid type and steel-concrete composite (c) seawalls (Ishikawa et al. 2011).....	176
Figure 5.3: Masonry historical buildings in front of shoreline, City Hall (Trieste, Italy) (a) and San Giuliano Church (La Valletta, Malta) (b)	178
Figure 5.4: Mechanical behaviour of masonry in compression	180
Figure 5.5: Compression parameters ψ and λ	182
Figure 5.6: Tensile mechanical behaviour of composite strengthening systems	184
Figure 5.7: Strain and stress diagrams for first failure mode	186
Figure 5.8: Strain and stress diagrams for second failure mode	186
Figure 5.9: Strain and stress diagrams for third failure mode	187
Figure 5.10: P-M interaction diagrams changing the composite mechanical percentage ω and fixed composite ultimate strain ϵ_{fu} equal to 2 ‰ (a), 6 ‰ (b), 10 ‰ (c) and 20 ‰ (d)	189

Figure 5.11: P-M interaction diagrams while changing composite ultimate strain ε_{fu} and at a fixed composite mechanical percentage ω equal to 0.5 % (a), 1.0 % (b), 2.0 % (c) and 4.0 % (d) 191

Figure 5.12: Maximum ultimate bending moment m_r – composite mechanical percentage ω diagram while changing the composite ultimate strain ε_{fu} 192

Figure 5.13: Dimensionless critical bending moment..... 194

Figure 5.14: Ultimate bending moment diagrams of masonry cross section for different composite proprieties (1 ‰ (a), 3 ‰ (b), 5 ‰ (c) and 10 ‰ (d)) and fixed external axial loads..... 195

Figure 5.15: Comparison between normalized external bending moment (demand) and bending capacity of cross section..... 197

Figure 5.16: Design chart of minimum composite mechanical percentage ω 197

Figure 5.17: Ultimate bending moment increase versus normalized axial load, assuming ε_{fu} equal to 2‰ (a), 6‰ (b), 10‰ (c) and 20‰ (d) at different ω values..... 199

Figure 5.18: Arch mechanism depending on restraint degree: beam stresses (a), arch mechanism for simply supported (b) and for optimum solution (c) 201

Figure 7.1: Fragility curves summary based on number of storeys and age of construction..... 223

Figure 7.2: Fragility curves related to out-of-plane mechanisms activation and damage state DS_5 depending on age of construction (AGE) and masonry types (MT): poor stone, tuff stone, hollow clay bricks, clay brick and full clay brick. 224

Figure 7.3: Fragility curves related to in-plane mechanisms activation and damage state DS_5 depending on age of construction (AGE) and masonry types (MT): poor stone, tuff stone, hollow clay bricks, clay brick and full clay brick. 225

Figure 7.4: Fragility curves comparison based on generic masonry buildings between in-plane and out-of-plane failure modes depending on ultimate limit state..... 226

Figure 7.5: Fragility curves comparison based on seismic masonry buildings between in-plane and out-of-plane failure modes depending on ultimate limit state..... 227

Figure 7.6: Fragility curves comparison based on gravitational masonry buildings between in-plane and out-of-plane failure modes depending on ultimate limit state..... 228

Figure 7.7: Number of buildings ratio related to different failure modes and building classes groups..... 229

Figure 8.1: Inundation maps in Lesina city (Foggia, Puglia) assuming 2 (a), 5 (b) and 10 (c) meters of inundation depth along the coastline..... 232

Figure 8.2: Inundation maps in Ispica city (Ragusa, Sicilia) assuming 2 (a), 5 (b) and 10 (c) meters of inundation depth along the coastline..... 233

Figure 8.3: Number of buildings damaged for several Cities in Calabria assuming 2 (a), 5 (b) and 10 (c) meters of inundation depth along the coastline 234

Figure 8.4: Reconstruction costs for several Cities in Calabria assuming 2 meters of inundation depth along the coastline based on DS₂ (a) and DS₅ (b) 235

Figure 8.5: Reconstruction costs for several Cities in Calabria assuming 5 meters of inundation depth along the coastline based on DS₂ (a) and DS₅ (b) 235

Figure 8.6: Reconstruction costs for several Cities in Calabria assuming 10 meters of inundation depth along the coastline based on DS₂ (a) and DS₅ (b)..... 236

Figure 8.7: Number of damaged buildings in Sicilian provinces assuming 2 (a), 5 (b) and 10 (c) meters of inundation depth along the coastline..... 238

Figure 8.8: Reconstruction costs in Sicily provinces assuming 2 meters of inundation depth along the coastline based on DS₂ (a) and DS₅ (b) 239

Figure 8.9: Reconstruction costs in Sicily provinces assuming 5 meters of inundation depth along the coastline based on DS₂ (a) and DS₅ (b) 240

Figure 8.10: Reconstruction costs in Sicily provinces assuming 10 meters of inundation depth along the coastline based on DS₂ (a) and DS₅ (b) 241

Figure 8.11: Number of damaged buildings in Calabria, Puglia and Basilicata provinces assuming 2 (a), 5 (b) and 10 (c) meters of inundation depth along the coastline 243

Figure 8.12: Reconstruction costs in Calabria, Puglia and Basilicata provinces assuming 2 (a), 5 (b) and 10 (c) meters of inundation depth along the coastline based on DS₅ 244

Figure 8.13: Number of damaged buildings in Italy regions assuming 2 (a), 5 (b) and 10 (c) meters of inundation depth along the coastline 247

Figure 8.14: Reconstruction costs in Italy regions assuming 2 meters of inundation depth along the coastline based on DS₂ (a) and DS₅ (b) 249

Figure 8.15: Reconstruction costs in Italy regions assuming 5 meters of inundation depth along the coastline based on DS₂ (a) and DS₅ (b) 251

Figure 8.16: Reconstruction costs in Italy regions assuming 10 meters of inundation depth along the coastline based on DS₂ (a) and DS₅ (b) 253

Chapter 1

Introduction: Overview of Tsunami Events

In the last decades, several tsunami events caused catastrophic effects in terms of casualties and structural damages and this is one of the main reasons that have engaged scientific attention to the vulnerability of Italian coastal buildings subjected to tsunami loads.

Tsunami is a Japanese word that means “*harbour wave*” and can be defined as a series of waves with variable long periods, mostly triggered by earthquake induced uplift or subsidence of the sea floor. Other causes include large landslides near the coast or underwater and undersea volcanic eruptions; in general, a tsunami is caused by a large displacement of water mass (Figure 1.1).

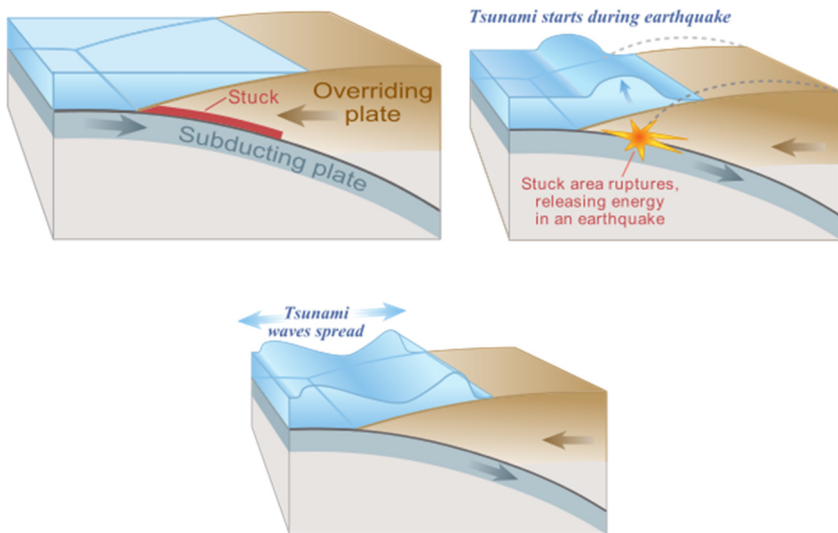


Figure 1.1: Tsunami genesis (image provided by United States Geological Survey agency)

Large tsunamis have historically affected the coasts of Japan, Alaska, Hawaii, South America and Southeast Asia. The Mediterranean Sea area is characterized by a high tsunami risk as it is geologically active; however, tsunamis with lower intensity are expected due to the small size of the basin than tsunamis generated in ocean. Furthermore, the time between the generation of the tsunami and the arrival of the wave on the coasts is limited.

In this chapter a quickly review is shown on the physical phenomenon in order to understand how a tsunami event born and grows. Furthermore a list of the main tsunami events is reported related to international and national events and an intensity scale is shown to compare different tsunami events depending on several factors.

1.1. Physical phenomenon

Normal ocean waves are caused by the wind, weather, tides, and currents while tsunamis are powered by a geological force. Tsunami waves are surface gravity waves where the displaced water mass moves under the influence of gravity and radiate across the ocean (Pelinovsky 2006 and Levin et al. 2009). Regular wind waves only involve motion of the uppermost layer of the water while tsunami waves involve displacement of the entire water column from surface to seafloor (Röbke et al. 2017).

Both common ocean waves and tsunami waves have a crest and a trough and can be described by their period, wavelength, crest, speed and amplitude (Figure 1.2).

The wave period is the measure of time it takes for the wave cycle to complete while the wavelength of this wave is the distance between two consecutive crests or peaks. The crest represents the highest part of a wave. The wavelength and the tsunami period give information on the

tsunami source. Wavelength ranges from 20 to 300 km characterize tsunamis generated by earthquakes while ranges from hundreds of metres to kilometres characterize tsunamis generated by landslides where the wavelength is much shorter.

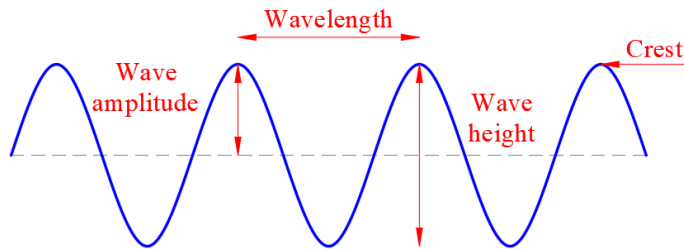


Figure 1.2: The main wave parameters

In the deep ocean, tsunamis have extremely long wavelengths which can be between 100 and 300 km, whereas normal ocean waves have wavelengths of only 30 or 40 meters. Furthermore, tsunamis are characterized by small amplitudes in the deep ocean of less than one meter and negligible wave steepness; this is the reason why they are not frequently noticed by people in ships.

Their period is very long about an hour in deep water while the common wave period is variable between 1 and 30 seconds. The tsunami wave speed is based on the water depth; typically, a tsunami wave has a velocity of about 800 km per hour in deep ocean while normal ocean waves have a wave speed of 10-100 km per hour but it is important to note that tsunami wave slows down dramatically as it approaches land and sea shallows.

The tsunami wave velocity can be calculated by the following equation in the ocean:

$$c_0 = \sqrt{g h}$$

where g is the gravitational acceleration and h is the sea water depth. As shown in the equation of wave velocity, it is obvious the reason why the flow velocity is higher offshore than near coastline.

Tsunami waves lose less energy in deep water because wave loss energy is inversely related to its wavelength and it becomes dangerous once shallow waters are reached near the coast. In fact, in coastal areas where water levels gradually become shallower, the wave will slow down dramatically, it becomes compressed and the inundation depth grows faster due to water depth decreasing (Figure 1.3).

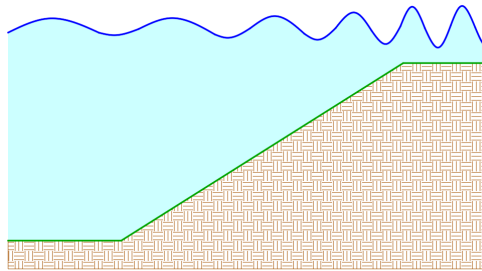


Figure 1.3: Wave propagation offshore and near coastline

The main wave parameters that characterize structural loads on buildings are:

- Inundation depth h : the depth of tsunami water level with respect to the grade plane, at the structure;
- Vertical velocity u ;
- Maximum momentum flux per unit mass per unit width $(h u)^2_{max}$.

It is important to note that maximum momentum flux per unit mass per unit width is not equal to multiplying the maximum inundation depth and the maximum vertical velocity, in fact, they may not occur at the same time.

In Chapter 2 the main international building codes will be analysed and how these parameters are taken into account in the tsunami load modelling on structures.

1.2. Historical event

Several technical reports are available in international scientific literature related to main tsunami events in last decades (Cuadra et al. 2012, Park et al. 2012):

- 2004/12/26 - *“The 2004 Indian Ocean Tsunami”*: A violent earthquake characterized by a 9.3 magnitude struck the Indian Ocean and it triggered a huge tsunami that mainly affected the Indonesia, Sri Lanka, India and Thailand coasts (Figure 1.4). The earthquake was the third largest earthquake recorded in historical database. Furthermore, it was one of the deadliest natural disasters recorded in human history because there were not any alert system covering the Indian Ocean due to the absence of major tsunami events since 1883;



Figure 1.4: An aerial photography post and pre tsunami event on Sumatra coast (2004)

- 2009/11/29 - *“The 2009 South Pacific Tsunami”*: an earthquake of 8.1 magnitude occurred in the Samoa Islands region triggering a tsunami that affected several countries, including Samoa,

American Samoa, Fiji, New Zealand, Tonga and French Polynesia. The recorded inundation depth was variable between 4 and 6 meters with low damages level on structures;

- 2010/02/27 - “*The 2010 Chilean Tsunami*”: an 8.8 earthquake offshore of Chilean coasts generated a tsunami which caused serious damage and casualties, it also caused minor effects in other Pacific nations;
- 2011/03/11 - “*The 2011 Great East Japan Tsunami*”: a 9.0 magnitude earthquake produced a tsunami characterized by inundation depth of 10 meters along Japanese coast in Tohoku region. The wave caused widespread devastation with a high number of casualties (Figure 1.5).



Figure 1.5: An aerial photography post and pre tsunami event on Japanese coast (2011)

According to technical reports, the events of Sumatra 2004 and Japan 2011 were the most severe in terms of human losses and damages to buildings and infrastructure.

In Italy, the main historical events affected the area near the Strait of Messina, the Gargano and Liguria areas (Tinti 2007, Caputo et al. 1987, Zecchi 2006):

- 1343/11/25: a violent earthquake affected the Neapolitan subsoil causing one of the first tidal waves recorded in Italy. The only proof available is reported in the manuscript "*Epistolae familiares*" written by famous Italian poet Petrarca that was in Naples during the tsunami event;
- 1627/07/30: An earthquake of the eleventh degree of the Mercalli scale caused a tsunami near San Severo in Foggia province that struck the Gargano promontory with waves characterized by inundation depth of 2.5 meters;
- 1693/01/11: An earthquake of 6.8 magnitude occurred in Val di Noto caused a tsunami in Sicily, affecting Syracuse, Ragusa, Augusta and Catania region where inundation depth of 15 meters were recorded;
- 1783/02/06: A seismic swarm struck Calabria and Sicily and it triggered a series of tidal waves that affected the Calabrian coast with particular reference to Messina and Reggio Calabria between 1783 and 1785. In particular, an earthquake caused a detachment of a huge part of a mountain close to Scilla and a tsunami occurred when debris dropped into the sea; the recorded inundation depth was of 9 meters;
- 1887/01/23: An earthquake of magnitude 6.3 occurred between Dianio Castello and Dianio Marina in Liguria causing a tsunami with waves of about 3 meters characterized by a retreat of water of about thirty meters and subsequent abnormal wave;
- 1908/12/08: an earthquake estimated at the eleventh degree on the Mercalli scale triggered a devastating tsunami near Messina, Reggio Calabria and several other Sicilian and Calabrian coastal

cities. In the following three days, there were more than sixty replicas of lower intensity and about two thousand aftershocks in the next two years. The historical reports recorded at least three large waves that characterized the tsunami after the earthquake with inundation depth of about 13 meters;

- 2002/12/30: a tsunami was triggered by the landslides of volcanic material due to the volcanic activity of Stromboli with inundation depth of 11 meters and high damages on coastal buildings.

The tsunami of Reggio Calabria – Messina in 1908 is one the worst tsunami events in Italian history in terms of casualties and construction damages. The main studies are proposed by Tinti et al. (2001, 2003, 2005) on the historical tsunami effects on Italian coasts.

1.3. Intensity scale

Several attempts have been made to provide tsunami intensity or magnitude scale to allow comparison between different events as with earthquakes events.

The intensity is a parameter that describes the effects of the analysed event, such as building or infrastructural damages and casualties.

Main earthquake intensity scales were provided by Mercalli-Sieberg and Richter and in particular, the former is a twelve-points scale based on structural damages. The magnitude parameter does not describe effects caused by the earthquake but it is related to the released energy during the event as reported in the Richter scale, introduced by C.F. Richter in 1935.

Similarly, the magnitude of a volcanic eruption is measured according to the eight-points Volcanic Explosivity Index introduced by Newhall and Self on 1982.

Papadopoulos and Imamura (2001) proposed a twelve-points tsunami intensity scale, which has been inspired by the long experience in post-tsunami events. The proposed new tsunami intensity scale incorporates twelve divisions and is consistent with the several twelve-grade seismic intensity scales established and extensively used in Europe and North America in about the last 100 years. The new scale is arranged according to three different aspects:

- (a) the effects on humans;
- (b) the effects on objects, including vessels of variable size, and on nature;
- (c) damages to buildings.

In particular, the twelve degrees are defined as follow:

I. Not felt

- a) Not felt even under the most favourable circumstances.
- b) No effect.
- c) No damage.

II. Scarcely felt

- a) Felt by few people on board in small vessels. Not observed in the coast.
- b) No effect.
- c) No damage.

III. Weak

- a) Felt by most people on board in small vessels. Observed by few people in the coast.
- b) No effect.
- c) No damage.

IV. Largely observed

a) Felt by all on board in small vessels and by few people on board in large vessels. Observed by most people in the coast.

b) Few small vessels move slightly onshore.

c) No damage.

V. Strong

a) Felt by all on board in large vessels and observed by all in the coast. Few people are frightened and run to higher ground.

b) Many small vessels move strongly onshore, few of them crash each other or overturn. Traces of sand layer are left behind in grounds of favourable conditions. Limited flooding of cultivated land.

c) Limited flooding of outdoors facilities (e.g. gardens) of near-shore structures.

VI. Slightly damaging

a) Many people are frightened and run to higher ground.

b) Most small vessels move violently onshore, or crash strongly each other, or overturn.

c) Damage and flooding in a few wooden structures. Most masonry buildings withstand.

VII. Damaging

a) Most people are frightened and try to run in higher ground.

b) Many small vessels damaged. Few large vessels oscillate violently. Objects of variable size and stability overturn and drift. Sand layer and accumulations of pebbles are left behind. Few aquaculture rafts washed away.

c) Many wooden structures damaged, few are demolished or washed away. Damage of grade 1 and flooding in a few masonry buildings.

VIII. Heavily damaging

a) All people escape to higher ground, a few are washed away.

b) Most of the small vessels are damaged, many are washed away.

Few large vessels are moved ashore or crashed each other. Big objects are drifted away. Erosion and littering in the beach. Extensive flooding. Slight damage in tsunami control forest, stop drifts. Many aquaculture rafts washed away, few partially damaged.

c) Most wooden structures are washed away or demolished. Damage of grade 2 in a few masonry buildings. Most reinforced concrete (RC) buildings sustain damage, in a few damage of grade 1 and flooding is observed.

IX. Destructive

a) Many people are washed away.

b) Most small vessels are destructed or washed away. Many large vessels are moved violently ashore, few are destructed. Extensive erosion and littering of the beach. Local ground subsidence. Partial destruction in tsunami control forest, stop drifts. Most aquaculture rafts washed away, many partially damaged.

c) Damage of grade 3 in many masonry buildings, few RC buildings suffer from damage grade 2.

X. Very destructive

a) General panic. Most people are washed away.

b) Most large vessels are moved violently ashore, many are destructed or collided with buildings. Small boulders from the sea bottom are moved inland. Cars overturned and drifted. Oil spill, fires start. Extensive ground subsidence.

c) Damage of grade 4 in many masonry buildings, few RC buildings suffer from damage grade 3. Artificial embankments collapse, port water breaks damaged.

XI. Devastating

b) Lifelines interrupted. Extensive fires. Water backwash drifts cars and other objects in the sea. Big boulders from the sea bottom are moved inland.

c) Damage of grade 5 in many masonry buildings. Few RC buildings suffer from damage grade 4, many suffer from damage grade 3.

XII. Completely devastating

c) Practically all masonry buildings demolished. Most RC buildings suffer from at least damage grade 3.

Chapter 2

State of Art Analysis

The second chapter focuses on main aspects about structural analyses and behaviour of buildings under tsunami loads available in international literature, research projects, building codes and guidelines.

A tsunami event is characterized by many uncertainty and it is complicated to predict building behaviour of structures due to land and wave characteristics that are strictly related to the interested area and earthquake or landslide that triggers the event. Many other studies are needed to improve current codes and evacuation systems.

In this chapter tsunami load models on structures are discussed according to main international building codes and guidelines. A critical review is provided on empirical fragility curves and structural behaviour depending on buildings structural material based on principal post-tsunami event of last twenty years and available on scientific papers.

2.1. International building codes

The main difficulties in analysing the effects of tsunamis are mainly related to the complexity of wave modelling and the high degree of uncertainties of the required parameters (Nouri et al. 2010). In particular, inundation depths and velocities are strongly influenced by coastal bathymetry (seabed geometry) near the shore, the topographic and morphological composition of the coastal areas of interest and the altimetry of structures.

The main horizontal forces related to a tsunami event are (Nistor et al. 2010):

- *Hydrostatic forces*: depending on the partial or total submersion of the structures;
- *Hydrodynamic forces*: based on the high wave velocity;
- *Debris impact forces*: caused by boats, cars, containers, wood and various debris dragged by the wave energy.

In addition, *buoyancy forces* are modelled as vertical component of tsunami loads and they are related to the inundated volume of the structure.

Main actual research project are trying to retrieve the inundation depth and the wave velocity based on the wave impact time on the buildings in order to provide empirical distribution of tsunami loads on structures; in particular a reverse technique is used depending on the videos obtained during the last events (mainly in the areas of Sumatra in 2004 and in the Tohoku region in 2011) and from the damages recorded on the structures.

The tsunami loads depend on several factors (Cawley 2014):

- Maximum vertical velocity u_{max} ;
- Inundation depth h_{max} ;
- Maximum momentum flux per unit mass per unit width $(h u)^2_{max}$;
- Mass and stiffness of debris (i.e. stiffness of debris is reduced due to impact with the tsunami wave);
- Structural exposure surface.

A further problem is related to the time influence of the wave parameters and in particular, it is not possible to establish if the maximum inundation depth and vertical velocity of wave are reached at the same time.

External pressure distribution integration is required in refined analyses to evaluate tsunami loads on structures depending on structural

exposed surface. International building codes propose simplified approaches characterized by closed form equations to evaluate tsunami loads on buildings.

2.1.1. Historical building codes evolution

An historical discussion is proposed on the main historical international building codes and guidelines evolution that introduced significant improvement in the tsunami loads modelling on structures.

In the international panorama, there are several approaches that assume different load distributions to model the tsunami effects on structures. The main studies and refined analyses have been developed in the United States and Japan as shown in the following list:

- *Development of Structural Standards in Flood and Tsunami Areas for the Island of Hawaii (Bretshneider, 1974):*

The study provides an approach to estimate the runup based on the sea level for the Hawaii coasts. The research was supported by a study of the coastal areas that led to realize detailed topographic maps. The proposed tsunami load equations have been validated by an extended experimental program; in the report tables are provided with drag coefficients and coefficients depending on the shape and size of the debris;

- *Design and Construction Standards for Residential Construction in Tsunami-Prone Areas in Hawaii (Dames & Moore, 1980):*

On commission of the *Federal Insurance Administration*, the first guidelines were realized for the structural design of buildings under tsunami loads. In particular, they provided design criteria for buildings and foundations under tsunami loads and an economic analysis for newly designed coastal structures;

- *1997 Uniforming Building Code (UBC 1997):*
The building code authorized by the *International Conference of Building Officials (ICBO)* offers several reflections on the design criteria of special resistant structures to tsunamis in the "*Appendix Chapter 31*" but it does not provide any equations for the evaluation of load distributions;
- *ASCE 7-98/16 "Minimum Design Loads for Buildings and other Structures":*
Provided by the *American Society of Civil Engineers Committee*, it proposed several load distributions with equations. In the next edition of 2002 (*ASCE 7-02*) equations are provided to calculate impact loads depending on specific structural elements. The latest edition of 2016 (*ASCE 7-16*) provides the most advanced approach to the tsunami design and in particular, it provides hazard maps, equations for horizontal and vertical load components, load combinations, load scenarios and specific energy analysis methods to assess the wave energy dissipation;
- *ASCE 24-98 "Flood Resistant Design and Construction":*
Provides minimum requirements for the design of tsunami resistant structures in areas classified with a high tsunami risk; it does not provide equations to describe tsunami loads;
- *International Building Code 2000 (IBC 2000):*
Commissioned by the *International Code Council*, it provides information on the construction of tsunami-resistant structures in the "*Appendix G*" for high tsunami risk areas, without providing equations to describe the wave effects on the structures;
- *The City and County of Honolulu Building Code (ROH):*
Commissioned by the *Department of Planning and Permitting of Honolulu of Hawaii*, it provides information on equivalent tsunami loads on the structures, load combinations and design

criteria for tsunami resistant structures. The provided equations are based on the studies of Dames and Moore in 1980;

- *Federal Emergency Management Agency Coastal Construction Manual (FEMA 2000/2012):*

In chapter 11, it introduces the equation to evaluate tsunami loads on specific structural elements. The manual aims to provide guidelines for the structural design of buildings in coastal areas with high tsunami risk. More refined analyses methods are discussed and proposed in the next edition *FEMA P-55* and the last one *FEMA P-646*;

- *Development of Design Guidelines for Structures that Serve as Tsunami Vertical Evacuation Sites, 2005:*

These guidelines are proposed by Yeh et al. (2005) to evaluate tsunami loads on structures committed by the *Washington State Department of Natural Resources*;

- *Guideline for Tsunami Evacuation Building, 2005/2011:*

Commissioned by the *Ministry of Land, Infrastructure, Transport and Tourism (MLIT)* and realized by the *Building Center of Japan*, it provides guidelines for the design of tsunami-resistant structures and design equations to evaluate equivalent tsunami loads on structures. The proposed approach is more conservative and simplified than the main U.S. codes *FEMA* and *ASCE* (characterized by refined analysis for specific buildings). In 2011, after the tsunami that devastated the Tohoku region, they were revised and the adopted approach was updated.

In the following, the main actual building codes and guidelines are analysed in detail.

2.1.2. *Structural Design Requirements for Tsunami Evacuation Buildings (SDRTEB)*

After the 2011 catastrophic tsunami event in Tohoku region, a team composed by the *Institute of Industrial Science*, the *University of Tokyo* and the *Building Research Institute* carried out a series of inspections to assess the damage level on structures. In November 2011, the *Ministry of Land, Infrastructure, Transport and Tourism* published interim guidelines (Nakano et al. 2011) based on *SDRTEB* paper and in-situ surveys proposed by Nakano et al. 2010.

It proposes a conservative and simplified approach to evaluate horizontal forces based on one equivalent hydrostatic force that combines the effect of both hydrostatic and hydrodynamic loads. In particular, the design inundation depth is assumed equal to the expected inundation depth increased by a coefficient η (Figure 2.1).

Therefore, the design tsunami pressure distribution is characterized by a triangular shape and it is applied on structural components:

$$q_z = \rho g \alpha (\eta h - z) = \rho g \alpha (h_{max} - z)$$

where:

- q_z : intensity of tsunami pressure at height z ;
- ρ : water density;
- g : gravity acceleration;
- η : inundation depth coefficient;
- α : wall openings ratio coefficient;
- h : expected inundation depth;
- z : location of acting pressure measured from ground.

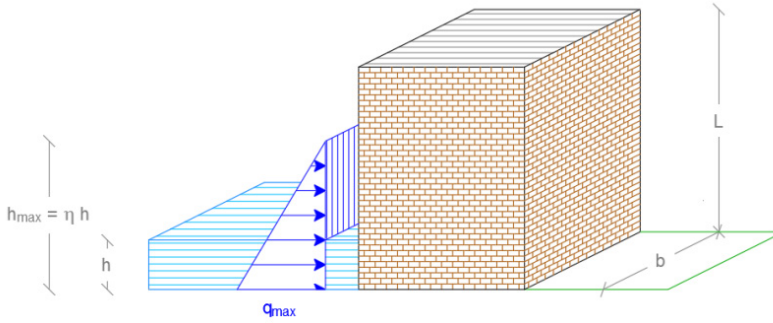


Figure 2.1: Design tsunami pressure distribution

The tsunami wave force can be evaluated integrating the wave pressure distribution between two generic heights z_1 and z_2 depending on the tsunami exposed surface area; the load can be reduced not less than 70% in case of wall opening (doors, windows, etc).

$$Q(z) = p g c \int_{z_1}^{z_2} (h_{max} - z) b dz$$

The inundation depth coefficient η depends on availability of specific tsunami energy dissipation structures commonly called *seawalls*. The seawalls represent an important prevention system in area with a high tsunami risk, a proper design is required and RC or steel materials are common used to build seawalls.

It can assumed a minimum value of 1.5 and a maximum value of 3 depending on the distance of the structure from shoreline or riverbank and the availability of the seawalls (Figure 2.2).

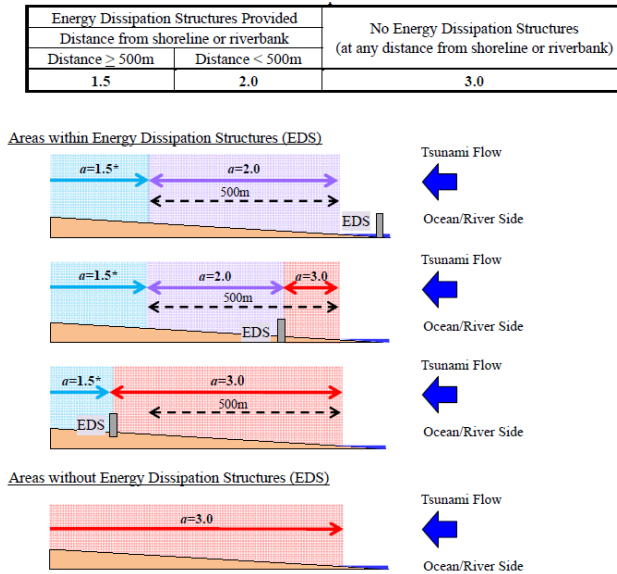


Figure 2.2: Inundation depth coefficient η depending on energy dissipation structures and distance from shoreline or riverbank (Nakano et al. 2011)

The buoyancy force represents vertical tsunami loads component and it is evaluable with following equation:

$$Q_z = p g V$$

Where V is the volume of the building inundated by the tsunami.

Following load combinations are proposed in the structural design of buildings under tsunami load.

$$G + P + 0.35S + T \text{ (regions of heavy snowfall)}$$

$$G + P + T \text{ (regions other than regions of heavy snowfall)}$$

Where:

- G represent dead load;
- P represent live load;
- S represent snow load;
- T represent tsunami load.

Furthermore, Japanese guidelines recommend to assume that the load in the perpendicular direction will be half or more of the load in the straight direction, as shown in Figure 2.3, because tsunami waves can potentially impact a structure from all directions. Furthermore, wave backwash effects are taken into account.

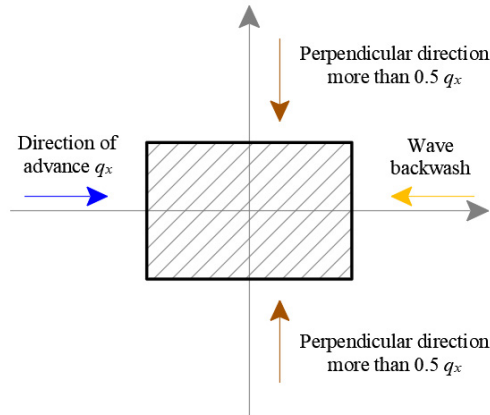


Figure 2.3: Horizontal load combination (Nakano et al. 2011)

For the structural framework design, the horizontal load capacity of the structure has to be equal to or greater than the horizontal tsunami load in all directions in terms of flexural and shear stresses. In particular, design criteria aims not to reach a building failure mode in terms of collapse, overturning and sliding of the structure.

The Japanese guidelines are based on previous edition of guidelines developed by Okada et al. (2005) and Asakura et al. (2002) to analyse the modelling of tsunami effects.

The previous edition of guidelines assumed that the inundation depth coefficient was always equal to the maximum value 3 and, in some cases, this could provide overestimated stresses.

With this approach, tsunami force depends on one parameter only, the inundation depth that is complicated to estimate and it can be

obtained via numerical simulation or hazard map. The method efficiency was validated by experimental study of Nakano (2010) by extended field surveys after the Sumatra tsunami in 2004, comparing real buildings damage with expected damages retrieved according to Japanese guideline approach.

2.1.3. Federal Emergency Management Agency – FEMA P-646

The *FEMA P-646* proposes tsunami load distribution equations based on the following assumptions:

- The tsunami water flow is composed by a mixture of sediment and seawater and in particular, the suspended sediment concentration in the fluid does not exceed 5%. Based on this assumption, the density of the tsunami flow fluid can be assumed equal to 1.1 times the fresh water density, or $\rho_s = 1.128 \text{ kg/m}^3$;
- It is suggested to increase the maximum runup (difference between the elevation furthest inundation inland point and the sea level) due to the strong influence of the site topography and bathymetry on the wave parameters based on empirical studies. In particular, the design maximum height R is equal to the expected value R^* increased by 30% or with a coefficient equal to 1.3:

$$R = 1.3 R^*$$

The aim is to take into account all potential analysis uncertainties. This coefficient is calibrated on experimental studies conducted by Yamazaki et al. (2011) on the Samoa Tsunami of 2009.

2.1.3.1. Hydrostatic forces

Hydrostatic forces occur when a fluid in a state of quietness or characterized by a very slow motion impacts a structure. It always acts perpendicularly to the analysed structural component (Figure 2.4). It is caused by different pressures depending on different water levels on the two opposite sides of the structure. Hydrostatic forces intensity is strongly dependent on exposed surface area and high effects are expected in the case of slender or thin elements.

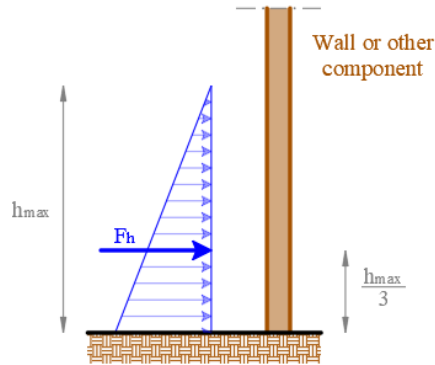


Figure 2.4: Hydrostatic force model

If the ground floor of the structure is waterproof, or in any case it has a degree of insulation such as to prevent the water infiltration, the horizontal hydrostatic force acting on the structural element is estimated with the following equation:

$$F_h = p_c A_w = \frac{1}{2} \rho_s g b h_{max}^2$$

Where:

p_c : is the hydrostatic pressure;

A_w : is the surface area of wall panel exposed to water flux;

s : is the fluid density including sediment;

g : is the acceleration of gravity;

b : is the wall width;

h_{max} : is the maximum inundation depth.

The pressure distribution is triangular and therefore the resultant is applied at $h_{max}/3$.

2.1.3.2. Buoyant forces

Buoyant forces depend on the water volume inside the structure and it is applied to its centre of gravity (Figure 2.5). It is a vertical load and must be balanced by the weight of the structural elements.

The buoyancy forces equation is:

$$F_b = \rho_s g V$$

Where V is the water volume inside the building.

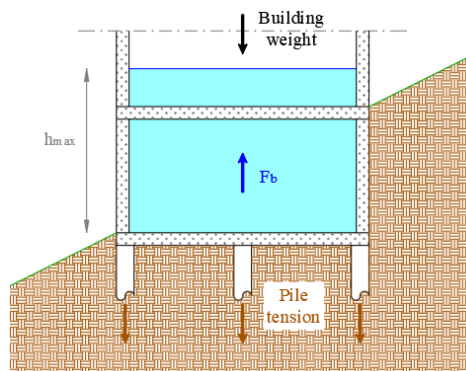


Figure 2.5: Buoyant forces model

It will be necessary to use pile foundation in case of vertical forces not balanced and in addition, liquefaction analyses are required.

2.1.3.3. *Hydrodynamic forces*

Hydrodynamic forces depend on wave vertical velocity, inundation depth, wave density and the geometry of the structure. (Figure 2.6).

Hydrodynamic forces can be evaluated with the following equation:

$$F_d = \frac{1}{2} \rho_s C_d B (h u^2)_{max}$$

Where:

C_d : is the drag coefficient;

B : is the width of the structural element analysed in the plane normal to the flow direction;

h : is the inundation depth;

u : is the wave vertical velocity.

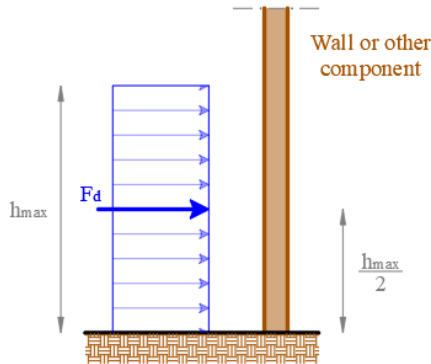


Figure 2.6: *Hydrodynamic forces model*

The pressure distribution is uniform and therefore the resultant is applied at half inundation depth, $h_{max}/2$.

The $(h u^2)_{max}$ parameter represents the maximum momentum flux per unit of mass and unit of width and it is important to note that it is different from $h_{max} u^2_{max}$ because it is not possible to establish if the maximum value of the inundation depth h_{max} and vertical velocity u_{max}

occurs at the same time. It can be evaluated through detailed numerical simulations or refined simulations available in literature.

In case of absence of data, the following analytical equation can be used depending on inundation maps parameters:

$$(h u^2)_{max} = g R^2 \left(0.125 - 0.235 \frac{z}{R} + 0.11 \left(\frac{z}{R} \right)^2 \right)$$

The previous formula is based on the non-linear one-dimensional theory of a fluid for shallow waters, in the absence of friction and considering sand for a ground with constant inclination. The results can be assumed for a preliminary design and numerical simulations.

2.1.3.4. Impulsive Forces

Impulsive forces are related to the wave impact on the structure and are estimated approximately as 1.5 times the hydrodynamic forces (Figure 2.7) as shown in experimental studies provided by Arnason in 2005.

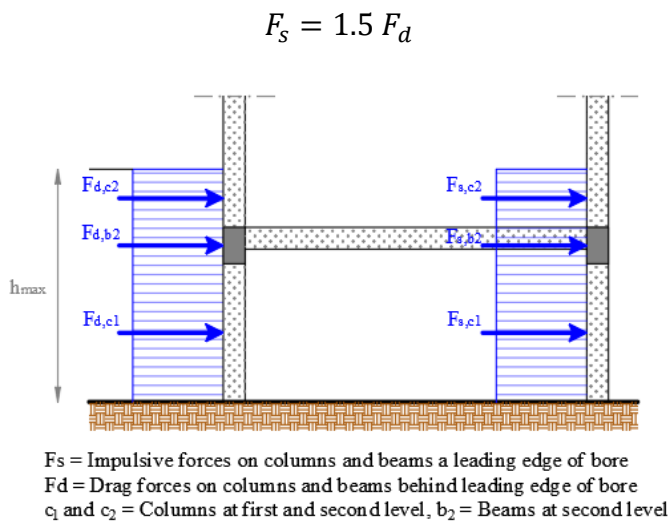


Figure 2.7: Impulsive forces model

2.1.3.5. *Floating debris impact forces*

The debris impact forces are related to any object with not negligible size (e.g. trees, boats, containers, vehicles, building debris). These forces are dependent on the analysed site, e.g. containers are taken into account in structures near harbours. In addition, debris impact force can cause significant damages to the structures and it is complicated to estimate due to problem uncertainties. It is possible to assume debris impact force equal to the following equation in according to *ASCE 7* at chapter 5:

$$F_i = 1.3 u_{max} \sqrt{k m_d (1 + c)}$$

Where:

I.3: is a coefficient for *risk category IV* for structures according to *ASCE 7* in chapter 5;

u_{max}: is the maximum vertical velocity;

c: is a hydrodynamic mass coefficient that takes into account the effect of debris on fluid and it depends on the debris size, shape and orientation;

k: represents the actual stiffness of the object reduced by the wave impact;

m_d: is the debris mass.

Impact forces are applied locally on single structural components at the inundation depth level (Figure 2.8). The probability that two or more debris impact the structure at same time is very low and can be neglected.

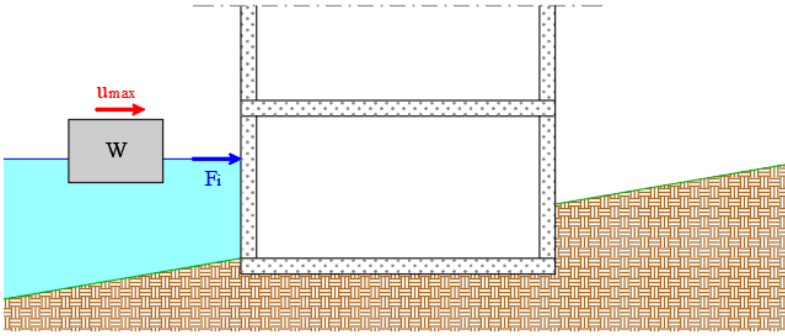


Figure 2.8: Floating debris impact forces model

The maximum vertical velocity has a huge influence on the assessment of impact forces and should be assessed through refined and advanced numerical simulations. In the case of lack of analyses, the following equation can be assumed:

$$u_{max} = \sqrt{2 g R \left(1 - \frac{z}{R}\right)}$$

The previous equation is based on the same assumptions for maximum momentum flux per unit of length and unit of mass equation.

2.1.3.6. Damming of accumulated waterborne debris

The debris accumulation on the structure can form a barrier, i.e. containers, and an additional horizontal hydrodynamic force can be modelled.

$$F_{dm} = \frac{1}{2} \rho_s C_d B_d (h u^2)_{max}$$

where B_d represents the debris width and it is suggested to assume a minimum value of 12 meters that represents the average size of a container.

2.1.3.7. *Load combinations*

Tsunami loads are not applied on the structure at the same time and therefore loads must be combined assuming particular load combinations. The following forces can be modelled on the structure:

1. Lifting forces reduce the weight of the structure and the overturning resistance of the structure due to buoyancy and hydrodynamic forces; therefore, these actions must be considered always in all load combinations;

2. *Impulsive forces* are characterized by short duration and impact a large part of the structure. External forces should be applied sequentially to all the structural elements but not at the same time. The impulsive forces are replaced by hydrodynamic forces when the wave impact effect ends.

3. *Debris impact forces* are characterized by short duration and caused by the impact of large floating debris on individual structural components. These forces must be combined with hydrodynamic forces and not with impulsive forces. The probability that two or more debris impact the structure at same time is very low and can be neglected, therefore it can be assumed that the impact occurs at a single moment at any point of the structure;

4. The *accumulation of debris* can increase the exposure area of hydrodynamic loads. It must be considered in the worst position of the buildings in terms of stress and combined with hydrodynamic forces applied on all structural components (Figure 2.9). Any positive shielding effect caused by debris is neglected as safety criterion;

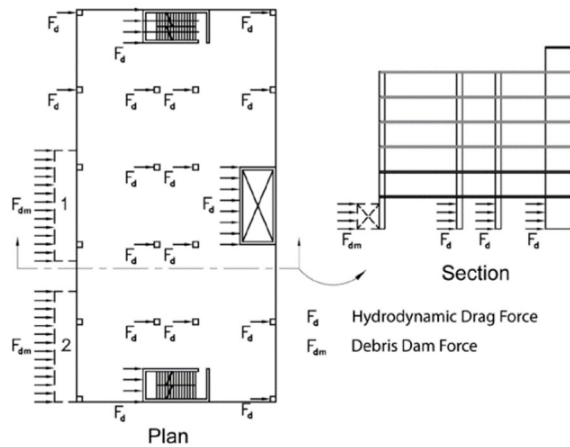


Figure 2.9: Load combinations (FEMA P-646)

5. The *slabs* design is independent from horizontal loads position on the structure.

The load combinations are based on *ASCE 7-10* and it is assumed that only refuge floor areas are occupied during the tsunami event. The tsunami loads T_s must be combined with gravitational loads using the following safety coefficients:

$$\text{Load Combination 1: } 1.2 D + 1.0 T_s + 1.0 L_{REF} + 0.25 L$$

$$\text{Load Combination 2: } 0.9 D + 1.0 T_s$$

Where:

D : self-weight loads;

T_s : tsunami loads;

L_{REF} : accidental loads on the "refuge area";

L : accidental loads outside the "refuge area".

A unitary load factor is used for tsunami forces T_s because the tsunami hazard level corresponding to the *Maximum Considered Tsunami* will be consistent with the 2500 years return period related to *Maximum Considered Earthquake* used in seismic design. Furthermore,

potential uncertainties in tsunami runup elevations are evaluated increasing the expected runup elevation R^* with a coefficient of 1.3.

Seismic loads are not combined with tsunami loads because it is neglected the possibility of a design level earthquake and maximum tsunami loading at the same time.

2.1.4. American Society of Civil Engineering – ASCE 7-16

The American code *ASCE 7-16* provides a refined and detailed analysis to design structures under tsunami loads and it is the latest building code. Hazard maps are provided for the *Maximum Considered Tsunami* (tsunami event with a return period of 2475 years) and for *Tsunami Design Zones* (area with high tsunami hazard level and it defines areas where structures require the design under tsunami loads).

The ASCE classifies buildings into four tsunami risk categories:

- *Risk Category I*: Buildings and other structures that represent a low hazard to human life in the event of failure;
- *Risk category II*: All buildings and other structures except those listed in Risk Categories I, III, and IV;
- *Risk category III*: Buildings and other structures , the failure of which could pose a substantial risk to human life as schools and universities;
- *Risk category IV*: buildings and structures of strategic importance.

During a tsunami, it is suggested to evacuate and not occupy structures in the first two risk categories.

The wave parameters required to model tsunami loads on structures, i.e. vertical velocity, inundation depth and maximum momentum flow, can be evaluated through two procedures:

- Energy grade line analysis: it is an energy method that permits to evaluate all wave parameters as inundation depth, vertical velocity and maximum momentum flux (Figure 2.10). It requires several input parameters as Froude number, Manning coefficient, runup elevation and a *DEM (Digital Elevation Model)* with a resolution at least of 10 metres to evaluate the altimetric trend.

The method validation and conservativeness of values are based on over 36'000 numerical analyses.

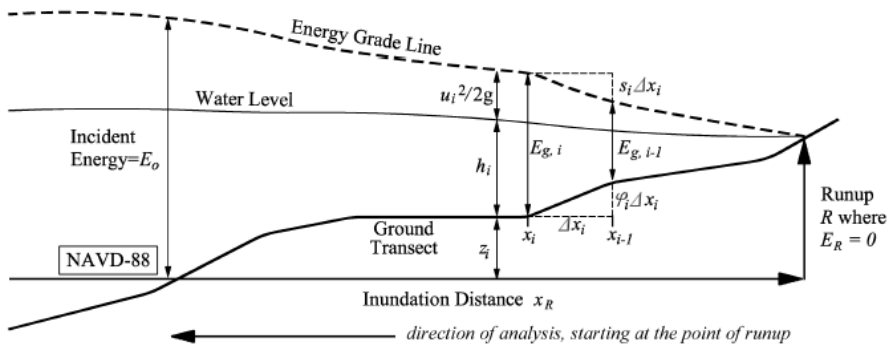


Figure 2.10: Emery grade line parameters (ASCE 7-16)

The building code provides all mathematical steps and equations to evaluate all wave parameters with the proposed method;

- Site-specific inundation analysis: it is a two-dimensional numerical analysis that requires waveform parameters and a high-resolution *DEM (Digital Elevation Model)*.

The building code proposes three different scenarios depending on the time history of the wave on the structure and in particular:

- *Load Case 1*: At an inundation depth of one-story, but not exceedance the maximum inundation depth, the interior shall be assumed not to be flooded to define the minimum condition of combined hydrodynamic force with buoyant force;

- *Load Case 2*: Depth at two-thirds of maximum inundation depth when the maximum velocity and maximum specific momentum flux shall be assumed to occur in either direction;
- *Load Case 3*: Maximum inundation depth when velocity shall be assumed at one-third of maximum in either direction

The *ASCE 7-16* introduces two rare load combinations:

$$0.9 D + F_{TSU} + H_{TSU}$$
$$1.2 D + F_{TSU} + 0.5 L + 0.2 S + H_{TSU}$$

Where:

F_{TSU} : tsunami loads;

H_{TSU} : tsunami- lateral loads on foundations;

D : self-weight loads;

L : accidental loads;

S : snow loads.

The design of the structural elements can assume linear elastic material behaviours as preliminary approach.

Furthermore, the *ASCE 7-16* proposes load factor "*Tsunami Importance Factors*" I_{TSU} , variable between 1 and 1.25, depending on the risk category of the building. The values were calibrated through a Monte Carlo simulation that involved millions of parameters combination.

The water wave inland is characterized by the presence of debris of various shapes and sizes which is the reason why the seawater mass density is amplified by a k_s coefficient equal to 1.1.

$$\rho_s = k_s \rho_{sw}$$

Similarly, it is recommended to amplify water specific weight by k_s coefficient in the evaluation of hydrostatic loads.

$$\gamma_s = k_s \gamma_{sw}$$

Where the specific weight density of water γ_{sw} is assumed equal to 1.025 kg/m^3 .

Great importance is given to the design of foundations, so it is necessary to take into account the phenomena of soil slip and erosion.

The main load distributions are:

- Hydrostatic forces;
- Hydrodynamic forces;
- Forces due to impact of debris.

The proposed equations are similar to *FEMA P-646* approach showed in previous paragraph, with load coefficients equation, i.e., drag coefficient and shape and size of debris coefficient.

In addition, it is not necessary to follow the proposed design criteria for buildings with one-to-two-storeys due to the high hydrodynamic loads, and furthermore, post-major tsunami event inspections in the last ten years showed a high vulnerability for this type of buildings.

2.1.5. Comparison and discussion

The building code analyses show two different approaches provided by Japanese guideline and main U.S. codes (*ASCE* and *FEMA*). The first one provides a simplified and conservative method assuming the tsunami loads modelled as a single equivalent hydrostatic distribution while the U.S. approach provides a marked distinction between hydrostatic and hydrodynamic forces with several load distributions.

The main difference consists in the number of parameters required to model tsunami loads; in particular, in the Japanese guidelines it is required only the maximum inundation depth, while the U.S. codes require several parameters as maximum inundation depth, maximum

vertical velocity and maximum momentum flux per unit mass per unit width. These parameters can be evaluated with simplified equations, hazard maps or refined numerical analyses. The Japanese approach can be extremely useful in the case of preliminary analysis, large-scale analysis, or in general, for analysis characterized by a low knowledge level. U.S. standards require a high knowledge level in terms of wave parameters, altimetric trend and structure details, therefore it is the best approach for single building design.

In particular, *ASCE 7-16* is the latest building code in terms of tsunami structural design and it provides a high degree of detail on the modelling of the effects of the wave impact on the structure. In addition, it provides a high degree of detail on load scenarios and combinations on tsunami loads modelling on structure and refined simulation analysis to retrieve water flux parameters (*Energy grade line analysis* and *Site-specific inundation analysis*).

2.2. Structural behaviour under tsunami loads

Post-tsunami event surveys permit to retrieve important information about buildings behaviour in terms of preferred collapse mechanisms depending on buildings structural materials and number of storeys.

2.2.1. *Masonry structures*

The main reports on masonry structures behaviour are related to Samoa buildings damages based on Indian Ocean Tsunami in 2004.

The reports available in literature show a high vulnerability under tsunami loads as shown in Figure 2.11. In particular, the main recorded collapse mechanisms are sliding failures, liquefaction event, flexural failure and in general, in-plane and out-of-plane local mechanisms

(Mallawaarachchi et al. 2008, Peiris et al. 2005). It is important to note that the construction quality in Sumatra was very poor and it is reasonable to consider that masonry buildings properly designed could exhibit a different structural behaviour under tsunami loads.



(a)



(b)



(c)



(d)



(e)

Figure 2.11: Out-of-plane mechanisms, liquefaction event and global collapse mechanisms of masonry buildings affected by the 2004 Indian Ocean Tsunami (a,b,c, Mallawaarachch et al. 2008; d, e, Peiris et al. 2005)

2.2.2. Reinforced concrete (RC) structures

RC structures show mainly columns collapse related to brittle failure and rarely ductile failure. (Chock 2011).

The main local mechanisms are characterized by soft storey mechanisms localized at ground floor or at first storey while, main global mechanisms are sliding failure at the ground floor and rarely the overturning of the entire structure (Hayashi et al. 2012), as shown in Figure 2.12.

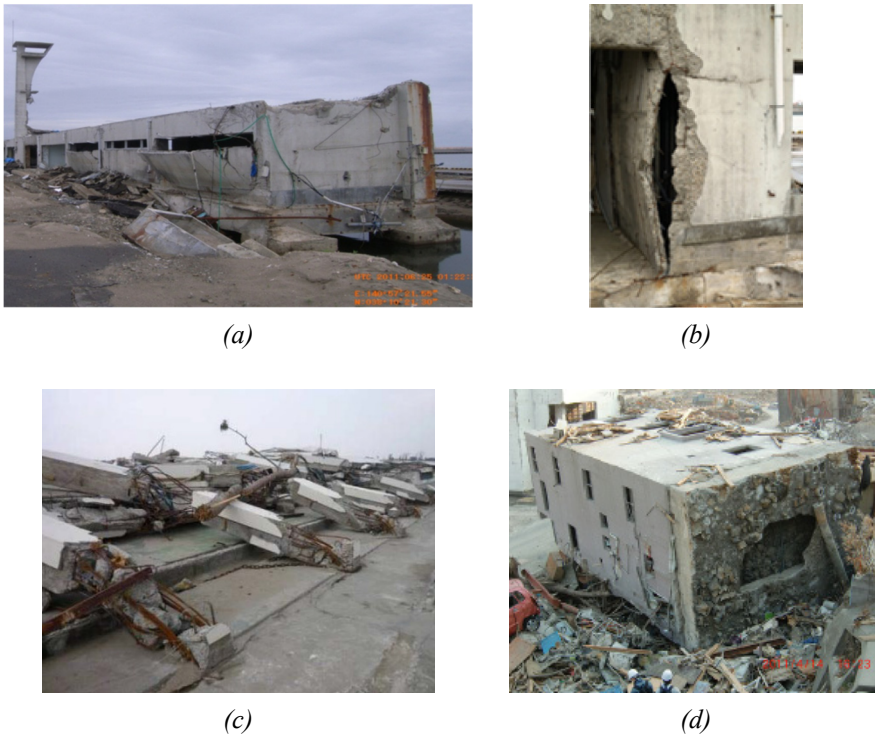


Figure 2.12: Main RC structures collapse mechanisms observed in Tohoku region, Japan, 2011

(a, b, c, Chock 2011; d, Hayashi, et al. 2012)

Infill walls show a high vulnerability to out-of-plane mechanisms and it is common to see circular openings in post-tsunami event surveys

as show in Figure 2.13. In particular, infill walls have a huge influence on buildings structural behaviour because in-plane mechanisms are related to structural resistance while tsunami loads evaluation is based on out-of-plane mechanisms. In fact, tsunami forces are surface forces linked to exposed surface and tsunami loads are strongly reduced in the case of infill walls collapse.



*Figure 2.13: Circular openings due to infill walls collapse in Chile (2010) and Thailand (2004)
(a, Al-Faesly et al. 2012; b, Foytong, et al. 2006)*

Columns in coastal RC buildings show a high vulnerability due to the impact of large debris (boats, vehicles or containers). In addition, debris accumulation could generate a dam effect that represent a huge increment in terms of loads on columns.

2.2.3. Steel structures

According to post-surveys event on steel structures, horizontal and vertical closure elements show a high vulnerability to out-of-plane mechanisms due to hydrostatic and hydrodynamic pressures acting on contact surfaces.

Furthermore, beams do not show high damages while columns show shear failures and in general, brittle failures. Another typical failure is

related to the buckling of compressed trusses. The most observed local mechanism is a soft storey mechanism due to the high deformability of steel structures.

As for RC structures, steel building could show overturning failure (Lignos 2011), as shown in Figure 2.14.



Figure 2.14: Effects of the Tohoku tsunami (2011) on steel structures (Lignos 2011)

2.2.4. Wooden structures

Wooden buildings show a high vulnerability to tsunami loads and an inadequate horizontal resistance to hydrostatic and hydrodynamic loads. In particular, a typical collapse mechanism is represented by soft storey mechanism at ground floor and the second storey exhibit a rigid translation (Cuadra et al. 2012) (Figure 2.15).



Figure 2.15: Effects of Tohoku Tsunami (2011) on wooden structures (Cuada et al. 2012)

Fires are the reason of complete destruction of the wooden structures as shown in Figure 2.16.



Figure 2.16: Fire in wooden buildings related to Tohoku tsunami in 2011

2.3. Empirical fragility curves

Empirical fragility curves are based on building damages recorded in post-tsunami event surveys and useful information are provided about building structural behaviour under tsunami loads depending on several parameters, i.e., buildings structural materials and number of storeys.

Teams of experts have collected data through field surveys, satellite images, *GPS (Global Positioning System)* and *GIS (Geographic Information System)* systems.

In particular, during the research, empirical fragility curves have been retrieved based on the following historical events:

- *The 2004 Indian Ocean Tsunami;*
- *The 2009 South Pacific Tsunami;*
- *The 2011 Great East Japan Tsunami.*

For previous events, there are not significant data in the international literature. In addition, only concrete and masonry buildings fragility curves are analysed due to the main goal of the research project that aims to clarify the structural behaviour of typical Italian residential buildings.

Furthermore, empirical fragility curves are analysed and compared based on buildings structural material while curves for cumulative building typologies are neglected because they do not provide significant results.

It is important to note that empirical fragility curves are strictly related to several parameters as local building types, materials quality, design code, coastal bathymetry, altimetric trend, and significant different results could be retrieved depending on the analysed tsunami.

In the literature, there is a lack of analytical fragility curves due to the absence of empirical and experimental data while main empirical fragility curves are related to few tsunami events (Koshimura et al. 2009).

Formally, fragility functions provide the probability of exceedance a specific damage state (*DS*) as a function of the structural demand parameter depending on the analysed hazard and it is usually assumed coincident with inundation depth, for the sake of simplicity. Furthermore, the lognormal distribution is typically used to define the fragility function (Porter et al., 2007).

2.3.1. “The 2004 Indian Ocean Tsunami”

Peiris et al. (2005) and Suppasri et al. (2011) provide main fragility curves based on the 2004 Indian Ocean tsunami.

In particular, Peiris et al. (2005) provide fragility curves related to residential masonry buildings in Sri Lanka, the data used are based on *Department of Census and Statistics of Sri Lanka* database, observations of the *Earthquake Engineering Field Investigation Team* and minor studies proposed in the literature.

Three different limit states are defined depending on the building damages according to available database as shown in Table 2.1.

Damage state (DS)	DS description
<i>Limit state 1</i>	Major damage to the entire building
<i>Limit state 2</i>	Partial damages such as to compromise the usability of the structure
<i>Limit state 3</i>	Partial damages such as not to compromise the usability of the structure

Table 2.1: Damage state definition (Peiris et al. 2005)

Fragility curves are provided as a function of the inundation depth and of the distance of structures from the coastline.

Fragility curves show that buildings far away from the coastline have less damages than structures near the coastline (Figure 2.17) as expected due to the reduced wave inundation depth and velocity that impact the structure. Wave parameters dissipation is caused by impact with structures, woods and altimetric trend. Fragility curves proposed by Peiris et al. (2005) provide the probability of exceedance a specific damage state depending on inundation depth.

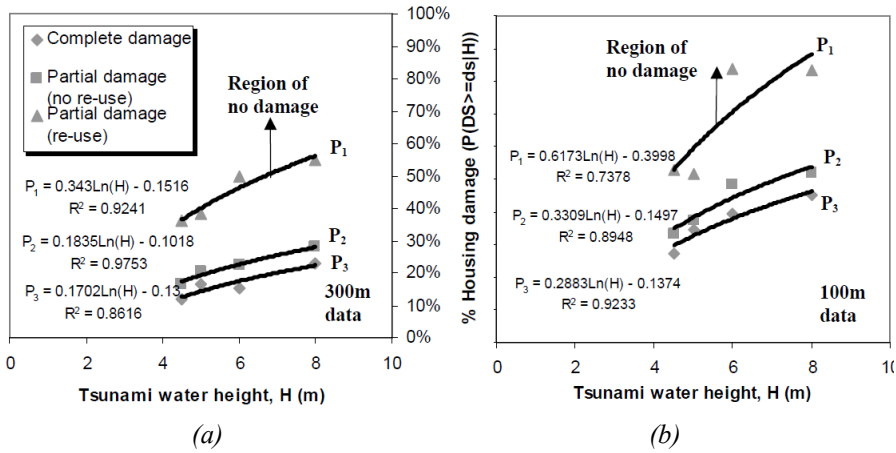


Figure 2.17: Fragility curves for masonry structures at a distance of 300 metres or more from the coast (a) and at a distance of 100 metres or more from the coast (b) (Periris et al. 2005)

Suppasri et al. (2011) provide fragility curves based on a semi-empirical approach assuming building damages linked to tsunami wave parameters obtained through numerical analysis. Structural damages are based on post-tsunami surveys and satellite images in Thailand.

Three limit states are defined depending on building damages as shown in Table 2.2.

Damage state (DS)	DS description
Limit state 1	Structural collapse
Limit state 2	Damage to structural elements (beams, columns and foundations)
Limit state 3	Damage to non-structural elements of vertical and horizontal closure

Table 2.2: Damage state definition (Suppasri et al. 2011)

Unfortunately, fragility curves are referred only to RC buildings as shown in Figure 2.18.

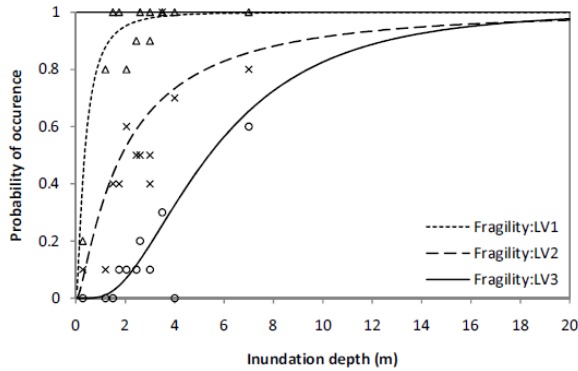


Figure 2.18: Fragility curves for RC buildings (Suppasri et al. 2011)

2.3.2. “The 2009 South Pacific Tsunami”

Reese et al. (2011) provide empirical fragility curves related to 2009 South Pacific tsunami based on damage database realized by a New Zealand team through post-event surveys considering about 200 buildings in 12 villages. The damage degrees are classified in six damage states as shown in Table 2.3.

Damage state (DS)		DS description
DS_0	None	None
DS_1	Light	Non-structural damage only
DS_2	Minor	Significant non-structural damage, minor structural damage
DS_3	Moderate	Significant structural and non-structural damage
DS_4	Severe	Irreparable structural damage, will require demolition
DS_5	Collapse	Complete structural collapse

Table 2.3: Damage state definition (Reese et al. 2011)

Reese et al. aims to clarify and analyse structures behaviour under tsunami loads depending on several parameters, i.e., the presence of elements that can act as a shield to the structure, impact of debris and buildings structural material.

Fragility curves for masonry buildings are shown Figure 2.19 and Figure 2.20.

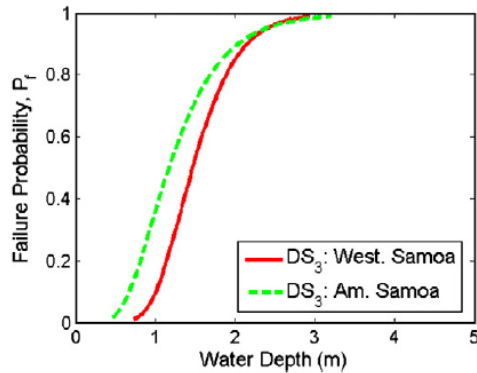


Figure 2.19: Fragility curves related to DS3 for American Samoa and Samoa buildings (Reese et al. 2011)

Figure 2.19 shows a similar structural behaviour of masonry buildings in two different areas due to similar construction and design techniques probably adopted, any difference could be related to topography effects, impact of debris or other variables that are complicated to take into account.

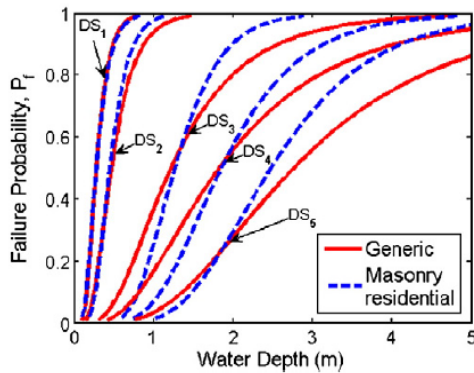


Figure 2.20: Fragility curves for masonry buildings (Reese et al. 2011)

Vegetation and obstructions can lead to a reduction of inundation depth, vertical velocity and debris that impact the structures.

Figure 2.21 shows the influence of shielded and unshielded buildings for residential masonry buildings related to DS_3 – DS_5 while DS_1 – DS_2 are neglected because the number of samples available was small and statistically significant conclusions could not be drawn. Shielded surveyed buildings are identified with a green line while unshielded buildings with a blue line.

As expected, the damage state probability of exceedance is less for a shielded structure than for a non-shielded structure for all analysed damage states depending on inundation depth.

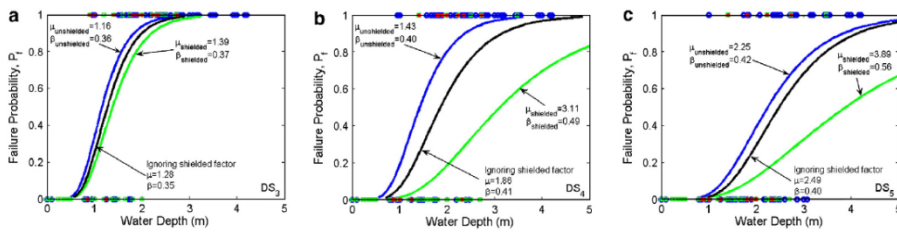


Figure 2.21: Effect of shielding on building fragilities: DS_3 (a), DS_4 (b) and DS_5 (c) (Reese et al. 2011)

Fragility curves for residential masonry buildings are provided depending on debris impact for limit states DS_3 and DS_4 (Figure 2.22). The remaining limit states are neglected due to lack of data. The results show a significant influence of the debris impact in risk assessment of residential buildings under tsunami loads.

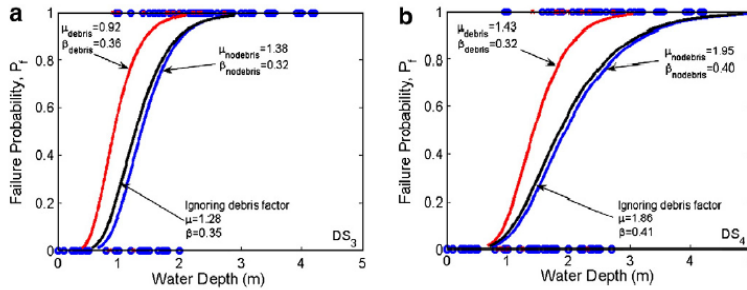


Figure 2.22: Effect of debris impact on building fragilities: DS_3 (a) and DS_4 (b) (Reese et al. 2011)

In addition, fragility curves are provided depending on buildings structural materials based on masonry, RC and timber residential buildings; it is important to note that masonry buildings data are greater than other buildings structural material data. Furthermore, in this case, only limit states DS_3 , DS_4 and DS_5 were analysed due to the lack of data.

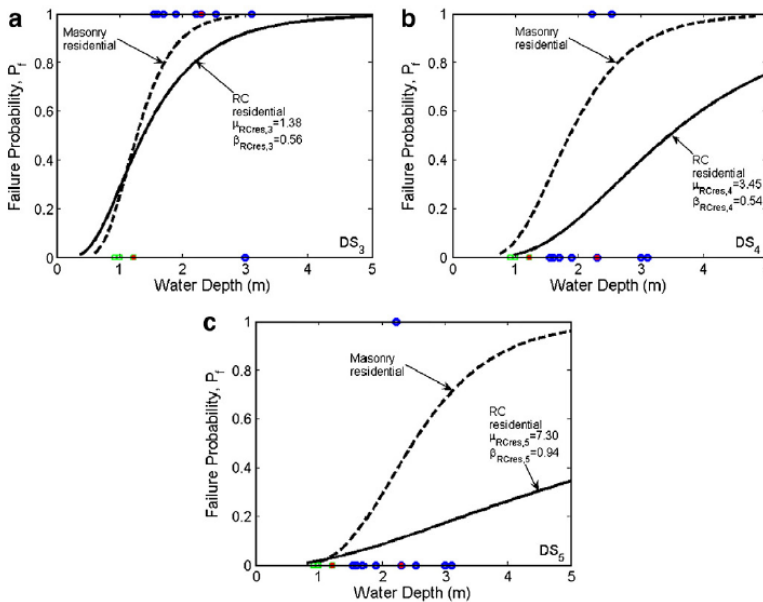


Figure 2.23: Fragility curves for masonry and RC residential buildings (Reese et al. 2011)

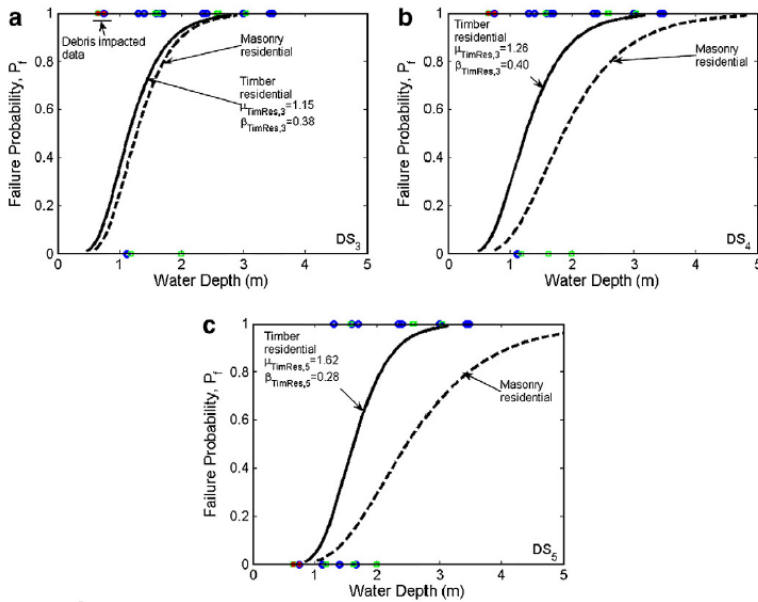


Figure 2.24: Fragility curves for masonry and timber residential buildings (Reese et al. 2011)

The results show a higher vulnerability of timber buildings under tsunami loads than other buildings structural material while RC structures show the best structural behaviour. In particular, the difference is high for limit states DS_4 and DS_5 while for DS_3 the differences are less obvious.

2.3.3. “The 2011 Great East Japan Tsunami”

Suppasri et al. (2013) propose empirical fragility curves related to 2011 Japan tsunami. The fragility curves were realized based on "Ministry of Land, Infrastructure and Transportation of Japan" database containing post-tsunami event surveys on more than 250'000 structures and damage levels are classified depending on buildings structural material, number of storeys and geographical location. The

inundation depth on each structure was obtained through surveys, high-resolution satellite images and multimedia material (photos and videos).

Six different damage states are defined depending on the recorded damages as shown in Table 2.4 and therefore, probability of exceedance of a specific damage level can be plotted depending on the inundation depth.

Damage level	Classification	Description	Condition
1	Minor damage	There is no significant structural or nonstructural damage, possibly only minor flooding	Possible to be use immediately after minor floor and wall clean up
2	Moderate damage	Slight damages to non-structural components	Possible to be use after moderate repair
3	Major damage	Heavy damages to some walls but no damages in columns	Possible to be use after major repairs
4	Complete damage	Heavy damages to several walls and some columns	Possible to be use after a complete repair and retrofitting
5	Collapsed	Destructive damage to walls (more than half of wall density) and several columns (bend or destroyed)	Loss of functionality (system collapse). Non-repairable or great cost for retrofitting
6	Washed away	Washed away, only foundation remained, total overturned	Non-repairable, requires total reconstruction

Table 2.4: Damage state definition (Suppasri et al. 2013)

Fragility curves are provided depending on buildings structural material considering RC, steel, wood and masonry residential buildings (Figure 2.25).

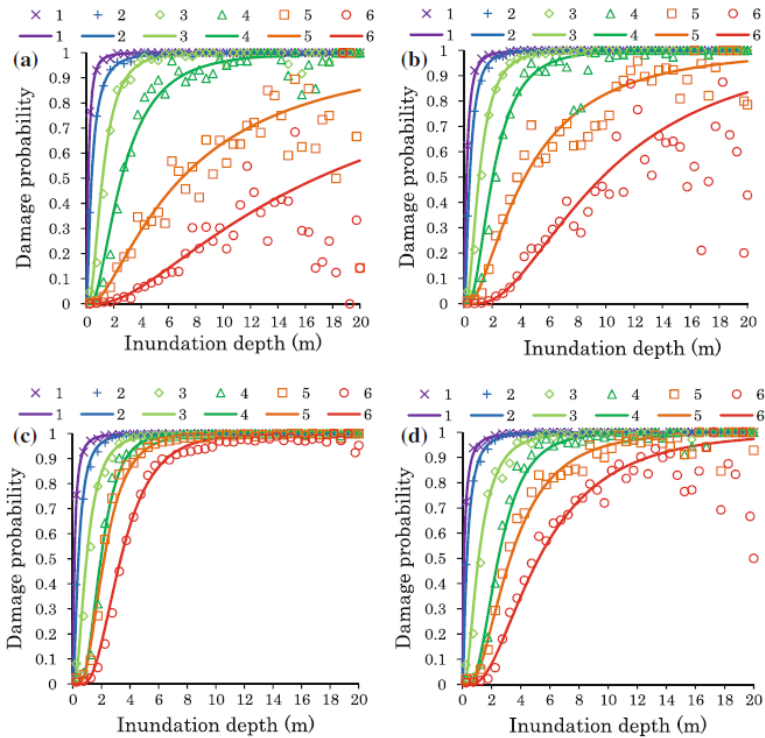


Figure 2.25: Fragility curves for different buildings structural material:
 RC (a), steel (b), wood (c) and masonry (d) residential buildings
 (Suppasri et al. 2013)

RC and steel structures exhibit the best structural behaviour under tsunami loads while wood and masonry buildings show a high vulnerability. Furthermore, for moderate limit states, the buildings structural material influence is not marked while for high limit state construction materials have a high impact on structural behaviour.

In addition, the fragility curves are realized depending on number of storeys and buildings structural material (RC and wood residential buildings) as show in Figure 2.26.

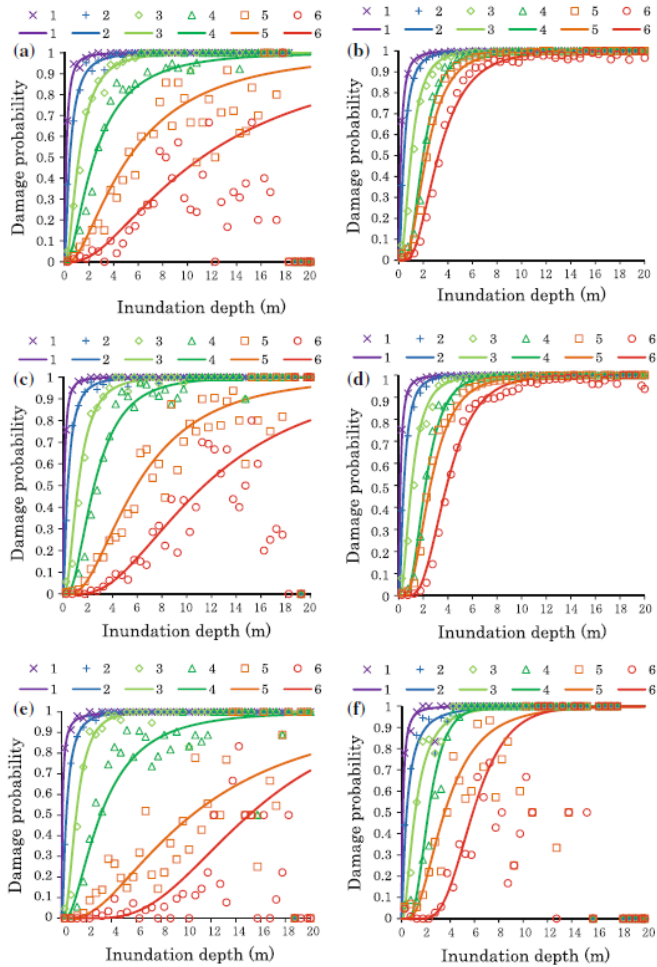


Figure 2.26: Fragility curves for different buildings structural material and number of storeys: RC single storey (a), wood single storey (b), RC two storeys (c), wood two storeys (d), RC three or more storeys (e) and wood (three or more storeys) (f) residential buildings (Suppasri et al. 2013)

It is interesting to note how the number of storeys has a huge influence on buildings behaviour under the same inundation depth and in particular, tall structures show a better response than buildings with one or two storeys due to columns and wall design and high gravitational loads acting in load bearing elements.

In addition, for high damage level the scattered data level is greater than low damage level due to the high degree of uncertainties that cause structural elements damages and building collapse. In addition, damages for low damage states are less scattered because the structural response is affected by local features of the structures, independently on many others. Damages in higher damage states (like those involving partial or total collapses) are more scattered because the global response is affected by many parameters as number of storeys, structural features, materials quality and design criterions. Consequentially, high damages data are more scattered than low damages as shown in Figure 2.26.

Suppasri et al. (2013) also provide fragility curves in order to investigate the effects of two different coastal topographies on building damage assuming the same data provided by *MLIT* (2012) along the region from Miyako in Sanriku area to Minami Soma in Fukushima.

Figure 2.27 and Figure 2.28 show the possible range of damage probability for each type of material for damage states DS_5 and DS_6 . Other damage states are not taken into account due to lack of data and because the damage probabilities of exceedance are not greatly affected by structural materials compared to high damage states.

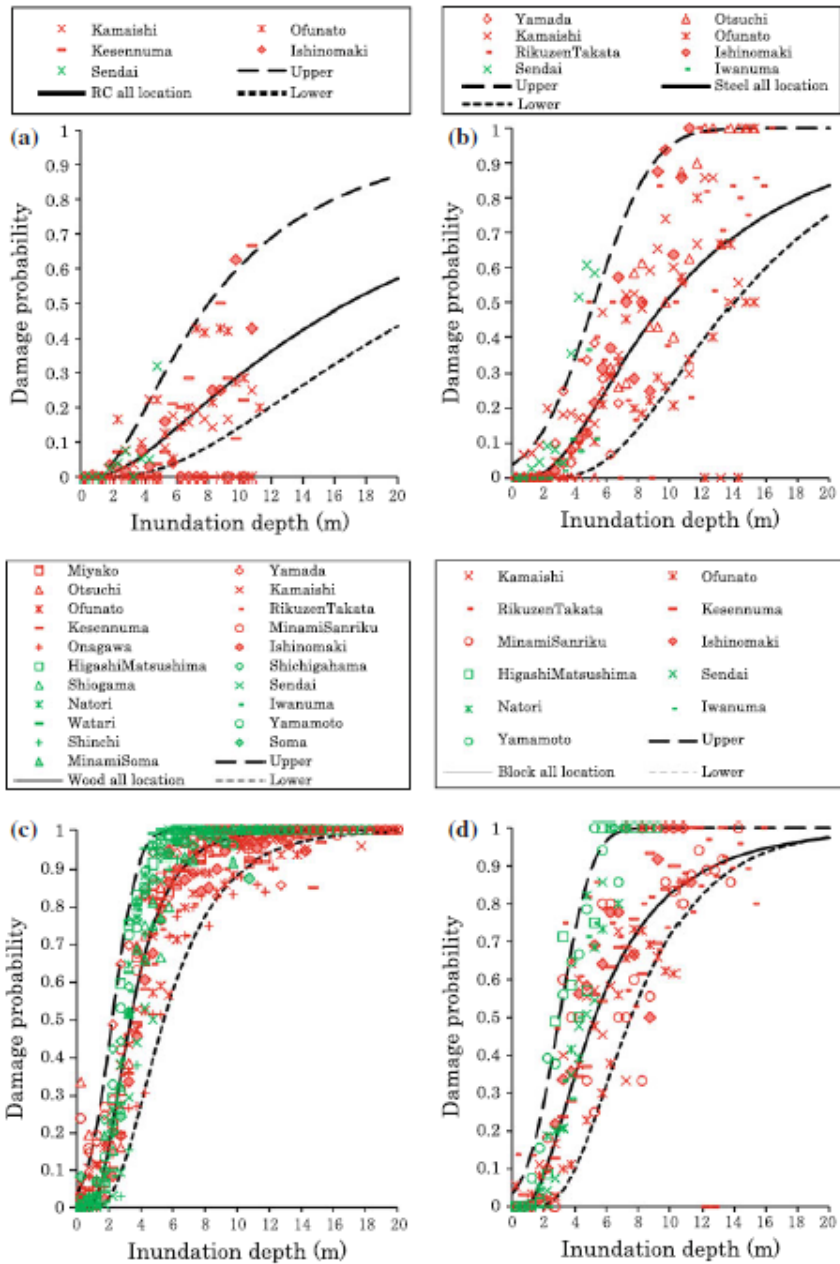


Figure 2.27: Fragility curves for different buildings structural material: RC (a), steel (b), wood (c) and masonry (d) residential buildings (Suppasri et al. 2013)

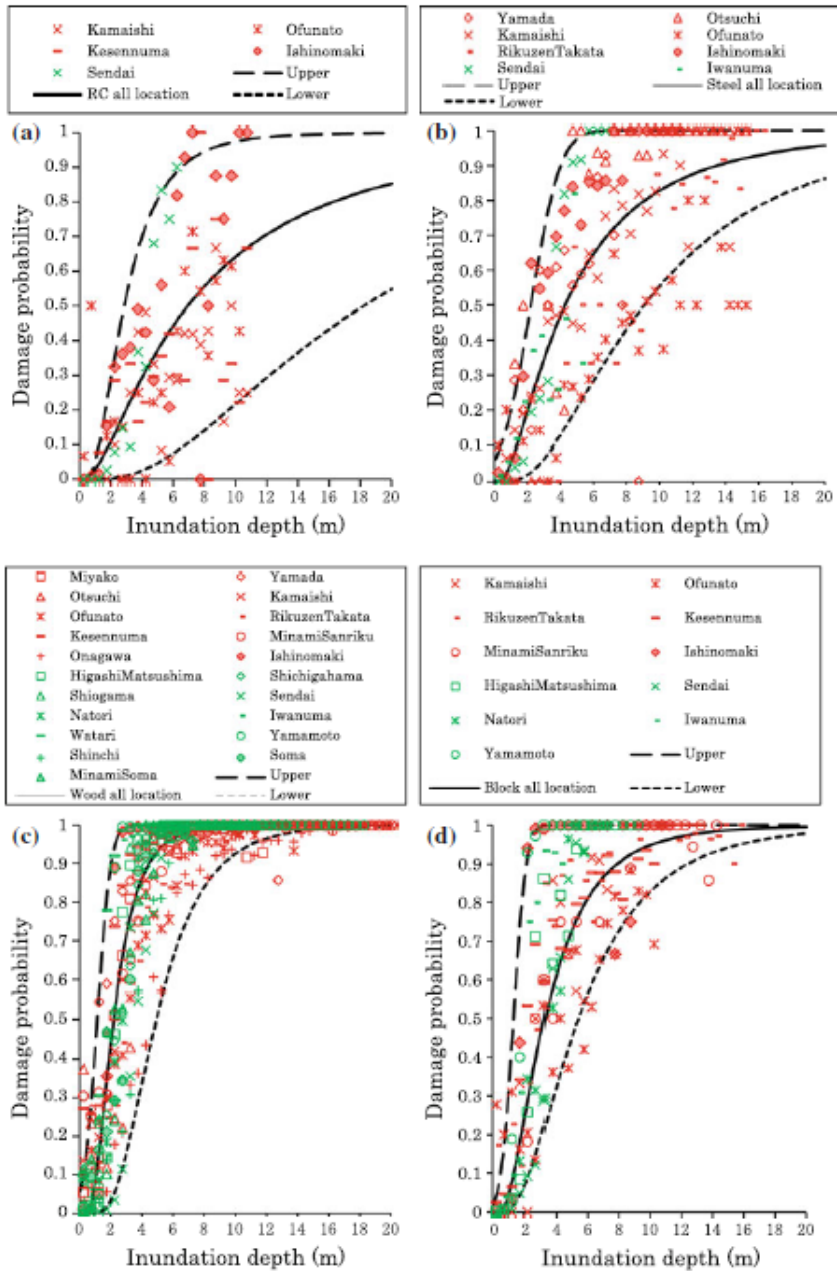


Figure 2.28: Fragility curves for different buildings structural material: RC (a), steel (b), wood (c) and masonry (d) residential buildings (Suppasri et al. 2013)

Coastal topography has a significant influence on building damages. At the same tsunami inundation depth, buildings along the Sanriku ria coast suffered greater damage than buildings from the plain coast in Sendai due to higher flow velocity along the ria coast.

2.3.4. Comparison and discussion

A preliminary analysis focuses on the comparison between principal empirical fragility curves available in international literature in order to clarify the structural behaviour of coastal buildings under tsunami loads depending on buildings structural material.

The buildings behaviour is strongly dependent on the construction techniques and the design codes in the analysed area. For example, in Japan, *MLIT* database shows a high concentration of timber buildings that are a typical Japanese construction in coastal areas while a high number of masonry buildings are built in Indian and Pacific Oceans coasts characterized by a low construction quality.

Furthermore, it is necessary to emphasize that empirical fragility curves are influenced by several parameters depending on the specific tsunami event analysed as construction techniques, buildings structural material, design codes, topography of inundated areas, bathymetry near the coast, debris characteristics (i.e. containers near a harbour) and presence of natural (trees) or artificial (seawalls) dissipative structures.

It is important to note that natural and artificial elements as trees and buildings could assume the meaning of shelters for buildings and could dissipate wave force.

Therefore, empirical fragility curves are based mainly on post event surveys and the results are strictly related to local buildings typologies. In addition, cumulative empirical fragility curves for a specific structural material do not take into account structural characteristics (i.e.

number of storeys), the distance of building from the coast and direction of water flow, etc.

Fragility curves provide the probability of exceedance a specific damage state (*DS*) as a function of inundation depth only and other parameters are not taken into account as vertical velocity or maximum momentum flux per unit mass per unit width. This choice is justified by the simplicity to retrieve inundation depths on buildings after a tsunami event through surveys.

It is interesting to note how the number of storeys influence the structural behaviour of buildings under tsunami loads, in particular structures with three or more storeys show a better behaviour than buildings with one or two storeys (Suppasri et al. 2013).

Furthermore, comparison between empirical fragility curves has been realized in order to clarify the structural behaviour of buildings under tsunami loads and to quantify the influence of regional characteristics on fragility curves. Some limitations have been found comparing fragility curves in the literature because each research team defines its own damage states. For example, Peiris et al. (2005) provide fragility curves strictly dependent on the distance of buildings from coastline and they are not available any other studies with these characteristics.

Therefore, comparison between fragility curves of masonry and RC buildings are performed regarding Suppasri et al. (2013) studies (Figure 2.29) in order to clarify the building structural materials influence on structural behaviour in case of tsunami event.

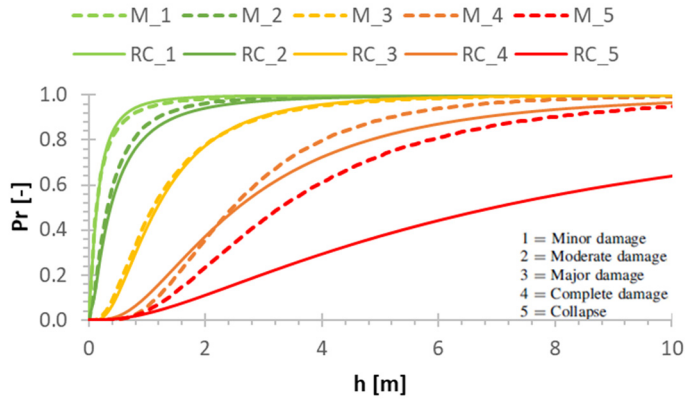


Figure 2.29: Comparison between fragility curves of masonry and RC buildings related to 2001 Great East Japan tsunami

Comparison shows that buildings structural material influence is negligible for low damage levels to structural and non-structural elements ($DS_1 - DS_3$). While a huge influence is exhibited for high damage levels regarding structural elements and the collapse of the entire structure ($DS_4 - DS_5$); in particular, RC buildings show a better response than masonry structures.

In addition, comparisons between fragility curves are performed based on different tsunami events regarding *The 2011 Great East Japan Tsunami*, *The 2004 Indian Ocean tsunami* and *The 2009 South Pacific Tsunami*. The results are shown in Figure 2.30 and Figure 2.31 for masonry and RC buildings respectively.

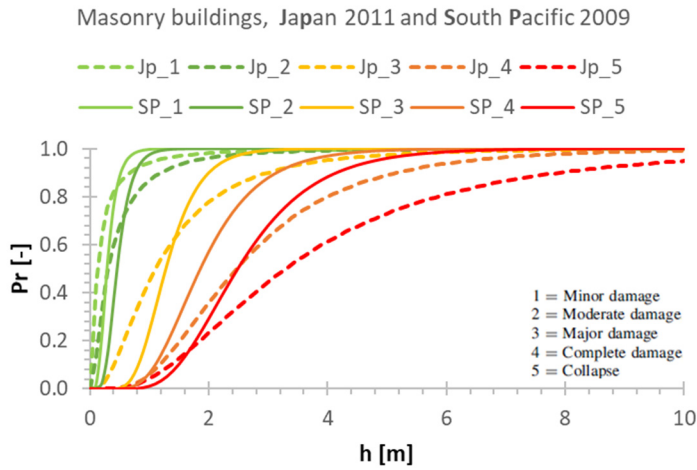


Figure 2.30: Comparison between fragility curves for masonry buildings based on The 2011 Great East Japan Tsunami and The 2009 South Pacific Tsunami

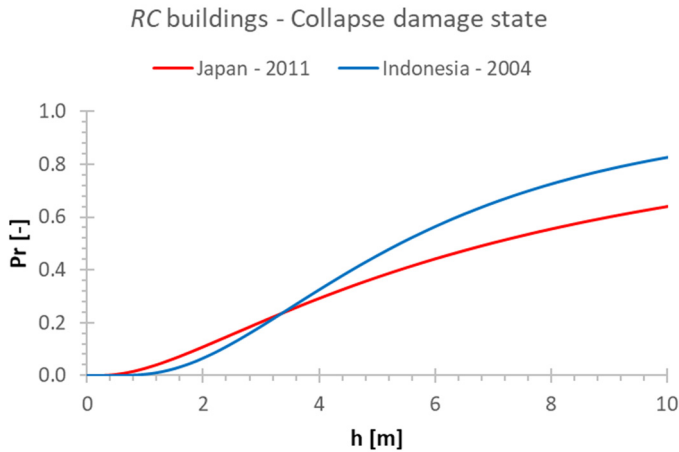


Figure 2.31: Comparison between fragility curves for RC buildings related to the 2011 Great East Japan Tsunami and the 2004 Indian Ocean Tsunami

Each comparison shows an appreciable match for low damage levels to structural and to non-structural elements while remarkable differences are recorded for high damage states regarding structural elements and collapse of structures. These differences are related to the

fact that empirical fragility curves are strictly related to local buildings type and regional characteristics in terms of structural material quality, design codes, debris type, terrain topography and coastal bathymetry.

Generally, Japanese buildings, as expected, show the best structural behaviour under tsunami loads compared with Sumatra and Samoa structures.

It is reasonable to assume that Italian coastal masonry residential buildings could show a better structural behaviour than Sumatra and Samoa structures due to best construction techniques and stone quality.

Chapter 3

Basis of fragility evaluation

In Chapter 3, the structural behaviour of coastal residential masonry buildings under tsunami loads is analysed and mechanical fragility curves are provided in order to realize damage scenarios in terms of number of damaged buildings, reconstruction costs and potential casualties. Furthermore, several building classes are defined to assess the influence of the structural evolution in terms of material quality and design code on building behaviour under (seismic and) tsunami loads.

Fragility curves are strongly influenced by buildings structural material, structural design, construction techniques and altimetric trend as shown in main empirical fragility curves (Reese et al. 2011, Suppasri et al. 2013) based on post-tsunami event surveys available in international scientific literature. Therefore, empirical fragility curves cannot be used to describe the structural behaviour of Italian buildings and specific mechanical fragility curves shall be defined to simulate the structural behaviour of typical Italian coastal masonry buildings in case of tsunami event.

3.1. Masonry building behaviour under tsunami loads

Masonry buildings behaviour under tsunami loads is influenced by local structural elements behaviour. The activation of in-plane and out-of-plane local mechanisms is taken into account instead of global mechanisms activation due to the complexity to study masonry

aggregates in large-scale analysis and the high material variability and inhomogeneity. In-plane mechanisms are analysed in elements with prevailing longitudinal length in the parallel direction to the tsunami flow while out-of-plane mechanisms activation is investigated in masonry walls with prevailing longitudinal length in the perpendicular direction to the tsunami wave.

After the building geometries definition, a "T" intersection between masonry walls of a generic building is analysed in order to clarify the in-plane mechanisms activation (Figure 3.1.a). Conversely, masonry walls behaviour between two transverse walls is examined (Figure 3.1.b) to assess out-of-plane mechanisms vulnerability of masonry walls under tsunami loads.

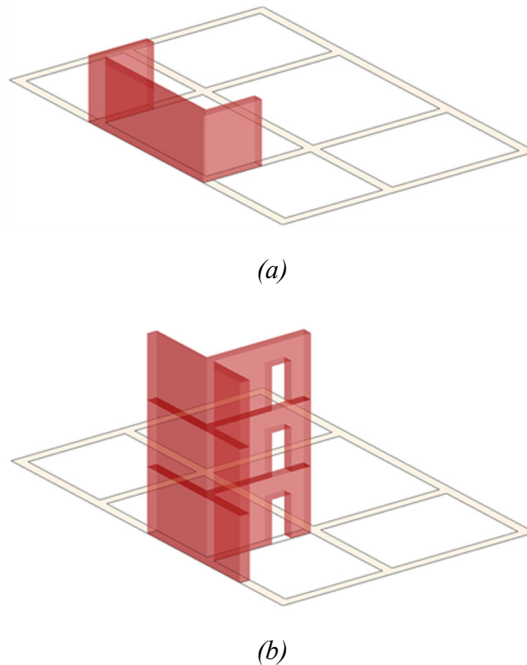


Figure 3.1: Masonry walls structural model adopted for in-plane (a) and out-of-plane (b) mechanisms analyses

Highest stresses in terms of bending moment and shear are localized at buildings ground floor (Figure 3.2) according to preliminary framed structures analysis, as expected for surface forces. Therefore, local mechanisms activation analyses are developed considering only masonry walls at ground floor due to higher stresses in terms of bending and shear stress.

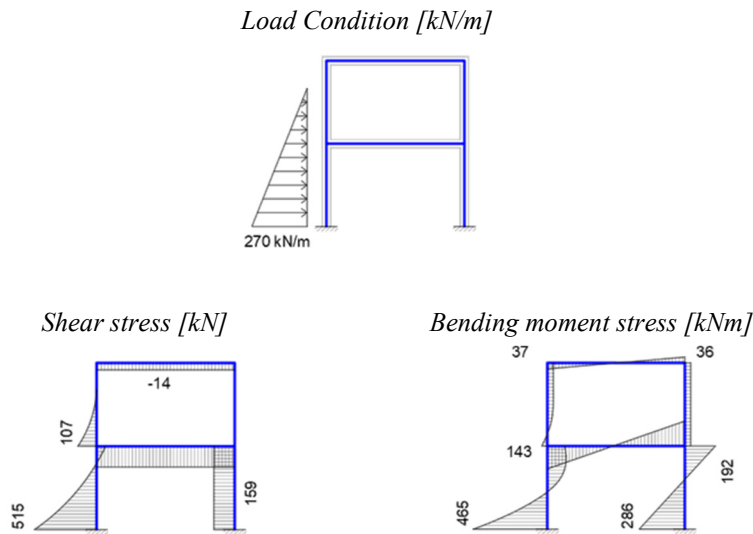


Figure 3.2: Stress distribution in a frame structure under triangular pressure distribution

3.2. Building classes definition

Several building classes are defined for Italian coastal residential masonry buildings in order to perform a large-scale analysis, to simulate buildings differences along Italian coasts and to assess the structural behaviour of masonry buildings under tsunami loads.

The building classes definition are based on the data provided by the *ISTAT* database in terms of material type (masonry or RC), number of storeys and age of construction. In particular, buildings with three or

more storeys show a better structural behaviour than structures with one or two storeys according to Suppasri et al. (2013). Tall structures are characterized by ground floor columns with larger geometrical size and consequently higher structural capacity than squat structure. Two different classes are assumed in order to consider the influence of the number of storeys:

- *Low buildings* with one or two storeys;
- *Medium-high buildings* with three or more storeys.

Another important aspect assumed to define building classes is related to the age of construction and in particular to the gradual improvement over time of construction techniques, buildings structural material and design codes. Furthermore, the historical evolution of seismic areas in Italy (Figure 3.3) plays an important role in the structural behaviour of buildings under tsunami loads as shown in the fragility curves results. The historical evolution of seismic area classification shows that in particular Sicily and Calabria areas have been classified as seismic prone since 1909 after the *Reggio Calabria and Messina earthquake* in 1908, while the coastal areas of central and northern Italy were classified as seismic prone only after 1981 due to the related earthquake the year before.



(a)



(b)

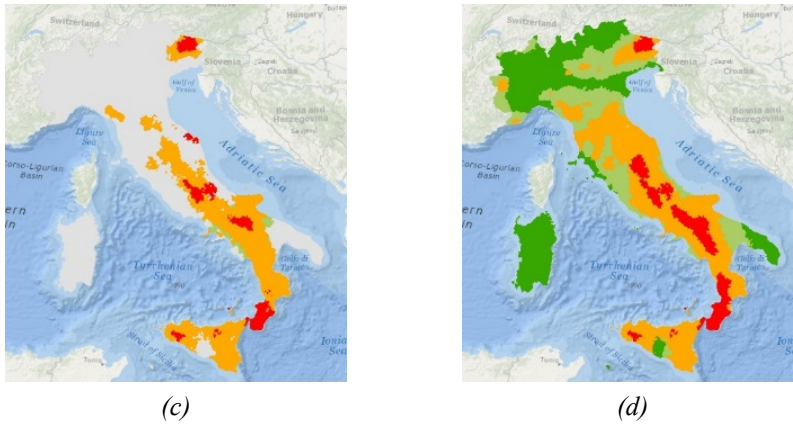


Figure 3.3: Evolution of the seismic areas in Italy:
 Decree-Law No. 193-1909 (a), Decree-Law No. 640-1935 (b),
 Ministerial Decree No. 9/10/1981 (c), O.P.C.M. No. 3274-2003 (d)

Twelve building classes are defined based on previously assumption in order to assess the vulnerability of masonry buildings under tsunami loads. Each building class allows to simulate material mechanical properties and typical buildings geometry of existing coastal masonry structures along Italian coasts with simple structural models.

Building classes are based on age of construction, number of storeys and design codes depending on *ISTAT* database updated every ten years. Therefore, four different ages of construction are defined based on the following assumptions:

- *AGE_0*: it considers all buildings built before 1919. In 1919 only a part of Calabria and some Sicilian cities were classified as seismic areas, therefore it is possible to assume that all buildings were designed only for gravitational loads as safe side criterion;
- *AGE_1*: it considers all residential masonry buildings built between 1920 and 1980. The seismic areas were defined depending on regions affected by earthquakes. Therefore, a large number of buildings is still designed only for gravitational loads

and a large part of the national territory is not classified as seismic area;

- *AGE_2*: it considers all residential masonry buildings built between 1980 and 2005. The national territory is divided into four seismic categories according to *O.P.C.M. 3274 (2003)*, where the fourth group is characterized by the lowest seismic risk. Therefore, it is still possible to separate buildings designed for gravitational or seismic loads;
- *AGE_3*: it considers all residential masonry buildings built from 2006 until today. The entire national territory is classified in seismic areas since the *O.P.C.M. 3274 (2003)*, therefore all buildings built in *AGE_3* are designed for seismic loads.

Masonry buildings designed for gravitational loads before the 1920s are not related to particular codes or guidelines. Main empirical design equations are retrieved for structural masonry walls by means of a bibliographic research in historical literature. Empirical equations allow to define wall thickness depending on structural geometric characteristics as number of storeys, length or height of building.

International studies in literature show a huge influence of the number of storeys on buildings behaviour under tsunami loads and therefore, building classes are divided into two sub-categories: low rise buildings (number of storeys less than or equal to two) and medium-high rise buildings (number of storeys equal to three or more). Furthermore, it was observed that the stock of masonry buildings with more than five floors is practically negligible compared to the remaining part of the building population as shown in Figure 3.4; therefore, an upper limit of five storeys is assumed for medium-high rise masonry buildings.

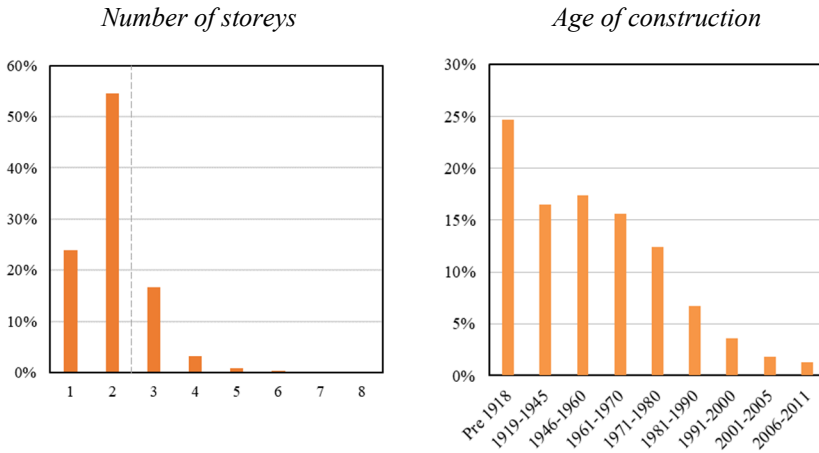


Figure 3.4: Masonry buildings distribution depending on number of floors (a) and age of construction (b) (ISTAT 2001 and ISTAT 2011 data)

The ratio of buildings built in *AGE_3* is negligible if compared with other construction ages (Figure 3.4.b) and it is assumed to merge *AGE_2* and *AGE_3* as safe side criterion.

In conclusion, ten building classes are considered to assess the vulnerability of masonry structures under tsunami loads as shown in the following figure with their respective acronyms (Figure 3.5).

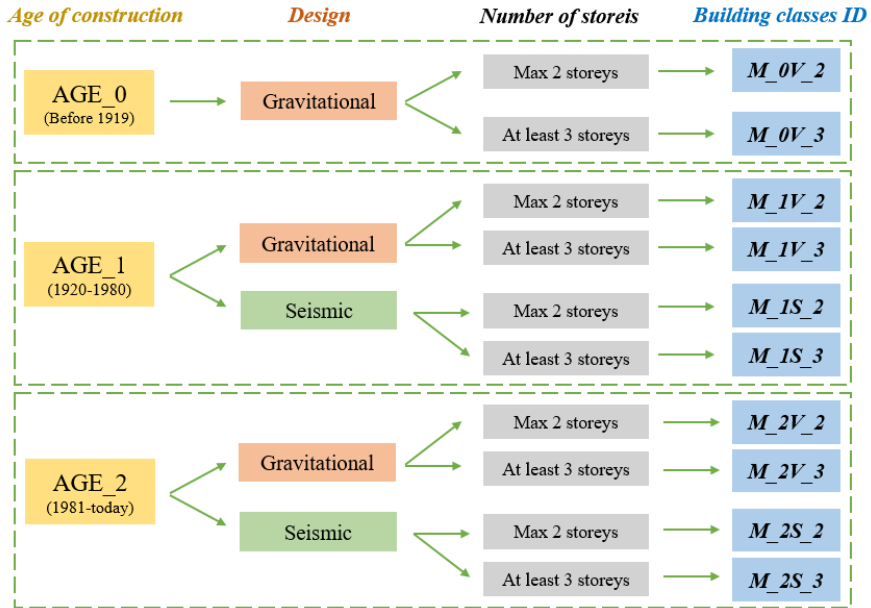


Figure 3.5: Building classes for masonry buildings and acronyms

3.3. Structural models generation

Large-scale vulnerability analysis required a population of typical buildings representative of the existing buildings according to the building classes introduced in the previous paragraph.

Monte Carlo simulation method was used to generate several structural models for each building class. A *Monte Carlo* simulation generates a finite number of random realizations of uncertain parameters based on their probability distributions. Each realization of uncertain parameters is used to generate a structural model and structural analyses are based on the building population provided by Monte Carlo simulation in order to assess the structural capacity depending on damage states.

Therefore, the *Monte Carlo* method simulation provided the population of buildings based on a set of random variables that represent the uncertain parameters in terms of load conditions, structural geometry and material mechanical parameters. A population of 1'000'000 buildings was generated for each building classes.

The main input parameters and their distribution are based on the *National Group for Earthquake Defence (GNDT)* database (Figure 3.6) in terms of geometrical properties of the building (inter-storey height), material mechanical properties (specific weight) and floor gravitational loads for generic floors and flat roofs. Normal probability distribution is defined with a mean and standard deviation for inter-storey height and slab gravitational loads for generic floors and flat roofs, while a constant value is defined for the materials specific weight. In addition, five different masonry types are defined: poor stone, tuff stone, hollow clay bricks, clay brick and full clay brick.

Parameter	Masonry substrates	μ	σ	Distribution	
γ_M [kN/m ³]	Poor stone	20.25	-	Constant	
	Tuff stone	19.25	-	Constant	
	Hollow clay brick	15.52	-	Constant	
	Clay brick	17.6	-	Constant	
	Full clay brick	14.32	-	Constant	
W [kN/m ²]	Flat roof W_e	Poor stone	2.64	1.4	Normal
		Tuff stone	2.92	1.33	Normal
		Hollow clay brick	3.02	3.45	Normal
		Clay brick	2.82	1.17	Normal
		Full clay brick	2.48	0.7	Normal
	Generic W_i	Poor stone	4.7	3.6	Normal
		Tuff stone	4.5	2.2	Normal
		Hollow clay brick	4.16	3.27	Normal
		Clay brick	4.07	2.21	Normal
		Full clay brick	3.75	1.29	Normal
h_p [m]	Poor stone	3.5	1.13	Normal	
	Tuff stone	3.5	1.1	Normal	
	Hollow clay brick	3.1	0.92	Normal	
	Clay brick	3.4	1.1	Normal	
	Full clay brick	3.22	1.11	Normal	

Figure 3.6: Monte Carlo simulation parameters based on the National Group for Earthquake Defence (GNDT) database

Furthermore, several parameters are taken into account by means of random values characterized by a constant distribution to simulate residential masonry buildings:

- *Number of storeys*: upper and lower bound depends on building classes;
- *Walls length*: based on building code limits or historical usual practices;
- *Compressive tensile strength σ_m* : based on building code limits according to *NTC 2008* and *NTC 2018* Italian building codes;
- *Wall modelling*: three different structural wall models are taken into account depending on building design approach for gravitational (type I or II) or seismic (type III) loads;
- *Wall opening ratio coefficient on external walls*: random values are assumed between 0% and 30% according to Japanese guidelines (Nakano et al. 2011) and *ASCE 7-16*;
- *Position coefficient of the opening on internal walls*: random values are assumed between zero and one.

The openings on the external and internal walls are assumed to be in the same position at each building storey as basic assumption.

A summary of the coefficient ranges are shown in Table 3.1 and Table 3.2.

Parameter	Design	Min [m]	Max [m]
Walls length	Gravitational	2.0	7.0
	Seismic	2.0	12.5
Position coefficient of the opening on internal walls	Gravitational	0.1 L	1.0 L
	Seismic	0.3 H_i	1.0 L

Table 3.1: Summary of the coefficient ranges depending on the design approach

Masonry substrates	Age of construction	Min [MPa]	Max [MPa]
Poor stone	AGE_0 and AGE_1	1.0	3.0
	AGE_2 and AGE_3	2.5	3.0
Tuff stone	AGE_0 and AGE_1	6.0	8.0
	AGE_2 and AGE_3	6.0	10.0
Hollow clay brick	AGE_0 and AGE_1	1.5	2.0
	AGE_2 and AGE_3	3.0	8.0
Clay brick	AGE_0 and AGE_1	3.0	8.0
	AGE_2 and AGE_3	4.0	10.0
Full clay brick	AGE_0 and AGE_1	3.0	4.4
	AGE_2 and AGE_3	5.0	10.0

Table 3.2: Summary of the compressive tensile strength ranges depending on the age of construction

The buildings distribution of a building class is represented in Table 3.3 and Table 3.4 where a generic column shows the building distribution depending on the masonry substrate for a specific building class. Tall buildings are not built of poor stone and a progressive increasing of the material quality usage is shown comparing gravitational and seismic building distribution.

Masonry substrates	M_0V_2	M_0V_3	M_1V_2	M_1V_3	M_2V_2	M_2V_3
Poor stone	40 %	0 %	30 %	0 %	0 %	0 %
Tuff stone	40 %	50 %	30 %	30 %	30 %	20 %
Hollow clay brick	10 %	10 %	20 %	20 %	10 %	10 %
Clay brick	10 %	40 %	20 %	50 %	50 %	50 %
Full clay brick	0 %	0 %	0 %	0 %	10 %	20 %

Table 3.3: Summary of the buildings distribution depending on the gravitational building class and the masonry substrates

Masonry substrates	M_1S_2	M_1S_3	M_2S_2	M_2S_3
Poor stone	0 %	0 %	0 %	0 %
Tuff stone	50 %	50 %	20 %	20 %
Hollow clay brick	0 %	0 %	20 %	20 %
Clay brick	50 %	50 %	40 %	40 %
Full clay brick	0 %	0 %	20 %	20 %

Table 3.4: Summary of the buildings distribution depending on the seismic building class and the masonry substrates

The study of the walls is usually conducted through a modelling in macro-elements that allows to simulate in-plane local mechanisms behaviour. The following structural component types can be identified in a masonry frame: *pier panels*, which provide load-carrying capacity to both gravitational and horizontal loads; *spandrel panels*, which distribute gravitational loads and provide coupling between adjoining piers under horizontal actions; and *joint panels*, which link pier and spandrel panels together (Augenti et al. 2010).

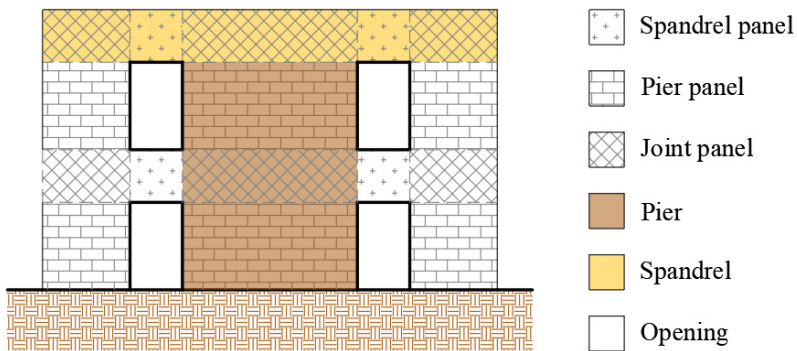


Figure 3.7: Macro elements in typical masonry frame

In particular, three different types of wall models can be found depending on the joint degree between walls:

- Wall model I: it is characterized by the absence of any horizontal connection between the walls and the masonry walls are modelled as isolated cantilevers. This is the common case of buildings without perimeter connection elements;

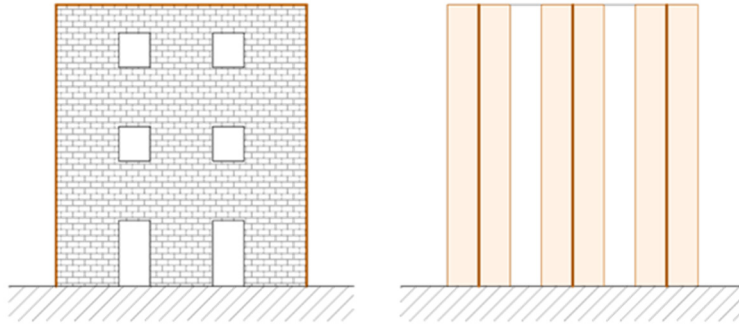


Figure 3.8: Wall model I

- Wall model II: the masonry walls are modelled as cantilever connected by trusses. Steel ties application in existing buildings allows to evolve wall model I into wall model II;

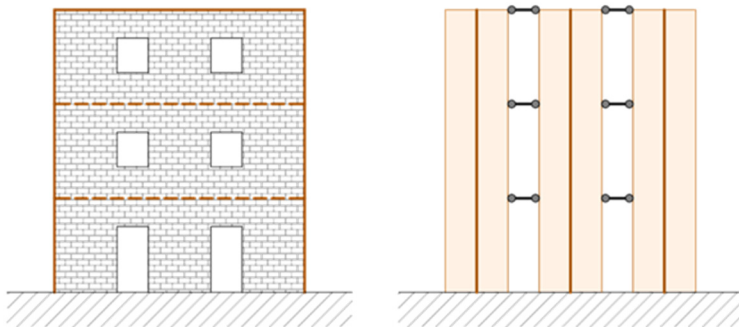


Figure 3.9: Wall model II

- Wall model III: it is the common case of shear type frame characterized by forbidden rotation at the end points of beams

and columns. This solution exhibits the best structural behaviour under horizontal forces and it is widely used in seismic analysis.

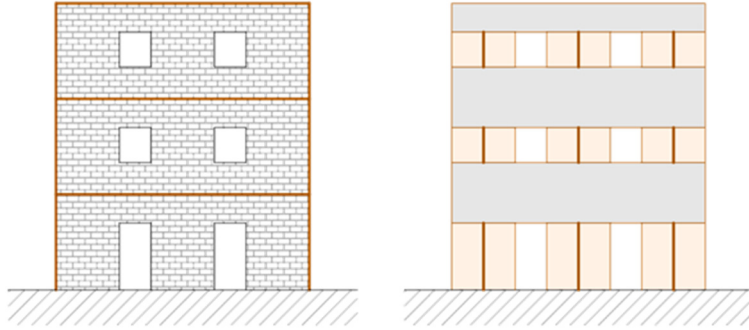


Figure 3.10: Wall model III

It is interesting to note that the second and third cases are related to statically indeterminate structures while the first wall model is an isostatic structure.

Wall model I and *wall model II* are generally assumed to model the structural behaviour of gravitational buildings, while *wall model III* is assumed to model seismic buildings. Structural analyses are performed depending on the wall models and the resultant stresses are compared to wall capacity (Augenti, 2004) in terms of bending moment and shear.

Therefore, an algorithm generates building models by means of several *Monte Carlo* simulations and it is completely developed in *Mathworks MATLAB* software. Each building model is based on different design criteria according to empirical design formula or design codes.

In particular, an accurate bibliographic research has been carried out in order to determine the main empirical formulations available in literature to design buildings under gravitational loads. The main studies were published between the 19th century and the first decades of the

twentieth century based on empirical observations and the main works were produced by: *Rondelet* (1812), *Curioni* (1870), *Breymann* (1884) and *Muller* (1920).

One of the first major works on wall thickness design of masonry buildings is provided by the French architect *Rondelet* in 1812, he proposed empirical equations to calculate masonry wall thickness based on empirical observation of about 280 existing Italian and French buildings. The design equation depends on the building height H and the wall length T :

- For external walls:

$$s = \frac{T + H}{48}$$

- For internal walls:

$$s = \frac{T + H}{36}$$

Curioni proposed an empirical equation in his book "*Raccolta di progetti di costruzioni in terra*" published in 1870, in Italian, where the wall thickness depends on the number of storeys n .

- For perimetric walls: $s = 0.45 + 0.12 n$
- For transverse walls: $s = 0.45 + 0.06 n$

In 1884, *Breymann* published a book series about design of civil constructions. The first volume was entirely dedicated to masonry constructions and it inspired several designers. Wall thickness design equation was dependent on the number of storeys n :

$$s_n = 0,025 \cdot t + 0,040 \cdot \sum_{i=1}^n h_i$$

Where t is the building height and h_i the inter-storey height as shown in Figure 3.11.

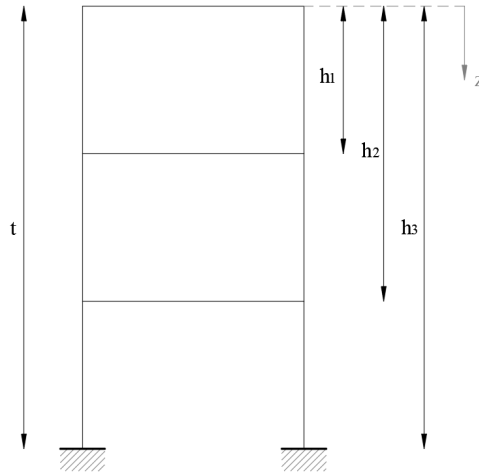


Figure 3.11: Structural parameters required to evaluate the wall thickness of a generic floor n according to Breyman equation

In 1920, *Milani* published "*L'Ossatura murale*" book containing design equations provided by various authors as *Rondelet*; in particular *Redtenbacher* and *Muller* proposed a wall thickness design equation depending on the building height H and the wall length T :

$$s = (T/40) + (H/25)$$

$$s = (T/40) + (H/36)$$

In the same book, a table for the minimum wall thickness was also reported depending on masonry materials quality (brick and stone wall); furthermore, bricks and stones are characterized respectively by minimum wall thickness of 30÷45 centimetres and a maximum of 100÷110 centimetres.

At the same time, *Marullier* (1914) proposed the "*Guida pratica per la costruzione degli edifici*" book including the design equations

proposed by *Rondelet* and it provided external and internal wall thicknesses of residential masonry buildings depending on the number of storeys (Table 3.5).

Storey	Brick wall		Stone wall	
	External	Internal	External	Internal
<i>P.5°</i>	0.40	0.40	0.55	0.45
<i>P.4°</i>	0.50	0.40	0.55	0.50
<i>P.3°</i>	0.60	0.50	0.65	0.55
<i>P.2°</i>	0.75	0.50	0.75	0.60
<i>P.1°</i>	0.90	0.65	0.90	0.65
<i>P.T.</i>	1.00	0.65	1.00	0.70

Table 3.5: Minimum wall thickness for masonry structures in metres proposed by *Marullier*

Historical and current Italian building codes provide simplified design approaches for simple masonry buildings where inter-storey height is less than 3.5 meters, maximum number of storeys is equal to three, maximum value of wall slenderness is equal to twelve and the following inequality is proposed based on elastic approach.

$$\sigma = \frac{N}{A} \leq 0.65 \frac{f_k}{\gamma_M}$$

Where N is the vertical load evaluated as the sum of the permanent and variable loads, A is the wall cross section area, f_k is the masonry characteristic compressive strength and γ_m is a load factor.

The conventional slenderness of masonry wall is defined as the ratio h_o/t where:

- h_o is the free inflection length of the wall equal to $\rho \cdot h$, where h is wall height and ρ is a constraint coefficient (Table 3.6);
- t is the wall thickness.

The ρ coefficient assumes the following values depending on a coefficient that represents the distance between the two consecutive transverse walls:

$\frac{h}{a}$	ρ
$\frac{h}{a} \leq 0.5$	1
$0.5 < \frac{h}{a} \leq 1$	$\frac{3}{2} - \frac{h}{a}$
$\frac{h}{a} > 1$	$\frac{1}{1 + \frac{h}{a} q}$

Table 3.6: ρ parameter depending on the ratio h/a according to NTC 2008

The simulated design of seismic buildings follows the evolution of the main seismic codes issued over the years and, in particular, the main historical building codes and guidelines in Italy are: *Circular Ministry of Public Works no. 21745* of 30/07/1981, the *Ministerial Decree* of 20/11/1987, the *O.P.C.M. no. 3274* of 20/03/2003 and the *New technical standards for construction* (NTC08) of 14/01/2008. Each building code and guidelines provide useful design criteria and approaches for masonry buildings regarding gravitational or seismic loads. The above building codes contain information about minimum wall thickness for seismic or not-seismic structures, material quality in terms of mechanical proprieties, number of storeys limitations for buildings in seismic areas and simplified design criteria.

Furthermore, the Italian building codes provide a simplified design approach for simple masonry buildings assuming a maximum length of load-bearing walls of 7 metres, a maximum number of storeys equal to three and the following inequality based on elastic approach.

$$\sigma = \frac{N}{A} \leq 0.25 \frac{f_k}{\gamma_M}$$

Where N is the vertical load evaluated as the sum of the permanent and variable loads, A is the wall area, f_k is the masonry characteristic compressive strength and γ_m is a load factor.

Therefore, structural analyses are performed based on building models generated by several Monte Carlo analyses for each building class depending on empirical design equations or historical codes and guidelines. In addition, local mechanisms activation are analysed comparing masonry walls capacity and external stresses provided by structural analysis in terms of bending and shear stresses for each masonry wall.

At the end, fragility curves are based on critical inundation depth that activates local mechanisms on masonry walls.

3.4. Structural analysis

The first step in assessing the capacity of existing structures under tsunami loads is to define tsunami loads model. International codes provide design approaches only for new buildings and there are not information about assessing structural capacity of existing buildings. Main building codes model tsunami loads on structures in several load components as hydrostatic loads, hydrodynamic loads, debris impact and impulsive loads. However, these models require high knowledge level and refined inundation simulation.

Structural analyses are performed assuming the tsunami loads model proposed by the Japanese guidelines due to adopted low knowledge level and large-scale approach. The method allows to model

tsunami loads by means of one equivalent hydrostatic load (Figure 3.12.a) where the expected inundation depth is increased by an inundation depth coefficient η in order to take into account indirectly both hydrostatic and hydrodynamic loads. The tsunami load evaluated using the Japanese model is a pressure per surface unit area and it depends on exposed surface to waves (Figure 3.12.b). The η coefficient has a huge impact on load intensity and consequentially on structural capacity and it is characterized by a minimum value of 1.5 and a maximum value of 3 depending on the presence of wave dissipative elements and the distance of structure from the coastline. Generically it is reasonable to assume the maximum value of 3 near Italian coastline due to the absence of specific dissipative elements. In addition, parametric analyses are performed considering different η values between its minimum and maximum value in order to obtain results comparable with empirical fragility curves that generally do not take into account the distance of the buildings from the coastline and shelter effects.

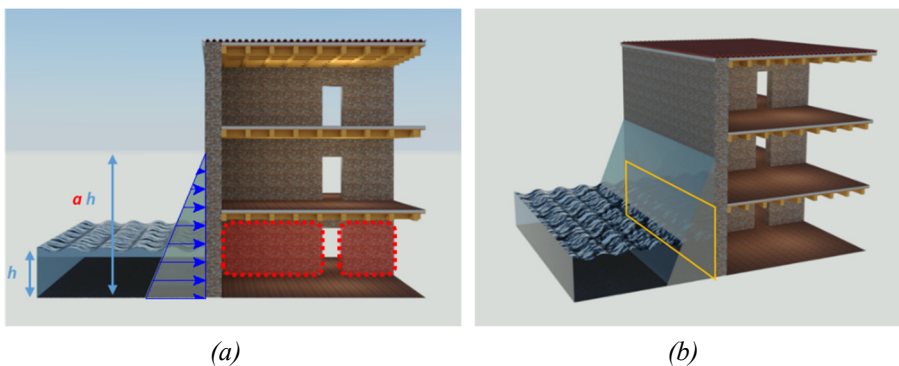


Figure 3.12: Tsunami load model according to Japanese guideline (a) and exposed surface to wave flow (b)

The vulnerability assessment of residential masonry buildings has been performed assuming a mechanical approach; the structural

analyses are based on local collapse mechanisms activation coherently with low knowledge level and large scale approach adopted in this study. In particular, it is simple to extrapolate a masonry wall panel from a generic masonry building and parametric analyses are performed for out-of-plane mechanisms (Pantò et al., 2017) due to the partial independent behaviour from the entire structure. On the opposite, a generic "T" intersection between masonry walls of a building is analysed involving the full height of the building in order to assess the in-plane mechanisms activation (Ismail et al., 2016); in fact the high in-plane stiffness of masonry walls has a crucial impact on stress distribution, hence the entire plane frame is analysed.

Linear analyses are performed assuming simplified mechanical models coherently with large scale approach adopted and in force control due to the assumed model for external loads. In particular, an equivalent hydrostatic load characterized by a triangular pressure distribution is applied to the masonry wall and wave inundation depth h is increased keeping the load slope constant (Figure 3.13) until local mechanism activation is reached.

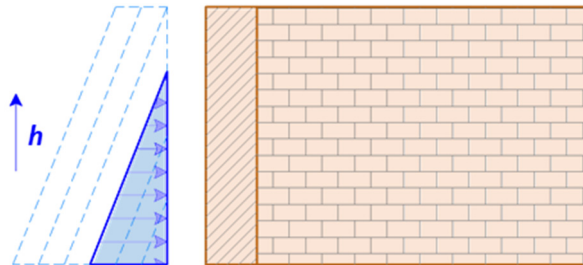


Figure 3.13: Local mechanisms activation model

A wall opening ratio coefficient α is taken into account because tsunami loads are surface forces and their intensities are strongly dependent on the wall influence area. Wall without opening retrieves

high tsunami loads and it is not reasonable; opening ratio is assumed between 0.0 and 0.3 according to *ASCE 7-16* and Japanese guidelines.

The analyses assumptions are the same of seismic analyses:

- Linear elastic distribution of normal stresses on the cross section;
- Constant plastic distribution of normal stresses on the cross section;
- Instability events are negligible;
- Tensile strength of masonry is negligible.

The behaviour of masonry walls under tsunami loads is not obvious in terms of local mechanisms activation because tsunami forces are superficial forces that depend on the exposed surface of the structure to the tsunami waves. It is important to observe that seismic forces are inertia forces depending on the mass of the structure. Consequently, the behaviour of structures under tsunami loads is not comparable to seismic behaviour.

Therefore, in-plane and out-of-plane local mechanisms are analysed based on seismic theory but different load conditions are assumed as triangular or trapezoidal load patterns. In fact, two different pressure distributions are obtained depending on the relationship between the masonry wall height H_i and design inundation depth h_{max} (Figure 3.14):

- *Triangular pressure distribution*: when the design inundation depth is less than or equal to the masonry wall height;

$$\frac{H_i}{h_{max}} > 1$$

- *Trapezoidal pressure distribution*: when the design inundation depth is greater than the masonry wall height.

$$\frac{H_i}{h_{max}} \leq 1$$

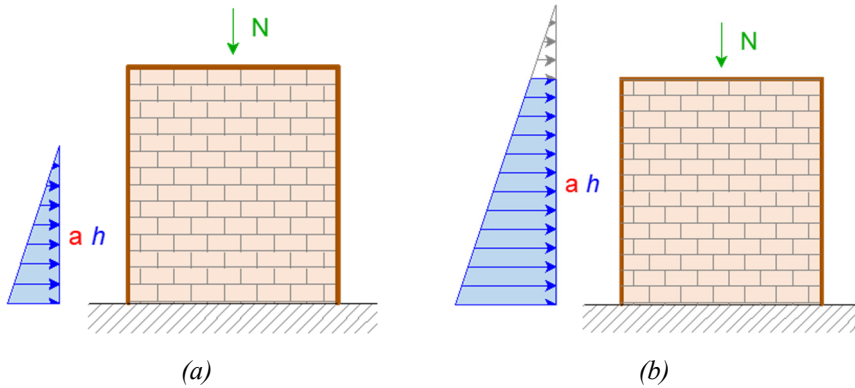


Figure 3.14: Masonry wall analysis: triangular (a) or trapezoidal (b) pressure distribution

Different types of interlocking among walls are neglected and in-plane and out-of-plane mechanisms are analysed for each building model.

3.4.1. In-plane mechanisms

In-plane mechanisms activation involves different flexural and shear failure modes. The probability of occurrence of different failure modes depends on several geometrical and structural parameters:

- Geometry of the structural elements: block aspect ratio and characteristics of cross section;
- Load pattern: vertical and horizontal load;
- Boundary conditions;
- Mechanical characteristic of masonry constituents regarding: mortar, blocks and interface.

The following failure modes are analysed:

- Flexural failure: it is characterized by corner crushing as shown in Figure 3.15 with tensile and compressive crack;

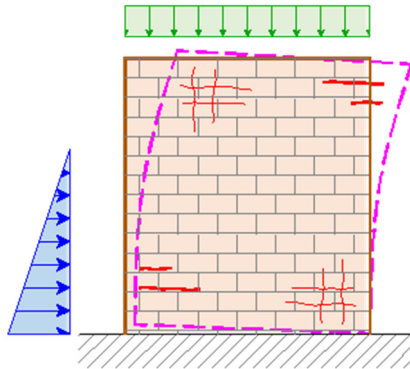


Figure 3.15: Flexural failure

- Sliding shear failure: the failure mode is attained with sliding on a horizontal joint plane. It is characterized by the formation of horizontal cracks (Figure 3.16). This mechanism is favoured by low friction coefficient values and low wall compression levels;

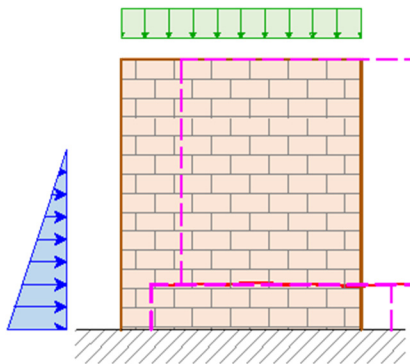


Figure 3.16: Sliding shear failure

- Diagonal shear failure: the failure mode is governed by critical diagonal crack formation (Figure 3.17).

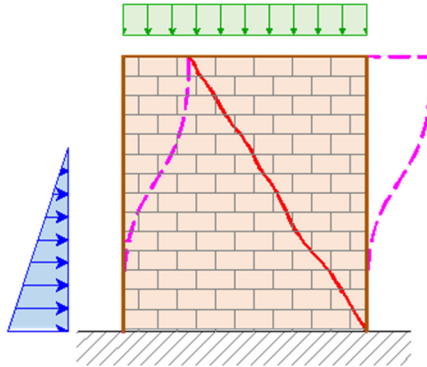


Figure 3.17: Diagonal shear failure

In-plane mechanisms activation is strongly dependent on geometrical characteristic and in particular on the L/b slenderness ratio of masonry wall. Flexural failure occurs in slender panels ($L/b > 1.5$) while shear failures occur in hollow panels ($L/b \leq 1$) due to low tensile shear capacity or sliding between mortar and stones.

Tsunami load resultant is variable during structural analyses and its application point depends on the inundation depth. For flexural failures, the point of application of tsunami load resultant is strictly necessary in order to define the most stressed cross section; seismic equations are not applicable due to linear bending moment diagram on masonry wall instead of the actual cubic function retrieved by triangular or trapezoidal tsunami pressure distribution. It is interesting to note that shear capacity is dependent only on wall geometrical and material mechanical parameters and it is independent on the inundation depth; this is the reason why seismic equations are still valid in case of the tsunami analysis.

The masonry wall extrapolated for in-plane local mechanisms analysis can be characterized by two cases: solid wall (total absence of openings) or walls with an opening length of 1 meter depending on *Monte Carlo* simulation results. The joint degree between walls is

3.4.1.1. *Wall model I*

The *wall model I* is a cantilever subjected to a triangular or trapezoidal load pattern (Figure 3.14), it is a statically determinate structural model and it is simple to retrieve maximum shear and bending moment stress in the fixed point by static equilibrium equation.

It is possible to provide closed form equation for critical inundation depth solving the equality between the external stress and cross section capacity for both triangular and trapezoidal pressure distributions.

Pressure distribution	Shear failure	Flexural failure
<i>Triangular</i>	$h_c = \frac{\sqrt{2 V_c}}{a \sqrt{\alpha g \rho L}}$	$h_c = \frac{\sqrt[3]{6 M_c}}{a \sqrt[3]{\alpha g \rho L}}$
<i>Trapezoidal</i>	$h_c = \frac{\alpha g \rho L H^2 + 2 V_c}{2 a \alpha g \rho L H}$	$h_c = \frac{2(3 M_c + \alpha g \rho L H^3)}{3 a \alpha g \rho L H^2}$

Table 3.7: Critical inundation depth equation for wall model I in terms of shear and flexural failure depending on triangular and trapezoidal pressure distribution

where V_c and M_c are respectively the shear and bending moment capacity for cross section.

It is important to note that in this case the panel height H is equal to building height due to the structural model adopted (Figure 3.18a).

3.4.1.2. *Wall model II*

The *wall model II* and the *wall model III* are statically indeterminate structural models; for the *wall model II*, force method is considered to solve the structural model removing trusses element and replacing them with unknowns forces (Figure 3.19). The choice of trusses as unknown forces is justified by the simple structural model that is represented by two cantilevers with concentrated forces.

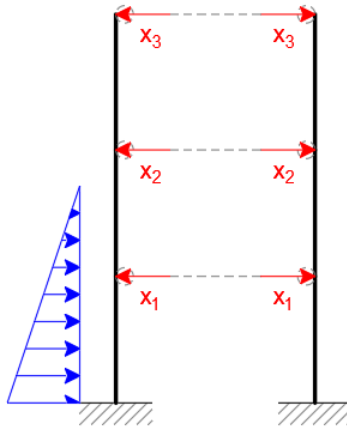


Figure 3.19: Wall model II and force method application for three storeys building model

The trusses have infinite axial stiffness as basic assumption and the number of unknowns is equal to the number of storeys of the structural model considered. With these assumptions, compatibility equations are evaluated assuming relative displacement of trusses equal to zero. The general solving equations can be written in matrix form as follows:

$$[D] \{x\} = \{b\}$$

where D represents the flexibility matrix, x the unknown forces vector and b the displacements vector.

The flexibility coefficients d_i take into account flexural and shear stiffness of masonry wall because wall length is not negligible.

$$d_i = \frac{h^3}{nEI} + 1.2 \frac{h}{GA}$$

Where h is the wall height, E is the Young or elastic modulus, G is the shear modulus, I is the cross section inertia, A the cross section area, n is a boundary condition coefficient and 1.2 is the shear coefficient.

The inverse of the flexibility is equal to the stiffness matrix K where the generic stiffness coefficient k_i is evaluated by the following equation:

$$k_i = \frac{1}{\frac{h^3}{nEI} + 1.2 \frac{h}{GA}}$$

An iterative method is developed on *Mathwork Matlab* software based on bisection convergence method in order to solve the compatibility equations and provide critical inundation depth that activates local in-plane mechanisms in masonry wall.

3.4.1.3. Wall model III

The *wall model III* is a statically indeterminate model and it is a common case for seismic buildings. The masonry walls are divided in frame elements and modelled as shear-type frames where horizontal storey displacements represent the model unknowns while joint rotations are equal to zero at each storeys as basic assumption.

Stresses are evaluated only on loaded storeys in terms of bending moment and shear, while unloaded storeys exhibit a rigid translation without any stress according to shear-type frame assumption.

The static model can be solved with simple shear balance equations where external triangular or trapezoidal pressure distributions are represented by equivalent joint shear stresses.

Four different load cases are taken into account, one for the triangular pressure distribution case (Figure 3.20.a) and three for the trapezoidal pressure distribution cases (Figure 3.20.b,c,d). In particular, the structural model depends on the relationship between the number of storeys n_s , the inundation depth h_{max} , the interstorey height H_i and the building height H .

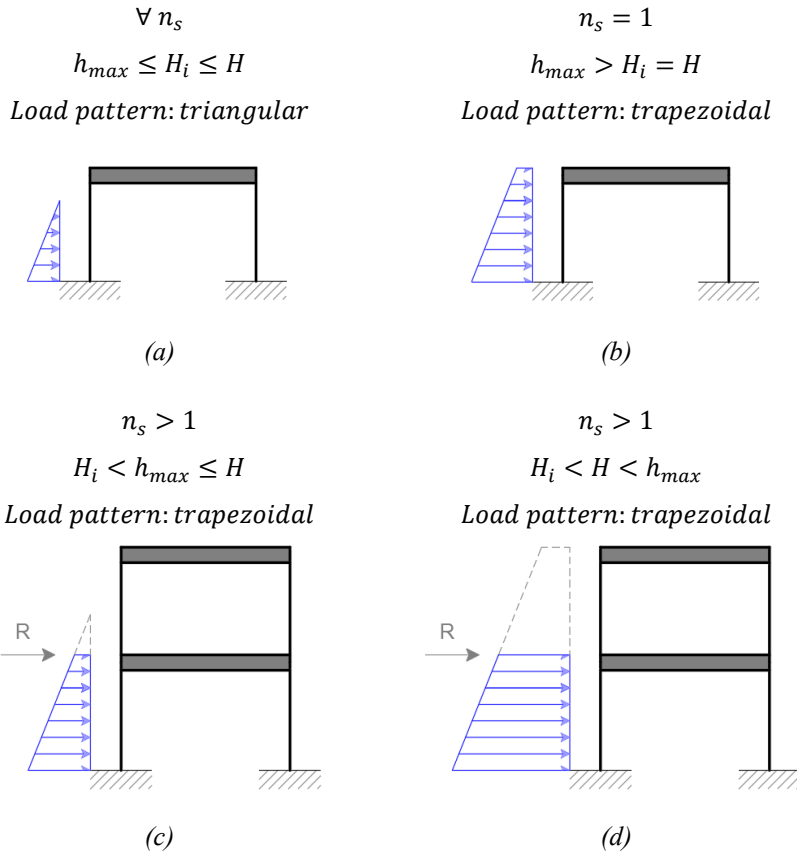


Figure 3.20: Structural models for wall model III

As for *wall model II* solution, an iterative method is developed on *Mathwork Matlab* software based on bisection convergence method in order to solve the static model and to provide critical inundation depth that activates local in-plane mechanisms in masonry wall.

3.4.1.4. Capacity model

For each in-plane mechanism, the cross section capacity is compared with external stress in terms of bending moment or shear stresses evaluated through linear elastic analyses in order to retrieve the

critical inundation depth that activates a specific local mechanism (Türkmen et al., 2020).

Two different cross section capacities are defined for shear failure modes corresponding to the first cracking occurrence and material rupture; in particular, cracking capacity is conventionally defined as half of the ultimate state capacity according to diagonal compression experimental tests available in literature (Prota et al. 2006).

For sliding and diagonal shear failures, the capacity equations are based on actual Italian building code *NTC 2018* assuming *Mohr-Coulomb* (V_a) and *Turnsek-Cacovic* (V_t) capacity criterion respectively for sliding and diagonal shear failures.

$$V_a = \left(\frac{1}{p} (\beta + \mu_a n) \right) N_u$$

Where:

- p : distribution coefficient of tangential stress acting on wall cross section;
- β : ratio between tangential and axial ultimate stress;
- μ_a : friction coefficient equal to 0.4 according to actual Italian building code *NTC18*;
- n : dimensionless external axial load;
- N_u : ultimate axial load.

$$V_t = \left(\beta \sqrt{1 + \frac{n}{p \beta}} \right) N_u$$

Where:

- p : distribution coefficient of tangential stress acting on wall cross section;
- n : dimensionless external axial load;
- N_u : ultimate axial load;
- β : ratio between tangential and axial ultimate stress.

The distribution coefficient of tangential stress acting on wall cross section has a lower bound value of 1 and an upper bound value of 1.5 according to several experimental tests. The lower bound value is common for squat masonry wall while 1.5 is related to slender walls depending on the relationship between wall length B and height H .

$$\text{Slender wall: } \frac{H}{B} \geq 1.5 \rightarrow p = 1.5$$

$$\text{Squat wall: } \frac{H}{B} < 1 \rightarrow p = 1.0$$

Furthermore, it is interesting to note that the upper bound limit is related to a parabolic distribution of tangential stresses on cross section while the lower bound limit is related to a constant distribution of tangential stresses (Figure 3.21).

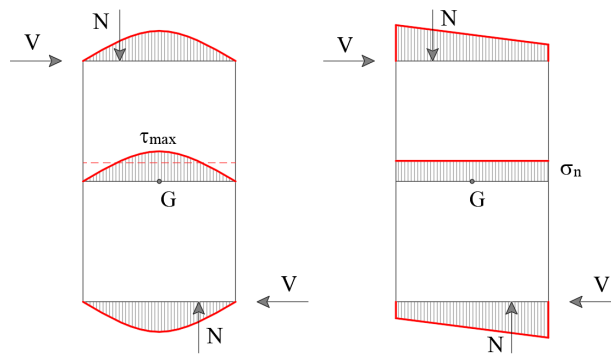


Figure 3.21: Distribution coefficient of tangential stress acting on wall cross section

The β coefficient represents a relationship between tangential and axial ultimate stress and it has been evaluated according to characteristic values provided by *Circolare esplicativa “Istruzioni per l’applicazione della normativa tecnica per la riparazione ed il rafforzamento degli edifici danneggiati dal sisma” n.21745* in 1981 and *Circolare esplicativa “Istruzioni per l’applicazione delle «Nuove norme tecniche per le costruzioni» di cui al decreto ministeriale 14 gennaio 2008” n.617* in 2009.

Masonry type	β
Poor stone	0.0277
Tuff stone	0.0245
Hollow clay bricks	0.0554
Clay brick	0.0465
Full clay brick	0.0299

Table 3.8: β coefficient values for different material types

The bending moment capacity model is defined for three different limit states corresponding to elastic (decompression), cracking (first cracking occurrence) and ultimate (material rupture) states. Their capacity models and PM domains (Figure 3.22) are available in the literature in dimensionless and parametric equations (Lignola et al. 2008).

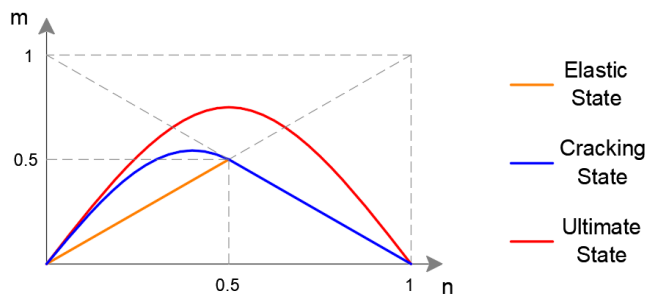


Figure 3.22: PM domains for elastic, cracking and ultimate states

The bending moment corresponding to decompression elastic limit state M_e is evaluated assuming compressed the entire section without any tensile fiber:

$$M_e = \frac{n}{6} s H^2 \sigma_m$$

Where:

n : dimensionless external axial load;

s : cross section depth;

H : cross section height;

σ_m : compression strength.

The cracking moment is calculated assuming partialized cross section:

$$M_{cr} = \frac{(n(3 - 4n))}{6} s H^2 \sigma_m$$

The ultimate bending moment M_r of masonry wall cross section is evaluated considering *stress-block* behaviour for compressed masonry according to actual Italian code *NTC18*:

$$M_r = \frac{(1 - n)}{2} s H^2 \sigma_m$$

The cracking moment M_{cr} and the ultimate bending moment M_r are similar for low external axial load as shown in Figure 3.22 and it is a common case for typical masonry walls. It is important to note that the external load depends on the inundation depth squared therefore, small inundation depth increments generate huge stress increments. It is reasonable to perform structural analyses only for elastic M_e and ultimate M_r limit state because cracking state analysis provides results

comparable to ultimate limit state analysis. The activation of the in-plane local mechanism occurs when the maximum external stress reaches the corresponding cross section capacity in terms of bending moment or shear stress. The equality between the cross section capacity and the external stress allows to retrieve the critical inundation depth h_c that activates a specific in-plane local mechanism. A closed form equation can be easily retrieved for *wall model I* while an iterative analysis is required for *wall model II* and *wall model III* due to complexity in inverting equation. The algorithm is implemented in *Mathworks Matlab* software using bisection convergence method in order to evaluate the critical inundation depth h_c for each defined damage state DS_i .

$$T_r = T_s \rightarrow h_{c,DSi}$$

$$M_r = M_s \rightarrow h_{c,DSi}$$

3.4.2. Out-of-plane mechanisms

Out-of-plane behaviour assessment of masonry walls is one of the most debated topics in the scientific community. One of the first attempts to describe out-of-plane mechanisms was provided by *Rondelet* in 1802, in particular, he proposed three different local mechanisms model depending on wall boundary conditions and geometry.

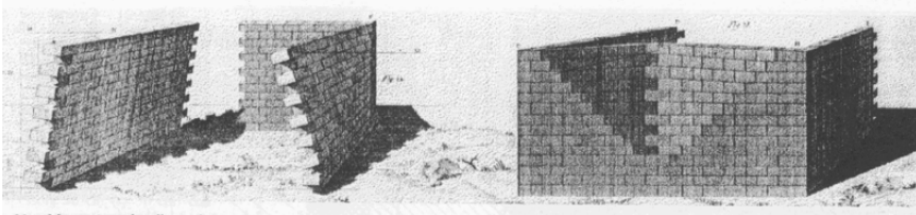


Figure 3.23: Out-of-plane mechanisms model proposed by Rondelet (1802)

However, out-of-plane mechanisms could involve portions of walls or the full wall (Maccarini et al., 2018).

Several works on seismic vulnerability assessment of masonry buildings by means of limit analysis procedures have been proposed. The research was restricted to the estimation of the seismic activation multiplier.

The out-of-plane local mechanisms activation depends on several structural details like as quality and mechanical properties of masonry, connections between structural elements, boundary condition and type of floors and roofs; for this reason it is complex to predict.

The out-of-plane mechanisms involve a kinematic mechanism characterized by the formation of oblique or vertical cracks (horizontal bending mechanisms) or horizontal cracks (vertical bending mechanisms). Masonry wall portions rotate around ideal plastic hinges situated at cracks.

The main out-of-plane mechanisms analysed are:

- *Vertical bending mechanisms;*
- *Horizontal bending mechanisms.*

A wall between two orthogonal walls is considered to study the out-of-plane mechanisms in terms of horizontal and vertical bending mechanisms. The activation of the local mechanism occurs when the maximum external stress reaches the corresponding cross section capacity in terms of bending moment (vertical bending mechanism) or axial load (horizontal bending mechanism) (Belliazzi et al. 2018a). The external loads are increased to reach the activation of out-of-plane local mechanism by means of the inundation depth, as calculated for in-plane mechanisms.

3.4.2.1. *Vertical bending mechanism*

Vertical bending mechanism occurs when the wall has a good connection in the upper and lower parts and a poor connection at the sides (Figure 3.24).

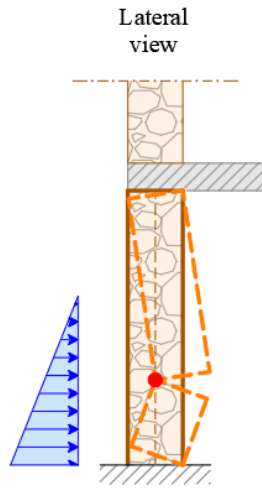
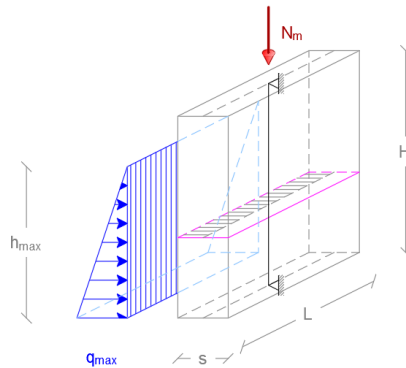


Figure 3.24: Vertical bending mechanism

The masonry wall has been modelled by means of beam elements (Figure 3.25) as a simple supported beam due to the regional scale approach adopted; it is a simplified assumption according to a safety criterion due to the actual bidimensional behaviour of masonry walls.



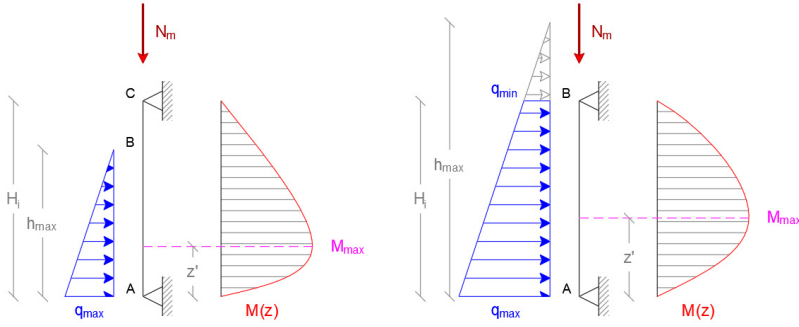


Figure 3.25: Vertical bending mechanism static model

The bending moment capacity M_r of the cross section is evaluated considering an external axial load N_m related to self-weight and floor loads that is beneficial for cross section capacity. The adopted capacity model is the same reported in §3.4.1.4 to evaluate ultimate bending moment capacity of a generic masonry wall cross section.

$$M_r = \frac{(1 - n)}{2} s H^2 \sigma_m$$

It is possible to calculate the equation of the maximum external bending moment M_s on the element depending on the zero of the shear function:

$$T_i(z) = 0 \rightarrow z' \rightarrow M_{max} = M_i(z')$$

The external bending moment function can be easily retrieved for both triangular M_{tri} and trapezoidal M_{tra} pressure distribution:

$$M_{tri} = \frac{\eta^3 \alpha \gamma_w h^3 (9 H_i^{3/2} - 9 \eta \sqrt{H_i} h + 2 \sqrt{3} \eta^{3/2} h^{3/2}) L}{54 H_i^{3/2}}$$

$$M_{tra} = -\frac{1}{54} \alpha \gamma_w (-3 \eta h + \sqrt{3} k) (-2 H_i^2 + 6 \eta H_i h + \eta h (-3 \eta h + \sqrt{3} k)) L$$

Where γ_w is equal to ρg and k coefficient is equal to:

$$k = \sqrt{H_i^2 - 3 \eta H_i h + 3 \eta^2 h^2}$$

The equality between the cross section capacity M_r and the external bending moment M_s does not allow to easily retrieve the inundation depth h_c within a closed form equation. An iterative analysis is implemented in *Mathworks Matlab* software using bisection convergence method in order to evaluate the critical inundation depth h_c for each defined damage state DS_i .

$$M_R = M_S \rightarrow h_{c,DS_i}$$

3.4.2.2. Horizontal bending mechanism

Horizontal bending mechanism is common in walls with a good joint degree to the side walls and free at the top (Figure 3.26).

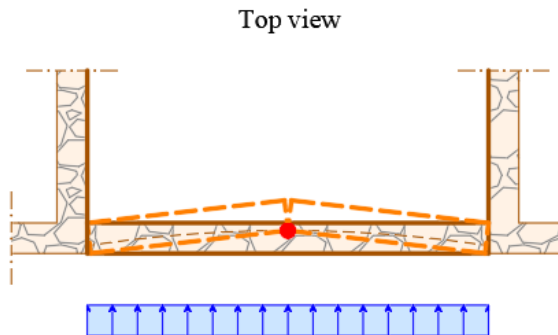


Figure 3.26: Horizontal bending mechanism

The horizontal out-of-plane mechanisms of masonry walls are highly dependent on connection degree between walls. Masonry walls without any connection with other walls exhibit rigid body behaviour such as free standing walls, they are characterized by zero axial loads

and they exhibit no bending moment capacity due to the no tension assumption.

The horizontal bending mechanism is characterized by the arch mechanism activation inside the masonry wall (Figure 3.27) and the mechanism activation is based on the equality between the external axial load N_s and the capacity of the cross section N_r in terms of compressed masonry.

In this case, the external axial load N_m does not contribute to the cross section capacity.

As for the static model of the vertical bending moment mechanism, the masonry wall is modelled as a one-dimensional element as a simply supported beam where the tsunami load is modelled as a distributed load. The distributed load intensity is considered assuming two different cases:

- *Load case 1*: load intensity is equal to the maximum value evaluated near the base;
- *Load case 2*: load intensity is evaluated by the ratio between the external tsunami load resultant R and wall interstorey height H_i :

$$q = \frac{R}{H_i} = \frac{q_{max} h_{max}}{2 H_i}$$

Load case 2 is assumed in the vulnerability assessment of masonry buildings under tsunami loads because the *Load case 1* provides unrealistic results due to the real exposed area linked to the external load.

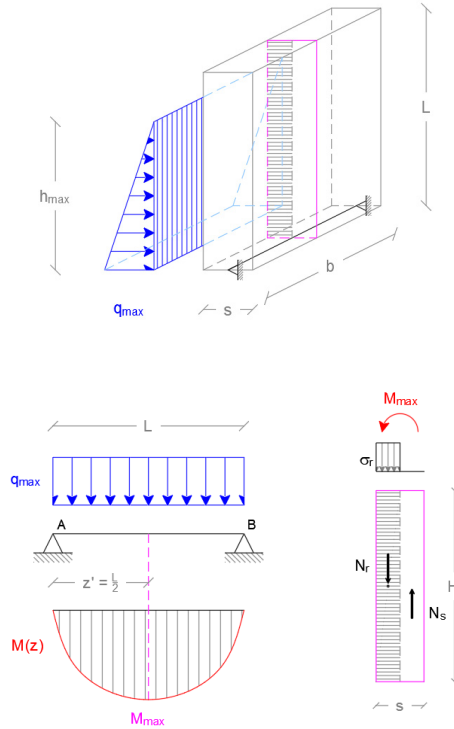


Figure 3.27: Horizontal bending mechanism static model for gravitational buildings

The cross section capacity N_r and external load N_s are evaluated considering the static model reported in Figure 3.27.

$$N_r = \sigma_m \frac{s}{2} H_i$$

$$N_s = \frac{M_s}{f} = \frac{q_{max} L^2}{8 f}$$

Where σ_m is the ultimate compressive stress of masonry and f is the distance between N_r and N_s in the section analysis. The parameter f is variable between $s/4$ and $s/2$ in order to consider walls design for gravitational or seismic loads and to take into account joint degree between structural walls. Buildings designed for seismic loads show a

better joint degree between walls than structures designed only for gravitational loads; for these reasons different boundary conditions are assumed in static mode and in particular, seismic buildings assume a beam restrained by rotational spring support as static model according to classis plasticity theory, while gravitational structures are modelled as simply supported beams.

In this case, it is simple to retrieve the critical inundation depth by means of a closed form equation for both gravitational $h_{c,g}$ and seismic $h_{c,s}$ buildings (Table 3.9 and Table 3.10).

Pressure distribution	Gravitational buildings	Seismic building
Triangular	$h_{c,g} = \frac{s H_i \sqrt{2 \sigma_m}}{\eta \sqrt{L^3 \alpha \gamma_w}}$	$h_{c,s} = \frac{2 s H_i \sqrt{\sigma_m}}{\eta \sqrt{L^3 \alpha \gamma_w}}$
Trapezoidal	$h_{c,g} = \frac{H_i \left(1 + \frac{2 s^2 \sigma_m}{L^3 \alpha \gamma_w} \right)}{2 \eta}$	$h_{c,g} = \frac{H_i \left(1 + \frac{4 s^2 \sigma_m}{L^3 \alpha \gamma_w} \right)}{2 \eta}$

Table 3.9: Critical inundation depth equation for horizontal bending mechanism in ultimate limit state condition

Pressure distribution	Gravitational buildings	Seismic building
Triangular	$h_{c,g} = \frac{2 s H_i \sqrt{\sigma_m}}{\eta \sqrt{L^3 \alpha \gamma_w}}$	$h_{c,s} = \frac{2 s H_i \sqrt{\frac{2}{3} \sigma_m}}{\eta \sqrt{L^3 \alpha \gamma_w}}$
Trapezoidal	$h_{c,g} = \frac{H_i \left(3 + \frac{4 s^2 \sigma_m}{L^3 \alpha \gamma_w} \right)}{6 \eta}$	$h_{c,g} = \frac{H_i \left(3 + \frac{8 s^2 \sigma_m}{L^3 \alpha \gamma_w} \right)}{6 \eta}$

Table 3.10: Critical inundation depth equation for horizontal bending mechanism in elastic conditions

3.5. Influence of parameters

Several parametric analyses are carried out in order to assess the effects of main geometrical and mechanical structural parameters on tsunami capacity. This is a basic step to provide vulnerability information on masonry Italian coastal buildings at a regional scale level and to design retrofit strategies in areas characterized by a high tsunami risk.

3.5.1. *Out-of-plane mechanisms*

Several analyses have been performed considering previous equations with mean values of each parameter, except: wall length L , wall thickness s and interstorey height H_i where the minimum and maximum values were considered for both vertical and horizontal bending mechanisms.

The density of water ρ incorporates that the tsunami flows consist of a mixture of sediment and seawater as reported in *FEMA P-646* (§2.1.3).

Different charts have been derived in order to compare the behaviour of gravitational and seismic buildings against activation of vertical and horizontal bending mechanisms (Belliazzi et al. 2019a).

3.5.1.1. *Vertical bending mechanism*

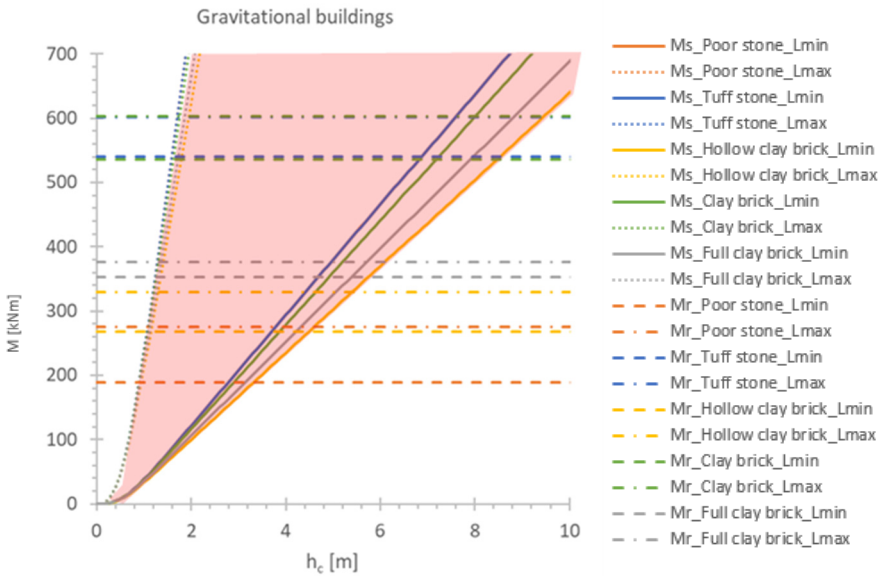
The out-of-plane mechanisms can be studied extrapolating a single wall from the generated structure and all the parameters that characterize the external load and cross section capacity depend on geometrical and mechanical parameters of the analysed wall.

The activation of the vertical out-of-plane mechanism occurs when maximum external bending moment equals the cross section capacity

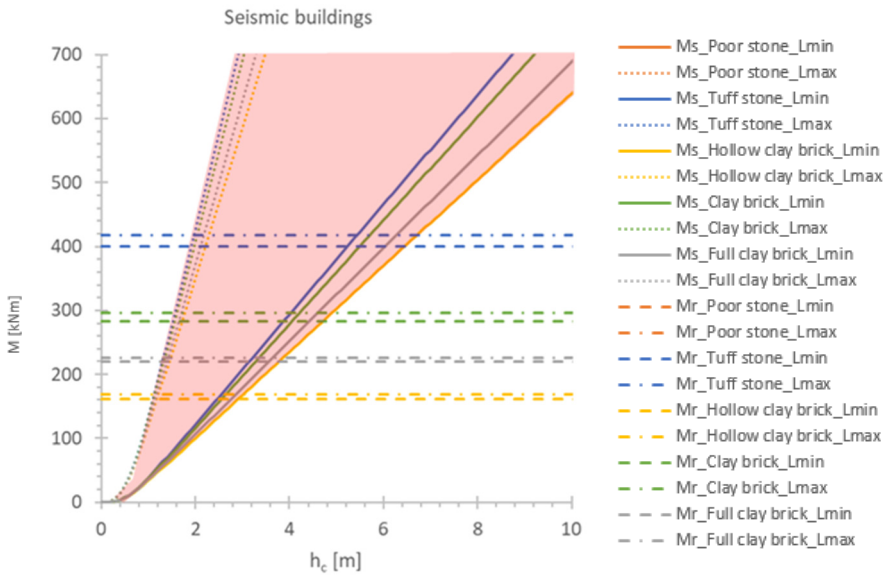
M_r ; the maximum external stress equation is simple to derive due to the considered static model (Figure 3.25) depending on triangular (M_{tri}) or trapezoidal (M_{tra}) load pattern. In each chart, five curves represent the external action M_s and capacity of cross section M_R for minimum and maximum values of investigated parameter.

In addition, an additional concentrated load N_m is considered on the top of the wall to model self-weight and effect of other storey weights.

In Figure 3.28 the influence of wall length L is shown on activation of vertical bending mechanism, in particular the critical point is defined by intersection between external demand and cross section capacity for a specific masonry type. In this chart it is possible to appreciate how gravitational buildings reveal a better behaviour under tsunami loads due to a greater mean thickness value compared to seismic buildings.

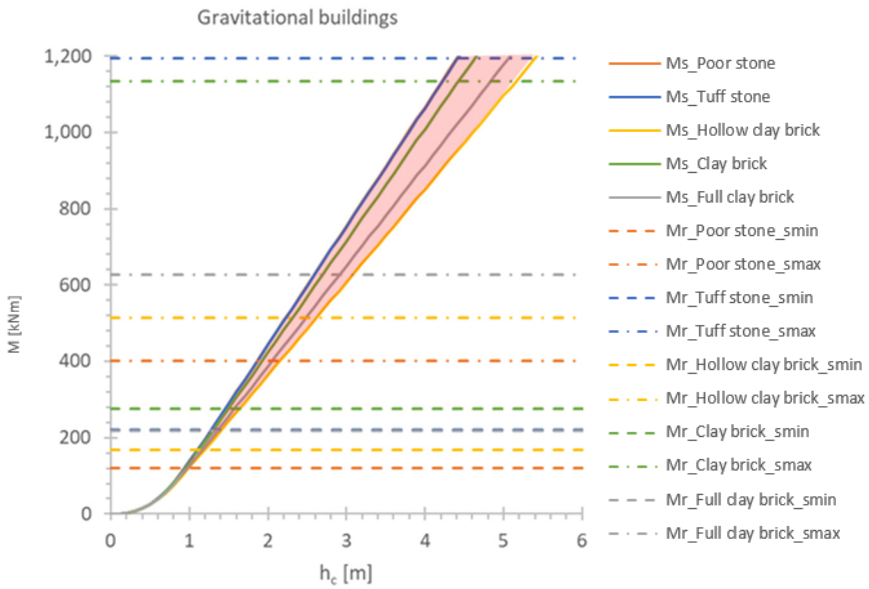


(a)



(b)

Figure 3.28: Vertical bending mechanism sensitivity to wall length L for gravitational (a) and seismic (b) buildings



(a)

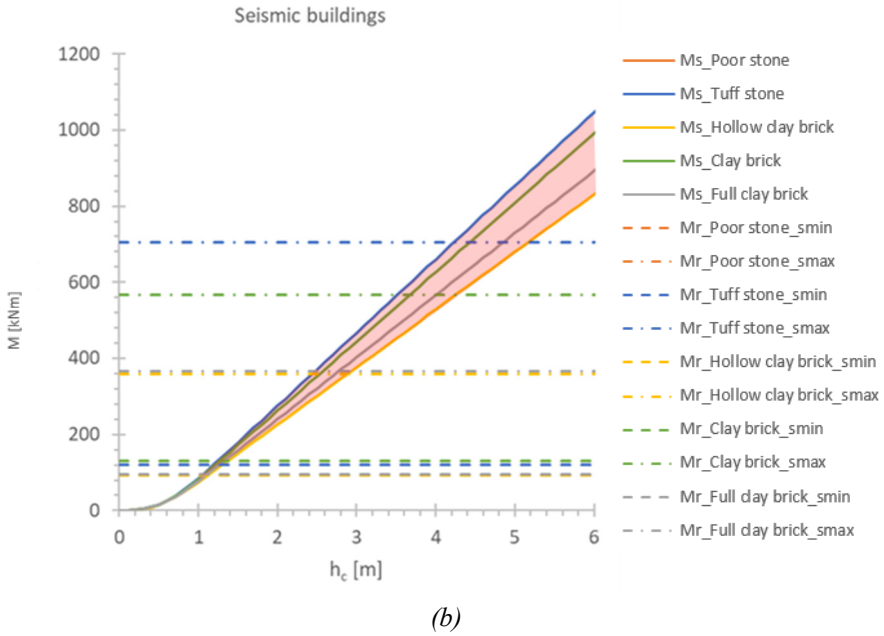
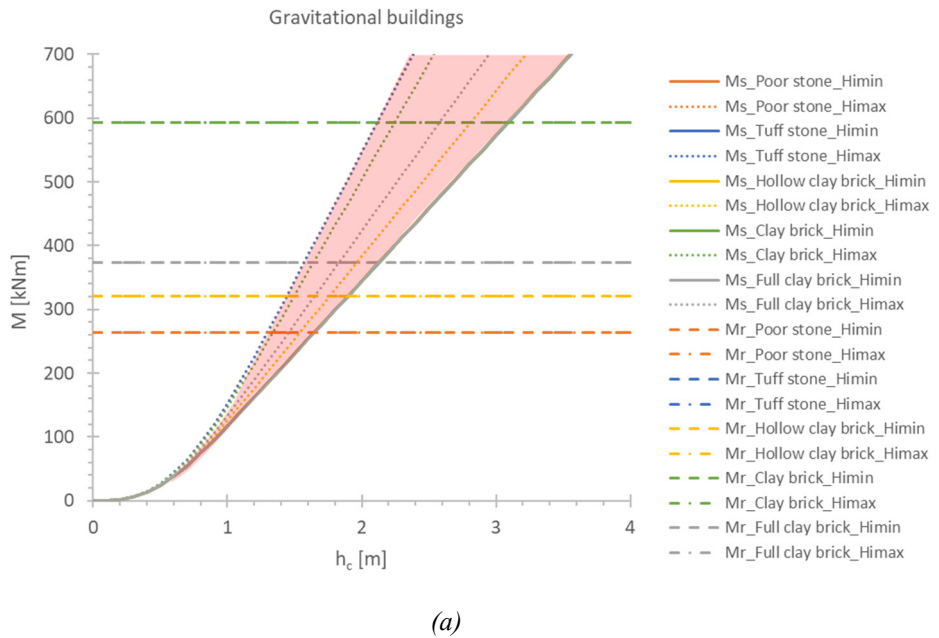
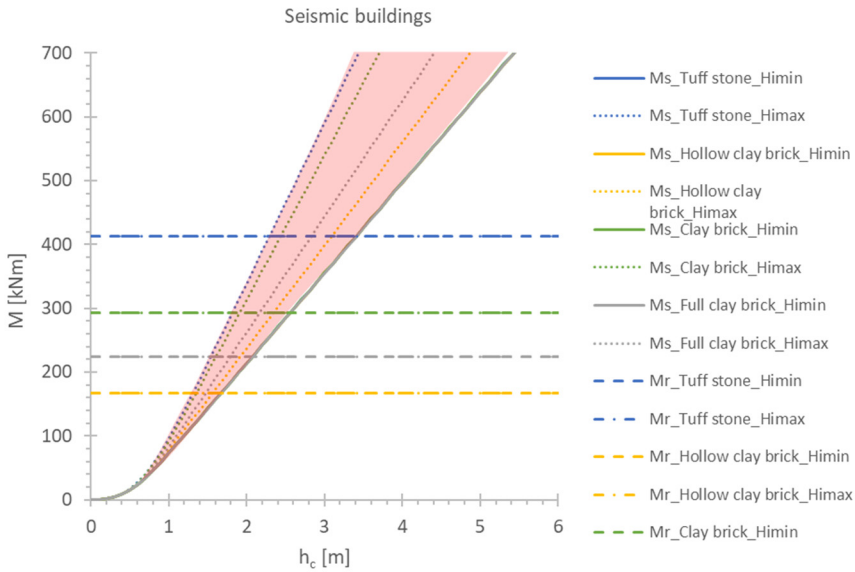


Figure 3.29: Vertical bending mechanism sensitivity to wall thickness s for gravitational (a) and seismic (b) buildings





(b)

Figure 3.30: Vertical bending mechanism sensitivity to interstorey height H_i for gravitational (a) and seismic (b) buildings

In Figure 3.29, the external demand is described by one curve only for each material quality because the equation is not influenced by the investigated parameter.

Comparing the charts, wall thickness (Figure 3.29) and interstorey height (Figure 3.30) have a huge influence on cross section capacity while the wall length (Figure 3.28) influences the external demand. The wall length L is the main parameter that describes the external demand because tsunami forces are superficial forces depending on the exposed surface. Gravitational buildings are designed by means of empirical equations depending on geometric parameters, therefore tall masonry structures require thicker walls and gravitational buildings with tuff stone have the best cross section capacity.

3.5.1.2. *Horizontal bending mechanism*

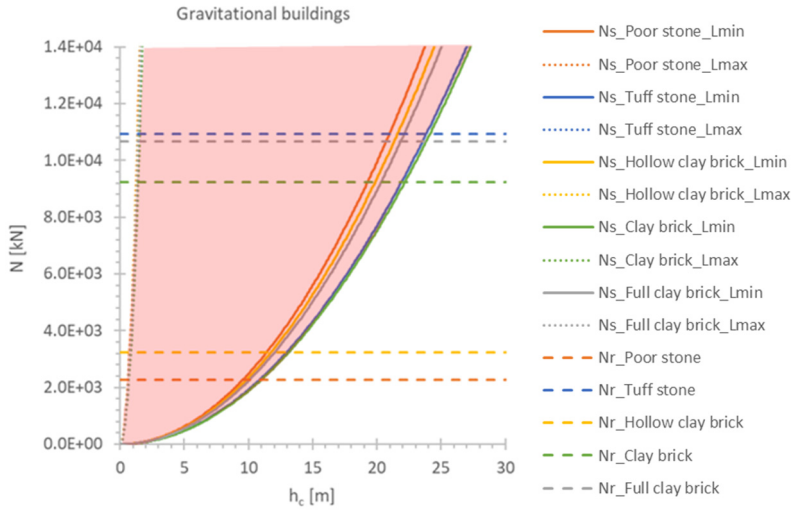
The horizontal out-of-plane mechanism is based on the equality between the external axial load N_s and the capacity of the cross section N_r due to the arch mechanism activation. The external demand is evaluated considering the static model reported in Figure 3.27.

The critical inundation depth that activates the local mechanisms is evaluated equating the external demand equation with the capacity of the cross section and the equations are reported in paragraph §3.4.2.2.

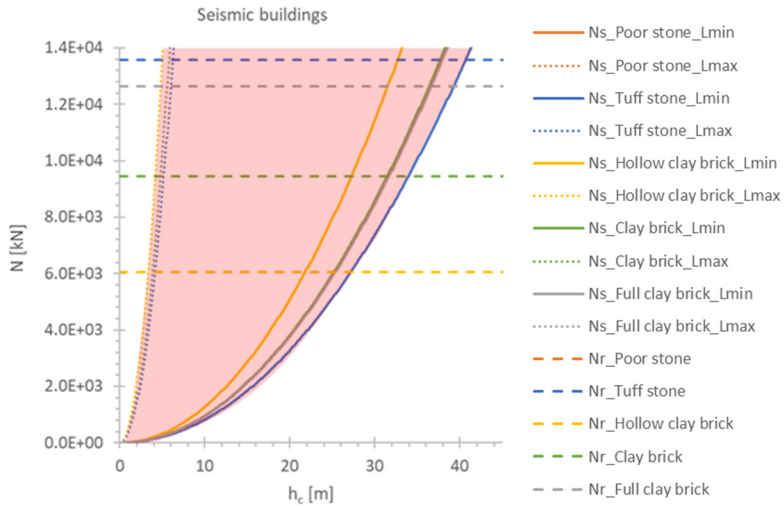
It is important to note that in the horizontal bending moment, the external distributed load is evaluated as the ratio between the wall load pattern resultant R and the interstorey height H_i . This assumption is necessary because the tsunami forces are superficial forces and extending local water pressure q_{max} is excessively conservative.

Similarly to vertical bending mechanism charts, several parametric analyses have been performed in order to clarify the influence of wall length L , wall thickness s and interstorey height H_i on horizontal bending mechanism activation.

In each chart, five curves represent the external demand N_s and capacity of cross section N_r for minimum and maximum values of investigated parameter.

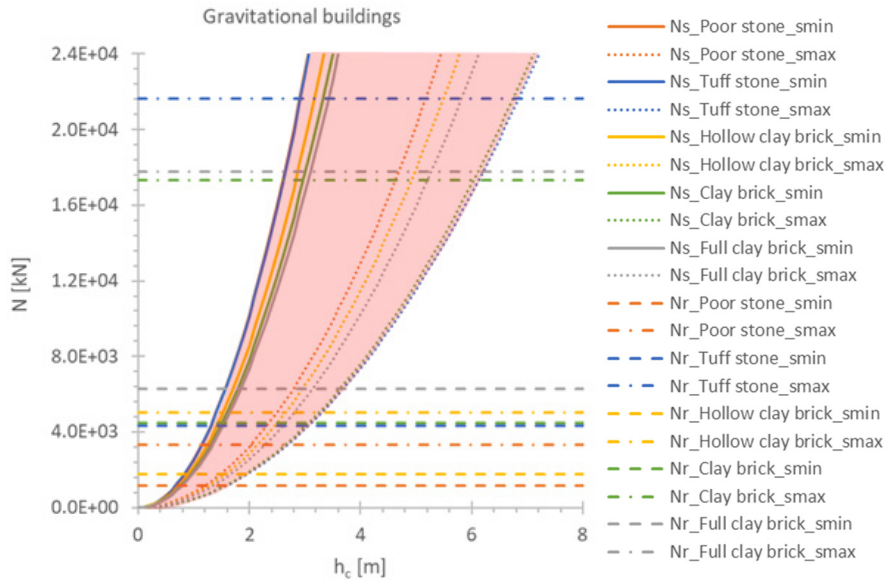


(a)

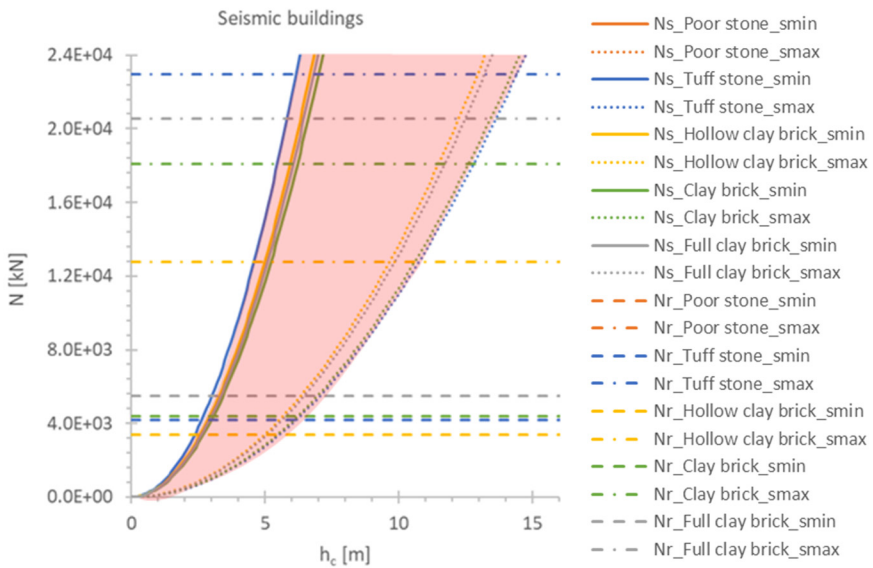


(b)

Figure 3.31: Horizontal bending mechanism sensitivity to wall length L for gravitational (a) and seismic (b) buildings

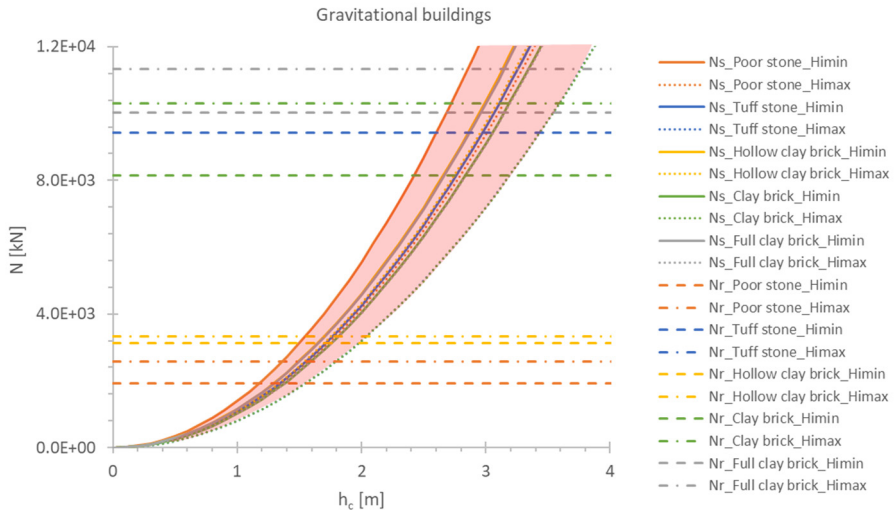


(a)

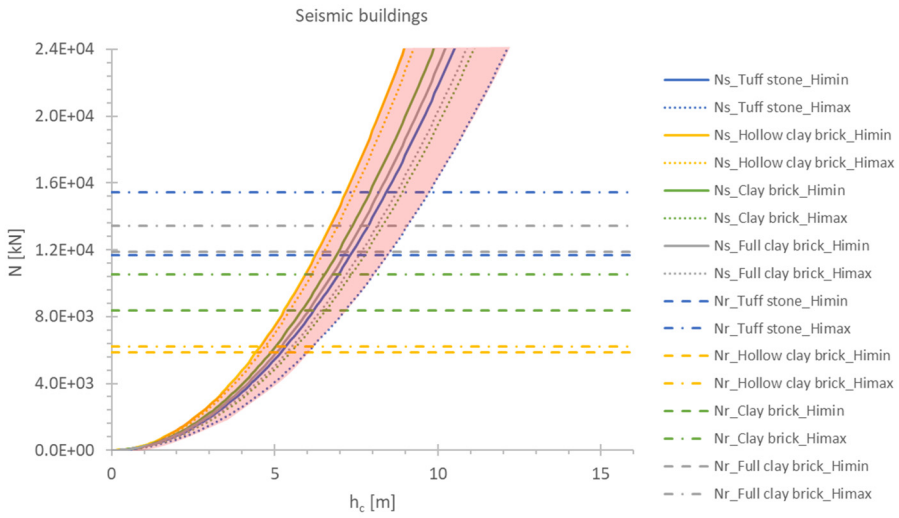


(b)

Figure 3.32: Horizontal bending mechanism sensitivity to wall thickness s for gravitational (a) and seismic (b) buildings



(a)



(b)

Figure 3.33: Horizontal bending mechanism sensitivity to interstorey height H_i for gravitational (a) and seismic (b) buildings

In Figure 3.31, the cross section capacity is described by only one curve for each material quality because the equation is not influenced by the investigated parameter.

Comparing the charts in Figure 3.31, Figure 3.32 and Figure 3.33 in terms of external axial load, the influence of wall length L is more noticeable than of wall thickness s and interstorey height H_i . Conversely, the axial load capacity of wall cross section has a huge influence depending on wall thickness s and interstorey height H_i similarly to vertical bending mechanisms. Seismic designed buildings exhibit a better behaviour than gravitational buildings due to a greater joint degree between walls.

It is important to note that in general, the charts between activation of vertical and horizontal bending mechanisms are not comparable because vertical bending mechanism charts are expressed in terms of bending moment while horizontal bending mechanism charts depend on axial load.

3.5.2. *In-plane mechanisms*

To assess the vulnerability of a masonry wall panel related to in-plane local mechanisms is more complex than out-of-plane mechanisms due to the influence of global behaviour of the entire structure on the single panel behaviour under tsunami loads. In fact, the number of spans plays an important rule on the lateral stiffness of the building and consequentially on the stress distribution between masonry wall panels.

A case study is analysed and comparison between external stresses and P - V domain are provided in terms of three main failure modes as flexural failure, sliding share failure and diagonal shear failure.

The structural model (Figure 3.34) is extrapolated by means of a random procedure from the tuff stone building population and the geometrical and mechanical parameters as shown in Table 3.11.

The density of water ρ assumes that the tsunami flows consist of a mixture of sediment and seawater as reported in *FEMA P-646* (§2.1.3) and the η coefficient is assumed equal to 3 according to upper bound limit provided by Japanese guidelines, in order to simulate a building near the shoreline.

Wall parameters	
B	5.0 m
$B1$	2.2 m
$B2$	1.8 m
H_i	4.0 m
H	7.5 m
s	0.9 m
L	4.5 m
σ_m	8 MPa
η	3
α	0.85

Table 3.11: Masonry building model parameters

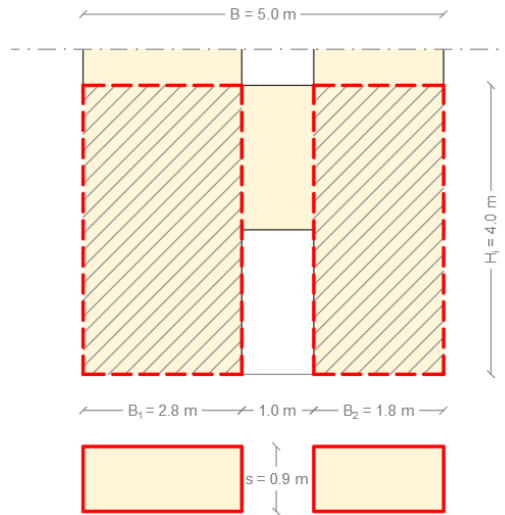


Figure 3.34: Masonry wall panels analysed for in-plane mechanisms

Structural analyses are performed on the extrapolated masonry buildings considering all three wall model cases in order to clarify the influence of the boundary conditions on in-plane local mechanisms activation and the structural behaviour of buildings under tsunami loads.

The analyses results are shown in Table 3.12 in terms of shear and bending moment stresses depending on the inundation depth.

Inundation depth		External Stresses					
h [m]	ηh [m]	V_s [kN]			M_s [kNm]		
		Wall model I	Wall model II	Wall model III	Wall model I	Wall model II	Wall model III
0.3	0.8	12.2	12.1	12.2	3.3	2.9	2.7
0.5	1.6	49.0	47.5	47.1	26.1	21.8	19.7
0.8	2.4	110.2	104.5	103.0	88.1	70.4	60.5
1.1	3.2	195.8	180.9	177.3	208.9	160.2	130.1
1.3	4.0	306.0	274.4	268.1	408.0	301.6	230.1
1.7	5.0	478.1	412.8	404.7	796.9	566.8	401.3
2.0	6.0	688.5	574.0	568.6	1377.0	952.2	627.1
2.3	7.0	937.1	758.1	759.8	2186.6	1482.7	907.6
2.7	8.0	1224.9	966.3	978.3	3269.7	2187.0	1242.7
3.0	9.0	1556.7	1202.3	1224.2	4682.7	3102.0	1632.4

Table 3.12: Analysis results in terms of shear and bending moment demand

The maximum expected inundation depth is assumed equal to three meters that it is equivalent to a fictitious inundation depth of nine meters according to Japanese guidelines in order to take into account indirectly both hydrostatic and hydrodynamic load components.

Regarding the cross section capacity, all failure modes are expressed in terms of P - V domain in order to simplify the comparison between external stresses and cross section capacity by means of one tool only.

Shear failure curves of both sliding shear and diagonal shear modes are independent on the wall model because all panels are slender and all the parameters are the same for each model case while flexural curve is dependent on the wall model and, in particular, it depends on boundary conditions and wall panel height.

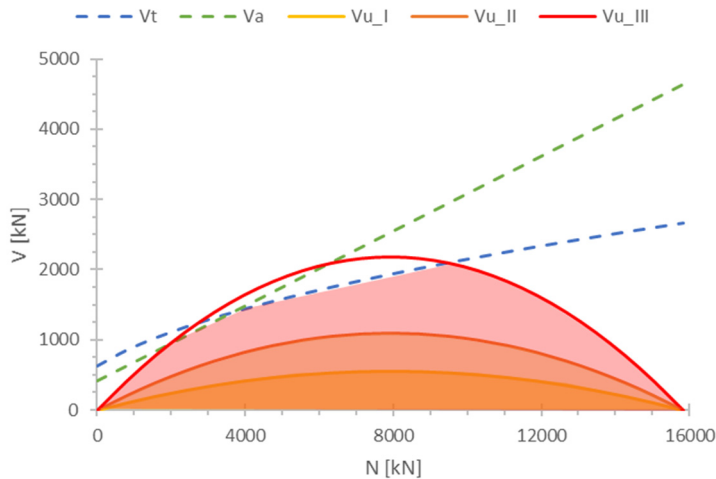


Figure 3.35: PV domain envelopes depending on shear and flexural failure modes and wall models

In Figure 3.35 shear failures are represented by means of dot lines while continuous lines represent flexural failure depending on the adopted wall model. In addition, P - V domain envelopes are shown for

all wall models and they are defined as the minimum critical shear value evaluated for each axial load value.

$$V_{env}(\bar{N}) = \min(V_t; V_a; V_u)$$

As expected, slender elements exhibit flexural failure mode (*wall model I* and *wall model II*) while no-slender elements could reach brittle failure (*wall model III*) depending on external axial loads.

Comparison between external shear loads and P - V domain allows to retrieve a relationship between the expected inundation depth (external loads) and the cross section axial loads (cross section capacity) as shown in Figure 3.36 depending on *wall model I*. The analysed cross section is related to the masonry wall panel characterized by the length B_l in the following example.

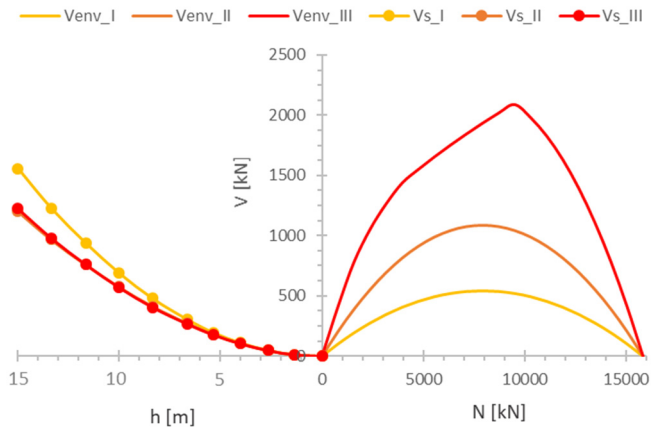


Figure 3.36: Comparison between external demand and cross section capacity in terms of shear stresses depending on wall model

Minimum and maximum admissible axial loads (N_{min} , N_{max}) that guarantee the cross section equilibrium are retrieved depending on expected inundation depth h , with a simple graphical method as shown in Figure 3.37. The green area represents the range of (V, N) points that

guarantee the cross section equilibrium while red areas represent (V, N) points that activate in-plane mechanisms.

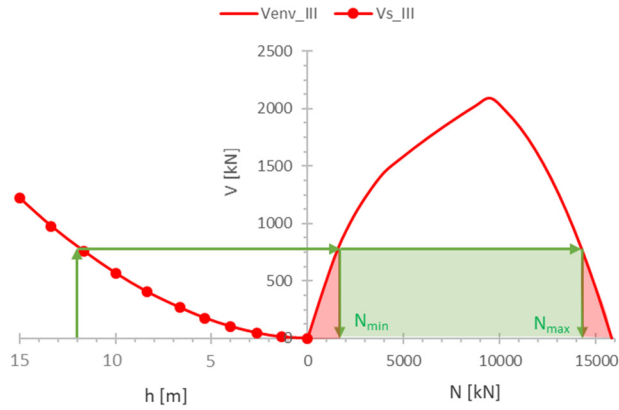


Figure 3.37: Minimum admissible external axial loads for wall model III for an inundation depth of 12 meters

A design chart (Figure 3.38) is provided for each wall model that provides the minimum admissible axial load N_{min} for a masonry wall panel depending on the expected inundation depth h .

The provided chart is based on a specific case study but the proposed method is applicable to any masonry wall panel.

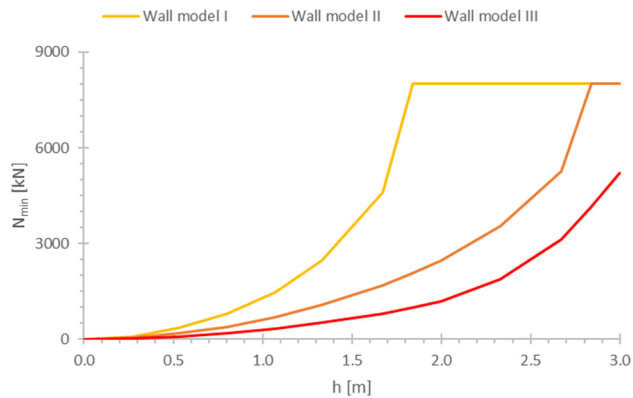


Figure 3.38: Design chart that provides the minimum admissible axial load for a masonry wall panel depending on expected inundation depth

In Figure 3.38, the discontinuity between the curve and the horizontal plateau represents in-plane mechanisms activation in terms of shear or flexural failure modes. In fact, the masonry wall panel does not increase the bearing load for higher inundation depths.

As expected, the *wall model III* shows the best structural performance comparing the curves in the design chart. In fact, the maximum admissible inundation depth is equal to 1.8 for *wall model I*, 2.8 for *wall model II* and greater than 3 meters for *wall model III*.

Chapter 4

Fragility curves and damage scenarios

In the last years, numerous catastrophic tsunami events have engaged scientific awareness to the vulnerability of Italian coastal masonry buildings subjected to tsunami loads. Tsunami vulnerability assessment represents a new research field in structural engineering and not many details are available on masonry walls behaviour under tsunami loads.

Therefore, fragility curves are retrieved based on the analysis method described in Chapter 3. Comparisons between mechanical and empirical fragility curves are provided in order to validate the structural analysis results.

In addition, one of the aims of the proposed work is to derive damage scenarios in terms of number of damaged buildings, reconstruction costs and potential casualties in the case of a tsunami event on the Italian coasts focusing on residential buildings. Damage scenarios provide preliminary information about high risk area in the case of a tsunami event along the Italian coasts.

An algorithm is developed by *GIS* system and *MathWorks MATLAB* scripts in order to analyse and manage the large amount of data produced. In addition, the *GIS* system allows to provide a simple and immediate graphical representation of the analyses results.

An inundation simulation is developed assuming three different attenuation laws based on simplified and refined approaches in order to retrieve inundation effects on buildings and population. In fact, building

damages are directly related to inundation depth through empirical or mechanical fragility curves. It is important to note that empirical fragility curves are based on post-tsunami event surveyor and, consequentially, buildings structural behaviour is strictly related to local building types as shown in paragraph §2.3; conversely mechanical fragility curves depend on structural analyses based on mechanical models assuming a regional scale approach as shown in paragraph §4.1.

The proposed algorithm aims to represent a fast tool that can be used as preliminary approach to define high tsunami risk areas. More refined simulations are required in order to analyse local 2D and 3D effects in the inundation simulation, friction between tsunami flow and different materials (e.g. terrain and asphalt), estimate several wave parameters as flow velocity and maximum momentum flux per unit mass per unit width. In particular, advanced flow parameters allow to perform refined structural analyses based on latest international building code as *ASCE 7-16* and to assess the structural behaviour of a specific building.

4.1. Fragility function

Fragility curves represent the probability of exceedance a specific damage state or performance as a function of an engineering demand parameter, e.g. the ground motion in seismic analysis. Therefore, mechanical fragility curves are derived in order to assess the vulnerability of Italian coastal masonry buildings under tsunami loads.

Uncertainties about materials and structural geometry are simulated by means of several *Monte Carlo* analyses.

Structural analyses are performed on one million buildings models for each building class and critical inundation depths are provided depending on in-plane and out-of-plane local mechanisms activation.

4.1.1. Damage state definition

Damage states *DS* are defined as damage degree on structures caused by a specific event, i.e., earthquake, landslide or tsunami. In literature, an unique definition for buildings damage states is not available in the case of tsunami events.

The Japanese *Ministry of Land, Infrastructure, Transport and Tourism (MLIT)* defines its own damage states based on post tsunami event surveys in Tohoku region in 2011 (Figure 4.1).

Damage State		Description	Use	Image
DS1	Minor Damage	Inundation below ground floor The building can be reused by removing mud below the floor boards	Possible to use immediately after minor floor and wall cleanup.	
	Moderate Damage	The building is inundated less than 1m above the floor (can be reused after a repair)	Possible to use after moderate repairs.	
DS3	Major Damage	The building is inundated more than 1m above the floor (below the ceiling)	Possible to use after major repairs.	
DS4	Complete Damage	The building is inundated above the ground floor level.	Major work is required for re-use of the building.	
DS5	Collapsed	The key structure is damaged, and difficult to repair to be used as it was before	Not repairable.	
DS6	Washed Away	The building is completely washed away except for the foundation	Not repairable.	

Figure 4.1: Damage states definition according to MLIT (Japan)

Therefore, damage states *DS* are proposed for masonry structures depending on damage degree of local mechanisms and *MLIT* definition; five different damage states are defined:

- *DS1*: Light damages on non-structural elements and negligible damages on structural elements;
- *DS2*: Slight damages on structural elements;
- *DS3*: Average damages on not load-bearing structural elements;
- *DS4*: High damages on floor-load bearing elements;
- *DS5*: High damages on floor-load bearing elements with floor loads.

In particular, damage degrees are related to in-plane and out-of-plane local mechanisms depending on elastic, cracking or ultimate state, in terms of bending moment and shear demand according to cross section capacity shown in paragraph §3.4.

Low damage states are related to low structural damages and they can be linked to elastic and cracking states, while high damage state can provide the structural collapse and plastic states are reached by the materials and for this reason are linked to ultimate state.

As preliminary approach, *DS2* is based on elastic failure, *DS3* depends on elastic or plastic failure while *DS5* is linked to plastic failure. Plastic failures are taken into account in *DS3* only in elements without floor loads because floor-load bearing elements could reach the floor collapse in the case of plastic failure and higher damages are expected (*DS4* or *DS5*).

DS1 and *DS4* are fictitious damage degrees based on *DS2* and *DS5* critical inundation depths, respectively. The first damage state *DS1* is assumed equal to half *DS2* critical inundation depth as basic assumption due to the inconsistent damages on structural elements and consequentially the impossibility to link the *DS1* to any local mechanism. In fact, Japanese *MLIT* assumes the building interior flooded without structural damages in the first damage state *DS1*.

4.1.2. Results and discussion

Least squares method is assumed to derive fragility curves and it is a mathematical regression analysis used to determine the line of best fit for a set of data. The method aims to create a curve that minimizes the sum of the squares of the errors generated by the difference between the observed data y_i (critical inundation depth provided by structural analyses) and the corresponding value obtained by lognormal function $f(h_i, (\mu, \sigma))$. A lognormal function is assumed according to several scientific papers available in literature that proof the validity of the adopted method (Porter et al. 2007) as shown in Figure 4.3.

$$S = \sum_{i=1}^n (y_i - f(h_i, (\mu, \sigma)))^2$$

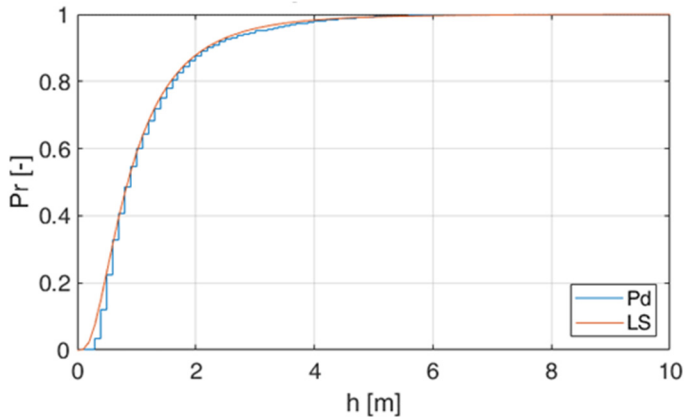


Figure 4.2: Discrete and continue fragility curves derived with least square estimation method

Fragility curves are retrieved considering several buildings population groups where the engineering demand parameter in terms of expected inundation depth is shown on the horizontal axis while the *DS* exceedance probability is on the vertical axis.

The inundation depth coefficient η is assumed constant or variable according to Japanese guidelines range in order to obtain fragility curves depending on distance of buildings from shoreline and to perform comparisons with empirical fragility curves.

Therefore, fragility curves are represented for a generic residential coastal Italian masonry building where different horizontal scales are shown depending on η coefficient (Figure 4.3).

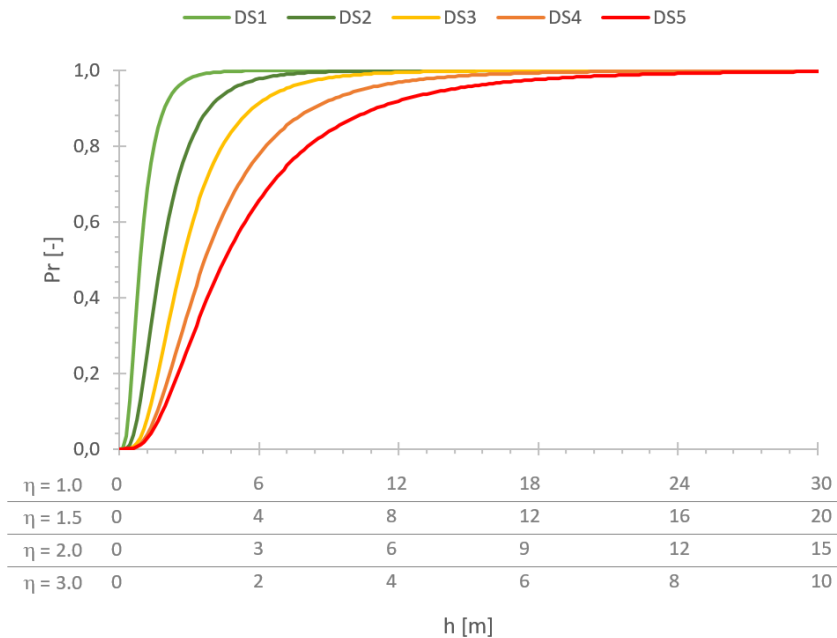


Figure 4.3: Fragility curves for generic masonry buildings

In Figure 4.4 and Figure 4.5 are shown fragility curves based on two different buildings population groups related to gravitational or seismic design approach, assuming η equal to 3.

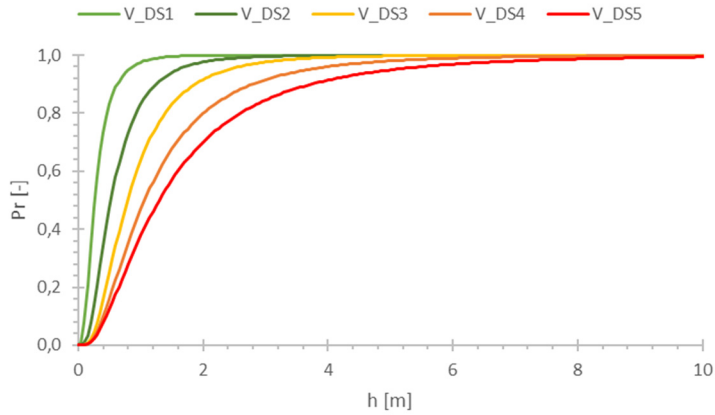


Figure 4.4: Fragility curves for gravitational buildings

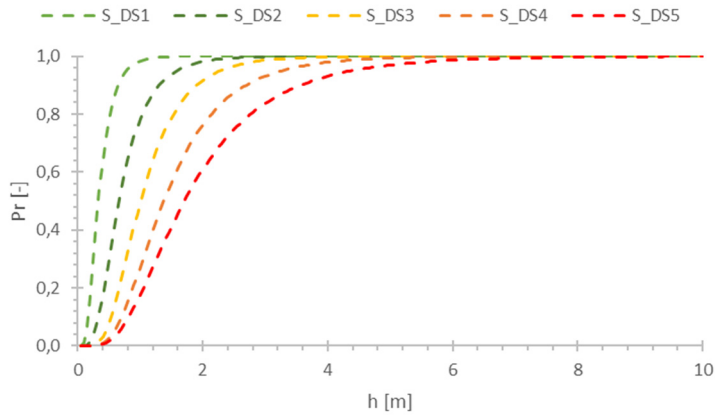


Figure 4.5: Fragility curves for seismic buildings

In Figure 4.6, fragility curves comparisons are shown between gravitational and seismic masonry buildings. Only DS_2 , DS_3 and DS_5 are shown because DS_1 and DS_4 are linked to other damage states.

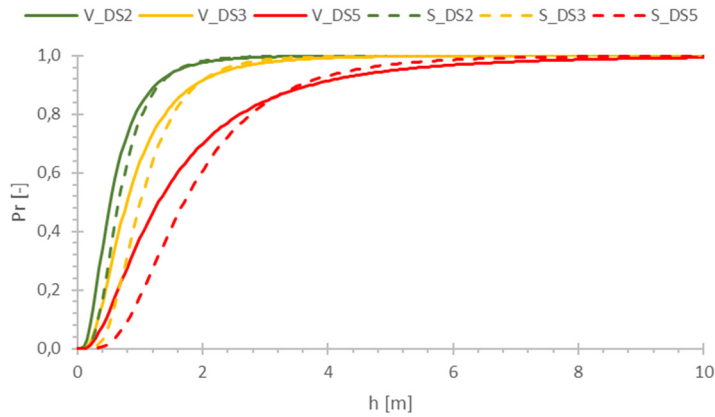


Figure 4.6: Fragility curves comparison between gravitational and seismic masonry buildings

Comparisons do not exhibit remarked differences in terms of fragility curves behaviour due to a cross section capacity balancing between gravitational and seismic buildings. In particular, gravitational buildings are characterized by high wall thickness and low material quality while seismic designed walls have low thickness and high compressive strength. In addition, maximum number of storeys and wall length limits are defined depending on the age of construction and buildings codes.

In Figure 4.7 and Figure 4.8, fragility curves are shown based on two different buildings population groups related to gravitational or seismic design approach assuming η equal to 3.

In Figure 4.9, fragility curves comparisons are shown between gravitational and seismic masonry buildings. Only DS_2 , DS_3 and DS_5 are shown because DS_1 and DS_4 are linked to other damage states.

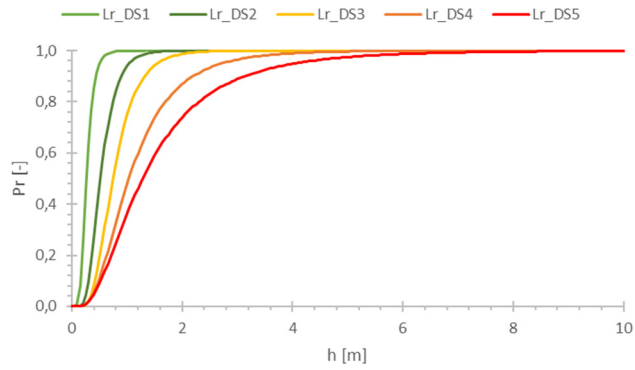


Figure 4.7: Fragility curves for low rise masonry buildings

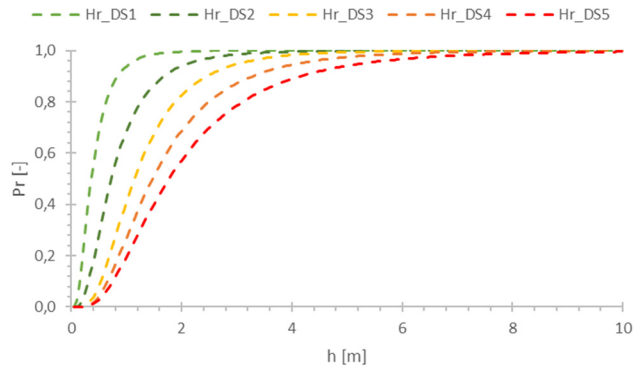


Figure 4.8: Fragility curves for medium-high rise masonry buildings

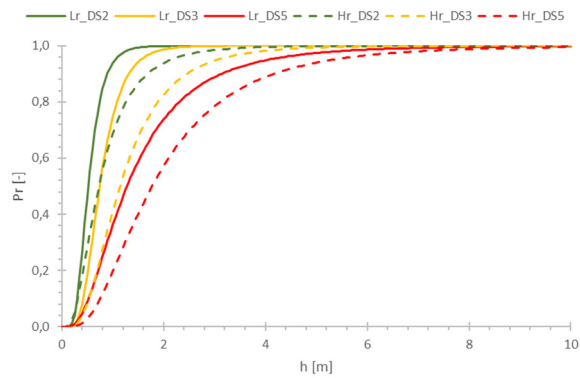


Figure 4.9: Fragility curves comparison between low and high rise masonry buildings

In line with Japanese empirical fragility curves available in literature (Suppasri et al. 2013), number of storeys has a high influence on structural behaviour and, in particular, the medium-high rise buildings are less vulnerable to tsunami loads than the low buildings due to higher wall thickness and consequently, higher cross section capacity.

In Figure 4.10, fragility curves comparisons are shown for different ages of construction related to DS_5 .

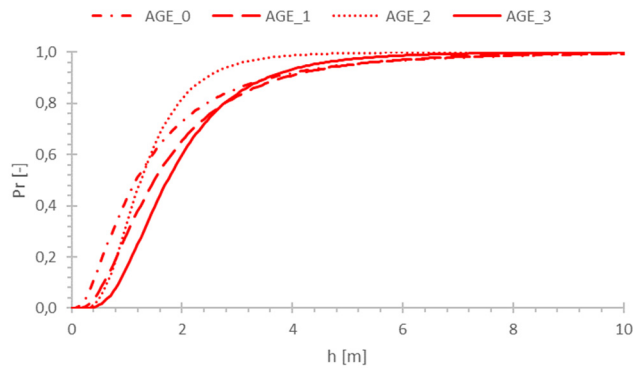


Figure 4.10: Fragility curves comparison between ages of construction for DS_5

As expected, a gradual increment of the structural behaviour under tsunami loads is shown due to the improvement of design approaches and construction techniques.

Furthermore, comparison between empirical and mechanical fragility curves are provided in order to validate the proposed study based on empirical fragility curves related to “*The 2009 South Pacific Tsunami*” (Reese et al. 2011) and “*The 2011 Great East Japan Tsunami*” (Suppasri et al. 2013).

A variable η coefficient is assumed in order to derive fragility curves comparable with empirical studies. In fact, different η coefficient values allow to simulate shield effects and the effects related to the distance between the buildings and the coastline. The building

population includes all building models generated by simulation analysis.

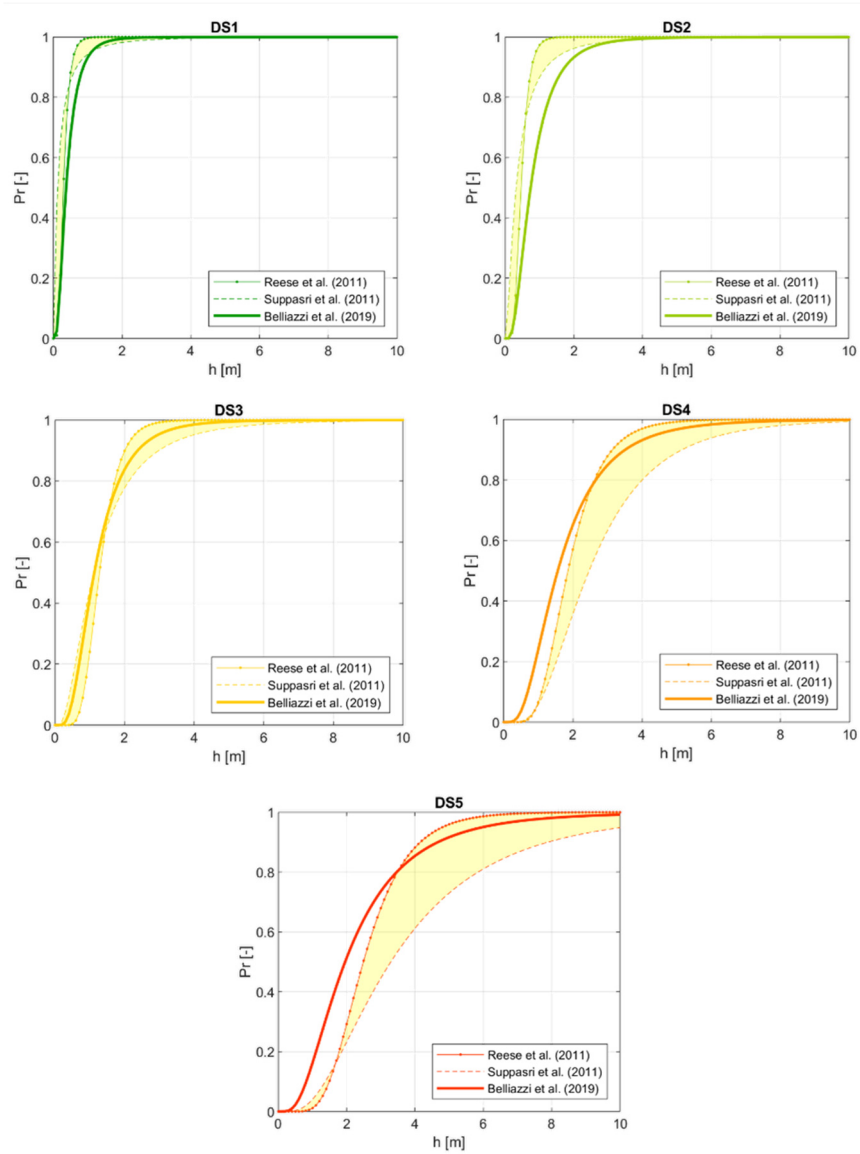


Figure 4.11: Comparison between empirical and mechanical fragility curves

The comparison (Figure 4.11) shows a good match between curves for low damage levels, i.e., DS_1 , DS_2 and DS_3 , while slight mismatch is shown for high damage levels, i.e., DS_4 and DS_5 . Differences are related to several uncertainties like as structural materials quality, number of storeys, age of construction, design criteria, unknown loads, collapse prediction, local mechanisms analysis and wave parameters. In fact, fragility functions are strictly related to local building typologies and it is reasonable to imagine that Italian stone quality is greater than Samoa materials quality.

In addition, a simplified and conservative approach is assumed instead of more refined structural analyses, as shown in American building codes, due to the low knowledge level reached in this study.

Design code and seismic area evolution play an important role in structural behaviour under tsunami loads and in particular, concrete buildings designed for earthquake loads overperforms buildings designed for gravitational loads only under tsunami loads because structural elements are designed for horizontal loads. In masonry buildings, the reduced thickness influences the structural capacity of load bearing elements more than the improvement of material mechanical properties.

Mechanical fragility curves are not currently available in the international scientific literature and they represent an important milestone in this scientific research on tsunami vulnerability assessment topic. It is important to note that the proposed curves are a first proposal and they may be improved in further studies and analyses.

4.2. Algorithm organization

The damage scenarios are evaluated by means of an automated algorithm developed in *MathWorks MATLAB* and it is composed by four

main steps as shown in Figure 4.12 and each step will be deepened in the following paragraphs:

- The input data is represented by the inundation depth along the Italian coastline;
- Inundation simulations are performed to evaluate the inland inundation depth assuming two simplified and one refined approach. In particular, the inland surface is divided in several grids based on potentially inundated areas according to New Zealand guidelines *DGL 08-16* and based on a *GIS* system;
- Damage prediction is based on empirical or mechanical fragility curves in terms of number of damaged buildings, reconstruction costs and potential casualties. Information about number of buildings, buildings structural material, building average plan areas and human census are provided by *ISTAT* database;
- Algorithm output is represented by thematic maps in a *GIS* environment in order to provide georeferenced results considering different scales of representation: grid, municipality, provincial and regional scale.

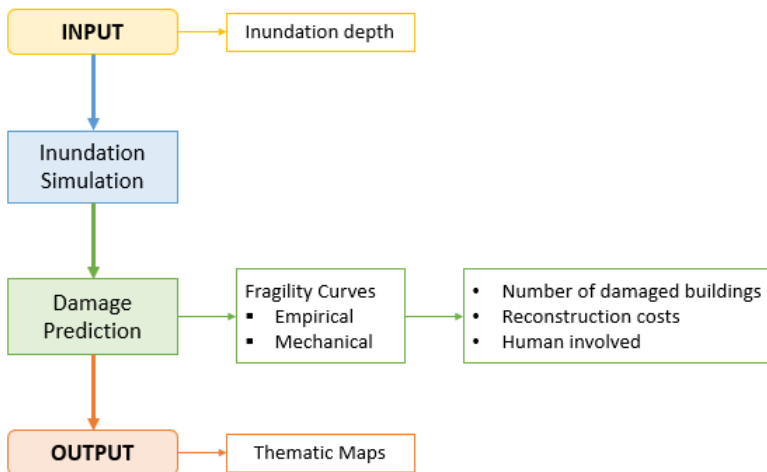


Figure 4.12: Algorithm flow chart

4.2.1. GIS system and census database

GIS, in full “*Geographic Information System*”, is a system designed to capture, store, manipulate, analyse, manage, and present spatial or geographic data. *GIS* applications are tools that allow users to create interactive queries, analyse spatial information, to edit data in maps and to present the results of all these operations. Furthermore, it is possible to link any information in terms of tables, images or text, to a place with specific geographical coordinates. *GIS* system allows to use different types of data: vector or raster and it allows to perform acquisition, recording, analysis, visualization and return of information derived from geographical data and it is composed by:

- *Digital data*: digital information to be displayed and analysed;
- *Hardware*: data visualization and processing;
- *Software*: allows to process digital data.

The software used in this work is “*QGIS*”, an open source software used to analyse and consult the damage scenarios.

The main residential buildings data are provided by *ISTAT* censuses (updated to 2001), based on municipal (Figure 4.13) and census areas (Belliazzi et al. 2017); the main information are related to the number of buildings depending on structural material (masonry or RC), number of storeys, age of construction (the database is updated every ten years), buildings area and demographic censuses.

In particular, the *ISTAT* database provides the total number of buildings and the number of buildings with three or more storeys for all buildings and for concrete structures, depending on the age of construction. Therefore, it is simple to evaluate the number of buildings with a maximum of two storeys for each age of construction. Consequentially, the masonry data are evaluated as difference of the previous data. In this work, the buildings classified as “other typologies”

have been added to masonry structures, on safe side since we count more buildings. Therefore, the buildings are linked to the building classes (Figure 3.5) according to *ISTAT* database.



Figure 4.13: Building data provided by *ISTAT* censuses for Sicily region

4.2.2. Potentially inundated area definition

ISTAT database has been filtered due to large amount of data and only coastal building information is requested to assess tsunami damage scenario. Therefore, three different database filtering procedures are developed according to a safety criterion.

In particular, potentially inundated areas (Belliazzi et al. 2018b) are defined according to New Zealand guideline *DGL 08-16* where potentially inundated areas can be evaluated assuming a simple attenuation law based on the simplified assumption that every meter of wave height along the coast corresponds to 200 m of inland inundation distance, in an assumed horizontal flat surface condition and without considering any obstacle to the wave flux (Figure 4.14).

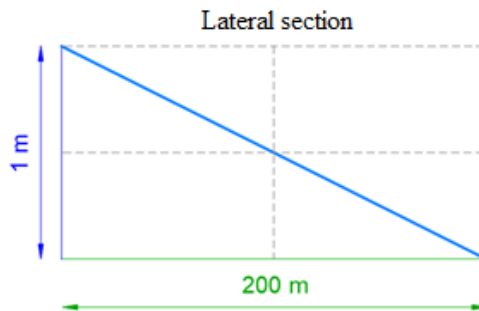


Figure 4.14: Wave attenuation law for the identification of areas potentially subjected to flooding

An inundation depth of 25 meters is assumed on the coastline to establish potentially inundated areas, considering the worst scenario in accordance with hazard maps provided by *TSUMAPS-NEAM* project (*Probabilistic TSUnami hazard MAPS for the NEAM Region*) (Figure 4.15). An inundation depth rounded up to 25 metres, as safety criterion, is obtained near the *Calabria* coasts and an inundation length of 5 kilometers is obtained according to *DGL 08-16* approach.

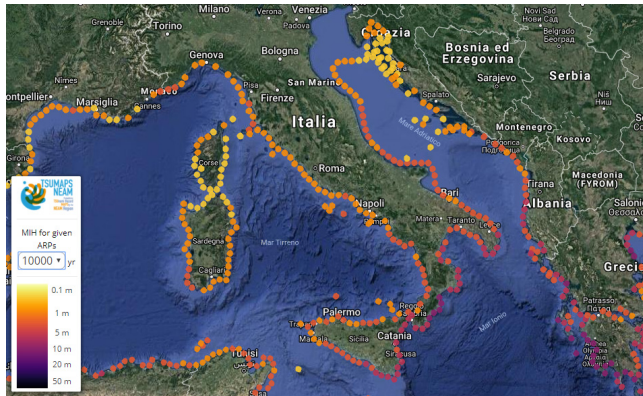


Figure 4.15: Example of a hazard map produced by the TSUMAPS-NEAM project

Figure 4.16 shows an application example of the proposed method for the Sicily region where the potentially inundated areas are represented by the hatched blue area; the northern part of the region is excluded because it is not characterized by high tsunami risk and the focus is on tsunami triggered in the east Mediterranean Sea.



Figure 4.16: Application example of the proposed method for the Sicily region according to DGL 08-16

Furthermore, the potentially inundated area has been discretized into a grid with spacing 50 m in urban areas and 100 m in rural areas (Figure 4.17) because the buildings density and the tsunami risk are

greater in urban areas than rural areas. In addition, high density grid allows to have a higher detail level in urban areas for the damage scenarios output.

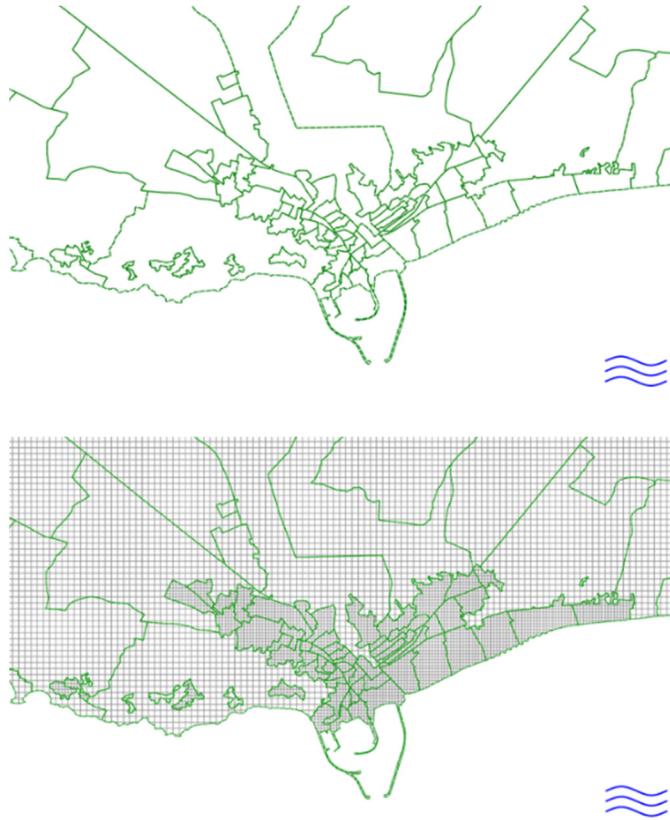


Figure 4.17: Example census areas (in green) and grids (in grey) for Gela city in Sicily region

A second database filter depends on altimetric trend inland. In particular, topographic elevation is added to each grid depending on *Digital Terrain Model (DTM)* with a resolution of 20 meters available at *Italian National Cartographic Portal (PCN) – GEOPORTAL* (Figure 4.18). The extrapolated altitude is based on the grid centre.

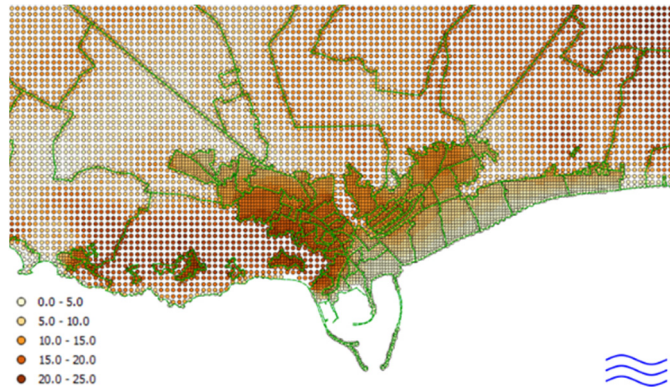


Figure 4.18: Grids altimetric trend represented by a colour gradient for Gela city in Sicily region

The grids with a topographical elevation greater than 25 meters are removed (Figure 4.19) assuming an expected inundation depth based on *DGL 08-16* approach and *TSUMAPS-NEAM* project.



Figure 4.19: Example of grid filter based on altimetric trend for Gela city in Sicily region.
The total number of grids in Sicily region is approximately equal to 230 000 grids

Furthermore, grids without residential buildings are neglected, e.g. rural areas, because they are not interesting for the goal of the project. In addition, this allows to manage less grids and the algorithm performances are increased.

A minimum distance between grid centre and coastline is evaluated for each grid assuming that the water follows the direction of minimum distance between grid centres and coastline as safety criterion (Figure 4.20). The defined lines represent the unidirectional flow direction of tsunami during damage scenarios.

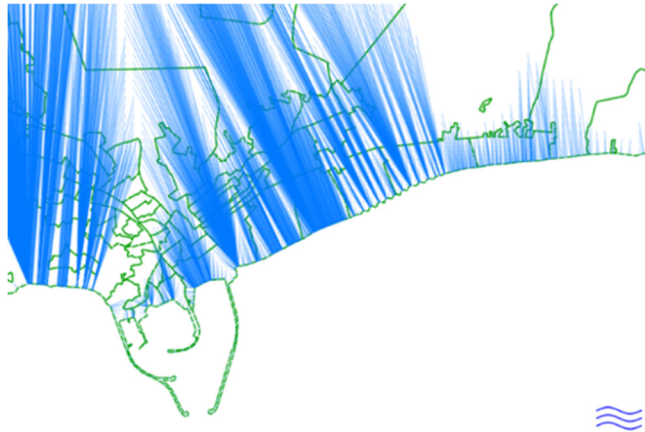


Figure 4.20: Example of minimum distances between grid centres and coastline for each grid for Gela city in Sicily region

The inundation depth inside the grid is assumed constant and it is applied as load to each building in the grid; it allows to assess the building damages and potential casualties through the empirical or mechanical fragility curves described in paragraph §2.3 and §4.1 respectively.

The proposed methodology has been extended along all the coasts interested by the Adriatic Sea, Ionian Sea and Sicily Sea, involving the following regions from north to south: Friuli Venezia Giulia, Veneto, Emilia Romagna, Marche, Abruzzo, Molise, Puglia, Basilicata, Calabria and Sicily. The order of magnitude of created grids number is about 1'400'000 in 10 regions (Figure 4.21). Other regions are neglected because the project is based on potentially tsunamis triggered in east Mediterranean Sea.



Figure 4.21: Potentially inundated areas discretized in 1 400 000 grids

Buildings distribution is assumed constant in each grid and the number of buildings is evaluated with a linear proportional function based on cities and grids areas.

$$\frac{Ed_{COM}}{Ed_{RET}} = \frac{A_{COM}}{A_{RET}}$$

Where Ed_{com} represents the number of buildings of a building class of a generic city (e.g., provided by *ISTAT* database), Ed_{ret} is the equation unknown, A_{com} is the city area (e.g., provided by *ISTAT* database) while A_{ret} represent the grid area.

4.2.3. In situ-surveys

In situ-surveys were performed in Calabria region in order to retrieve useful information for large scale analysis and damage scenarios. Several cities were chosen along the coastline based on buildings density (Figure 4.22) as shown in the following list:

Cities with high buildings density:

- Crotone (2095 buildings)
- Roccella Ionica (1375 buildings)
- Bovalino (1602 buildings)
- Locri (1274 buildings)
- Isola di Capo Rizzuto (2285 buildings)
- Cirò Marina (3067 buildings)

Cities with low buildings density:

- Squillace (185 buildings)
- Grotteria (81 buildings)
- Catanzaro (889 buildings)
- Ardore (917 buildings)
- Monasterace (793 buildings)
- Melissa (730 buildings)

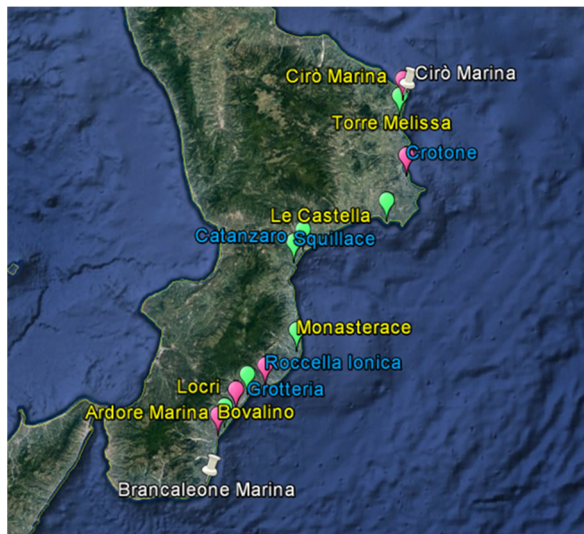


Figure 4.22: Cities inspected during in-situ surveys

Potentially inundated areas were evaluated according to New Zealand guidelines *DGL 08-16* in order to define inspection areas.

In situ-surveys provided important information about expected masonry material type and construction techniques. In addition, surveys provide a feedback of building census databases and they allow to validate the compatibility between actual topography trend and the potentially inundated areas retrieved by a simplified approach adopting a *DTM* with resolution of 20 meters.

4.3. Input data

The proposed damage scenarios algorithm requires only one input parameter that is represented by the inundation depth distribution along the Italian coasts. In particular, building damages are based on empirical or mechanical fragility curves where the probability of exceedance a specific damage state depends on only the inundation depth.

Empirical fragility curves assume the inundation depth as structural demand parameter due to recording ease in the post-tsunami event while in mechanical fragility curves, inundation depth is assumed as engineering demand parameter according to Japanese guidelines and coherently to the adopted regional scale approach. It is important to note that Japanese guidelines allow to describe tsunami loads on structures by means of an equivalent hydrostatic distribution depending on inundation depth only.

The input data depends on Italian coastline provided by “*Italian Institute for Environmental Protection and Research*” (*ISPRA*); in particular, the coastline is provided as an uninterrupted broken line where each point is characterized by its own inundation depth.

The inundation depth along the coasts can be evaluated with three different methods:

- A constant function;
- A random distribution;

- Refined geophysics simulation analysis assuming specific earthquake or submarine landslide.

First and second approaches are useful as preliminary approaches to define potentially high tsunami risk areas while the third method takes into account a specific event and it is recommended for refined and advanced analyses.

4.4. Inundation simulation

The inundation depth on coastline is provided by random population, constant value along the entire coastline or based on refined geophysics simulation related to specific earthquake or submarine landslide, as basic assumption.

The inland inundation simulation is performed assuming three different wave attenuation laws for the inundation depth:

- *Constant function*: the inundation depth value on coastline is assumed constant until a greater altimetric land value is reached;
- *Linear function*: the inundation depth on coastline decreases with a constant slope until a greater altimetric land value is reached;
- *Energy Grade Line (EGL) analysis*: it is the more refined analysis available in literature according to *ASCE 7-16* building code; more details are shown in paragraph §2.1.4.

The first two analyses represent a simple and fast approach to perform inundation simulations, in particular only two parameters are required: the inundation depth on the coastline and altimetric trend along the minimum distance line between a grid centre and the coastline. The slope of linear function attenuation law can be assumed according to DGL 08-16 guidelines as preliminary approach but it is important to note that the proposed method is valid only to define potentially inundated areas.

The third method represents the most refined proposed analysis and it requires several parameters as the inundation depth on the coastline, the altimetric trend along the minimum distance line between the grid centres and the coastline, the Froude number and the Manning coefficient.

Therefore, each minimum distance line between grid centres and coastline is discretized in several points and altitude values are extrapolated from a *DTM* in order to provide the altimetric trend along the minimum distance line and to perform the inundation simulation.

In each point of the minimum distance line, the expected inundation depth h_p is equal to the difference between the inundation depth h evaluated from the coastline altitude and the grid altitude value z_p . The inundation depth is compatible until h_p is positive, while the first negative h_p value defines the *run-up* height.

$$h_{p,i} = h_i - z_{p,i}$$

Figure 4.23 shows an application example of the constant and linear attenuation laws, in particular, two different points P_1 and P_2 characterized by the altitude values z_{p1} and z_{p2} are analysed in an inundation simulation. The case (a) represents an incompatible inundation for grid point P_1 due to negative h_p parameter, while the second case (b) shows a compatible inundation grid point P_2 .

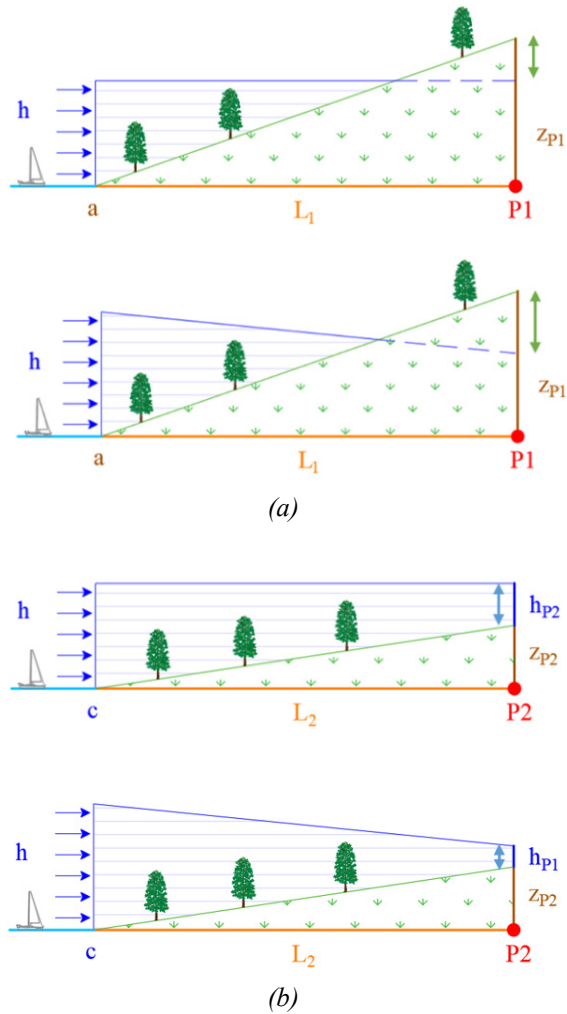


Figure 4.23: Example of constant attenuation laws: incompatible (a) and compatible (b) inundation

In Figure 4.24, an example application is shown of energy grade line (EGL) analysis compared to a constant attenuation law (CAL) analysis; the analysis is performed assuming as basic statement an inundation depth on coastline of 10 meters, a Manning coefficient equal to 0.04 and an unitary and constant Froude number.

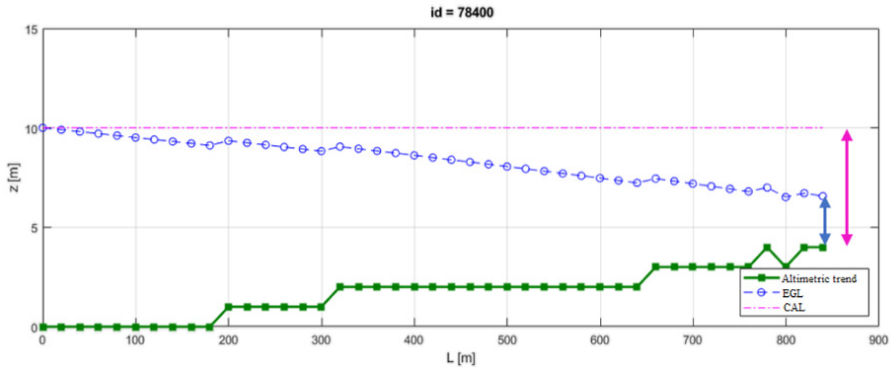


Figure 4.24: Example of EGL analysis compared to constant attenuation law (CAL)

4.5. Damage prediction and Output

The inundation depth calculated in a grid centre is assumed constant in the grid as basic assumption. The damages are linked to the inundation depth through empirical or mechanical fragility curves.

The building group Ed_{ret} of each building class is multiplied by the probability of exceedance, based on the expected inundation depth, depending on the relative fragility curves for each damage state, in order to obtain the number of damaged buildings.

The results in terms of municipality, province and region are based on the sum of the results of each grid.

Damage scenarios are evaluated depending on inundation simulations in terms of potential casualties, number of damaged building and reconstruction costs (Armigliato et al. 2019).

The number of buildings depending on buildings structural material are distributed proportionally in each grid, potential casualties are based on population census while reconstruction costs are based on building average plan areas; each building or population information is provided by the Italian census database (*ISTAT*).

In particular, the reconstruction costs are expressed for each damage state DS as a percentage of a generic cost of 1500 €/m² based on post-earthquake reconstruction costs:

- $DS_1 = 10\%$ of 1500 €/m²;
- $DS_2 = 30\%$ of 1500 €/m²;
- $DS_3 = 60\%$ of 1500 €/m²;
- $DS_4 = 100\%$ of 1500 €/m²;
- $DS_5 = 100\%$ of 1500 €/m².

The reconstruction cost is equal to the sum of all previous DS costs for a building characterized by a specific DS level.

$$C_{DS,n} = \sum_{i=1}^n C_{DS,i}$$

Analysis results are stored in "*shapefile ESRI*" vector files in order to link information to a specific geo-referenced geometry as points, lines or areas.

Thematic maps are realized to show the analysis results on grid, municipality, provincial and regional scale; in particular, every geometric elements contain specific information, for each analysis and specific DS , related to:

- Identifier id ;
- Altimetric value z_P (only for grids);
- Inundation depth h_P (only for grids);
- Damaged buildings;
- Reconstruction costs;
- Potential casualties.

In Figure 4.25 and Figure 4.26 a damage scenario example is shown in terms of thematic maps as algorithm output, while in Appendix B, complete example applications are provided and discussed for several damage scenarios.

The proposed damage scenario (Figure 4.25 and Figure 4.26) is based on the following assumptions: a constant inundation depth distribution along the coastline of 5 meters, a constant attenuation law and empirical fragility curves provided by Suppasri et al. (2013) related to “*The 2011 Great East Japan Tsunami*”. In addition, masonry and concrete buildings distributions are taken into account in the following damage scenarios.

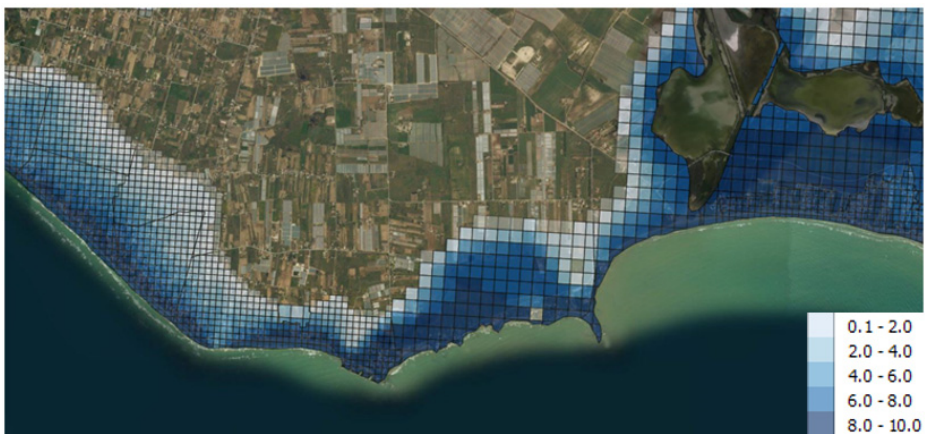
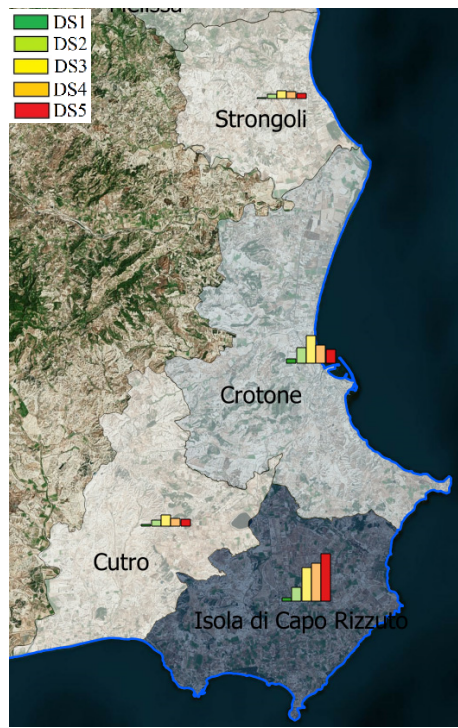


Figure 4.25: Example of inundation simulation in Ispica city (Ragusa, Sicily)



(a)



(b)



(c)

Figure 4.26: Example damage scenarios output in terms of thematic maps: city (a), provincial (b) and regional (c) scale assuming an inundation depth of 5 meters along the coast based on hazard maps provided by TSUMAPS-NEAM project.

Figure (b) shows reconstruction costs related to DS_2 while Figure (a) and (c) show number of damaged buildings by histograms representation.

Chapter 5

Prevention Systems

In the last decades several catastrophic tsunami events have stimulated the attention of the scientific community to clarify the structural behaviour of buildings under tsunami loads and prevention system.

The tsunami event is classified as an extraordinary event characterized by many uncertainties related to several factor as natural or artificial shelter, debris characteristics, altimetric trend, coastal bathymetry near the shore, earthquake damages and structural buildings behaviour.

Furthermore, it is impossible to predict a tsunami event but several prevention systems can be assumed in order to protect international community. The main prevention systems available related to a tsunami event are:

- Evacuation buildings;
- Artificial shelters;
- Early warning systems;
- Retrofitting systems.

The buildings behaviour under tsunami loads depend on many structural and geometrical parameters as materials quality, number of storeys, design approaches. Post-tsunami event surveys show a huge vulnerability of buildings with one or two storeys to tsunami loads independently from the buildings structural material. The most recent international code *ASCE 7-16* affirms that buildings with less than two

storeys must to be evacuated in the case of tsunami events due to high structural vulnerability.

The *ASCE 7-16* provides a design approach for tsunami evacuation buildings in areas with high tsunami risk in order to protect the population during a tsunami event.

In Figure 5.1 an evacuation building in Sendai City in Japan is represented, characterized by lack of vertical closure and this is due to the fact that tsunami forces are superficial forces depending on exposed surface of the structure to the tsunami waves.



Figure 5.1: Example of tsunami evacuation building in Sendai City (Japan)

Another important prevention system is represented by artificial shelters; they are similar to walls built on coastline or near the harbours.

It is an expensive system and it requires a specific design approach but it has high structural performance under tsunami loads and this is the reason why it is strongly recommended in areas with high tsunami risk as the Japanese coasts.

In Japan are commonly named seawalls and the first models were realized with soil but a high vulnerability was due to scour effects. In order to prevent geotechnical failure, piles foundations are taken into account depending on geotechnical parameters. An advanced type is realized made of concrete (Figure 5.2.a) but sliding mechanisms activation occurs and it is vulnerable to large debris impact and

impulsive loads. The latest technologies suggest to realize grid-type seawalls (Figure 5.2.b) in order to allow flow defluxion, or steel-concrete composite seawalls (Figure 5.2.c).

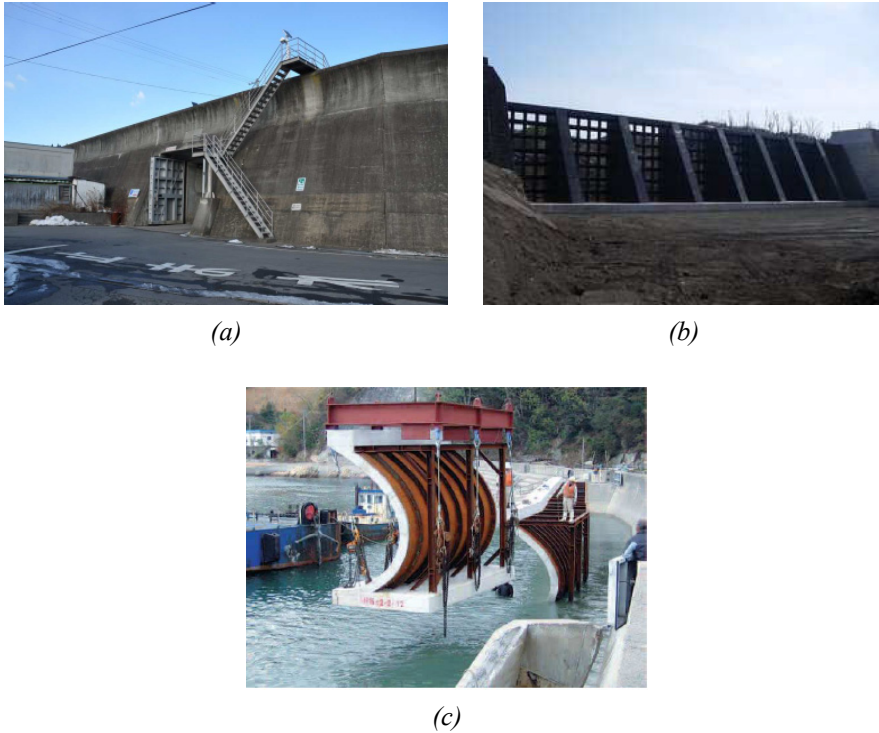


Figure 5.2: Examples of concrete (a), grid type and steel-concrete composite (c) seawalls (Ishikawa et al. 2011)

Another important flood prevention measure is represented by moveable flap-gate type breakwater built in Japanese harbours.

Furthermore, *ASCE 7/16* provides a design approach related to artificial shelters according to structural and geotechnical analysis.

Early warning systems represent a technology designed to mitigate natural disasters as tsunamis, floods, earthquakes, tornadoes, landslides, storms and forest fire.

A tsunami warning system is used to detect tsunamis in advance and provides warnings to prevent human losses and damages to property. It

is realized by a network of sensors to detect tsunamis and a communications infrastructure to issue timely alarms to allow coastal areas evacuation.

Warning system centres use seismic data about nearby recent earthquakes to determine if there is a possible local threat of a tsunami. Such systems are capable of issuing warnings to communities in less than 15 minutes through text messages, phone notifications, TV alerts and sirens. Furthermore, the epicentre, moment magnitude of an earthquake and the probable tsunami arrival times can be quickly calculated but it is almost always impossible to predict tsunami waves without uncertainties and false alarms could occur with these systems as a result.

Several science institutes monitor international sea levels to provide evacuation alarms and one of the most important is the *National Oceanic and Atmospheric Administration (NOAA)* that controls tsunami warnings for most of the Pacific Ocean.

NOAA tsunami warning centre in U.S. developed a specific tsunami warning and evacuation procedure with a 24-hour operational site to receive the warning and established methods of transmitting the warning that will be received by the affected population. Furthermore, it has established and designated evacuation routes for its citizens to high ground or to designated evacuation buildings. In addition, a tsunami evacuation map based on a tsunami inundation map based on assumed scenarios in *ASCE 7/16* is developed and provided to communities.

Another important prevention system is provided by the composite strengthening system with innovative materials as *FRP* and *FRCM* (Carozzi et al. 2015 and Kouris et al. 2018). The use of composite materials like as natural fibers represents a sustainability criterion in order to increase the existing building capacity against the activation of local mechanisms (Belliazzi et al. 2019b). Obviously, it is not

reasonable to apply strengthening systems to all existing buildings in tsunami prone area; in fact buildings characterized by one or two storeys show high vulnerability to tsunami loads as reported in *ASCE 7/16* and strengthening system application are economically advantageous. In fact, evacuation buildings represent one of the best solutions to preserve human life in the case of a tsunami event. Strengthening systems can be used in strategic buildings as hospital, fire and police stations in order to ensure their operation after catastrophic events. Another important aspect is related to preservation of historical heritage in terms of museums or historical buildings (Figure 5.3). In the following paragraph, strengthening system effects are clarified regarding bending capacity of cross sections and in terms of influence on local mechanisms activation for masonry walls under tsunami loads.



(a)



(b)

Figure 5.3: Masonry historical buildings in front of shoreline, City Hall (Trieste, Italy) (a) and San Giuliano Church (La Valletta, Malta) (b)

5.1. Strengthening system with innovative material

Strengthening system with innovative material is characterized by a low cost of manufacturing and time of installation, a higher compatibility with the masonry substrate for the rugged surfaces, a high durability and fire resistance (Caggegi et al. 2017). The masonry is a

brittle material; experimental tests showed that using *FRCM* on masonry can increase the ductility of the structural element. In addition, the reduced thickness of the retrofit system does not influence dynamic characteristics of the structure (Carpentieri et al. 2016), as the period of vibration looking at a combined seismic vulnerability, and the fiber mesh guarantees an improvement of bending strength in both principal directions of retrofitted elements. This method is not invasive on the structure and it is an important aspect in terms of monumental building strengthening. Furthermore, the composite retrofit system guarantees a tensile capacity to the masonry wall cross section and it is a significant improvement for the cross section behaviour due to the negligible tensile strength of unreinforced masonry in terms of bending moment capacity.

The application of the retrofit system is an important aspect, e.g. in the case of *FRCM* application, the masonry surface must be repaired removing refinement materials or weak surfaces and wetted with water to prevent shrinkage phenomena on the mortar matrix. Then a thin layer of mortar is applied on the masonry surface and the fibre grid or mesh is pressed on it.

In this paragraph, the behaviour of masonry walls under tsunami loads is analysed against bending local mechanisms activation and strengthening systems benefits are remarked in terms of *P-M* domain. A useful tool is provided with the aim to design retrofit systems depending on a critical parameter for tsunamis such as the expected inundation depth. All the results are normalized in order to provide generalizable results applicable to any masonry cross section and condition.

5.1.1. Materials behaviour

Several stress-strain relationships are proposed in international codes and guidelines in order to model the mechanical behaviour of

masonry and composite strengthening systems. The aim is to derive normalized equations to evaluate the ultimate bending moment of a masonry cross section reinforced with a composite strengthening system. Therefore, a non-linear behaviour is considered for masonry material according to *Eurocode 6 (EC6)* while a linear behaviour is assumed for the mechanical response of composite strengthening systems according to the Italian guidelines *CNR DT 200 R1/2013* and *CNR DT 215/2018*.

5.1.1.1. Masonry

The mechanical behaviour of masonry in compression is described by a non-linear behaviour defined by two functions as shown in Figure 5.4. In particular, it is composed by a first parabolic function from zero strain up to the first yielding strain and a second constant function from the yielding strain up to the ultimate strain.

$$\sigma_1[\varepsilon_m] = f_m \left(2 \frac{\varepsilon_m}{\varepsilon_{m0}} - \left(\frac{\varepsilon_m}{\varepsilon_{m0}} \right)^2 \right) \quad \text{if } 0 \leq \varepsilon_m \leq \varepsilon_{m0}$$

$$\sigma_2[\varepsilon_m] = f_m \quad \text{if } \varepsilon_{m0} \leq \varepsilon_m \leq \varepsilon_{mu}$$

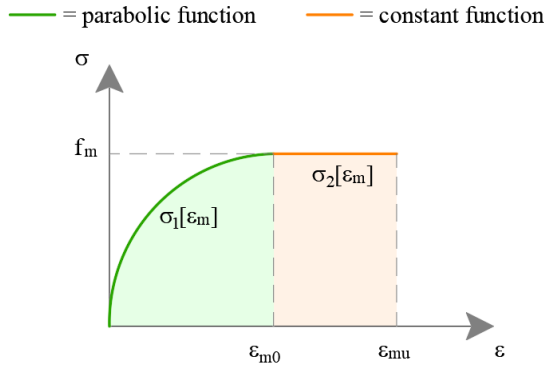


Figure 5.4: Mechanical behaviour of masonry in compression

The collapse is achieved when the ultimate strain of one of the materials is reached if the analysed cross section is characterized by more than one material with different behaviours and ultimate strains. The evaluation of ultimate bending moment is direct due to the stress-block theory application in classic masonry cross section analysis assuming only masonry material. In the case of strengthening systems applied to masonry walls, the section analysis must consider different failure modes such as crushing of masonry or rupture of strengthening system.

In the case of reinforcement rupture, the most compressed masonry fiber has a strain lower than the ultimate strain ε_{mu} and the classical stress-block theory is not applicable. The compressed masonry resultant could be evaluated with a fiber model of cross sections obtaining an acceptable approximated solution. An extension of stress-block theory is provided to obtain an exact solution in terms of an effective height ψ and an effective depth of compression zone centre λ . These parameters are evaluated assuming an equivalence between the actual behaviour and a fictitious rectangle (Figure 5.5) and fixing the maximum concrete strain ε_m .

$$\psi[\varepsilon_m] = \frac{\int_0^{\varepsilon_m} \sigma[\varepsilon_m] d\varepsilon_m}{f_m \varepsilon_m}$$

$$\lambda[\varepsilon_m] = 1 - \frac{\int_0^{\varepsilon_m} \varepsilon_m \sigma[\varepsilon_m] d\varepsilon_m}{f_m \varepsilon_m^2 \psi[\varepsilon_m]}$$

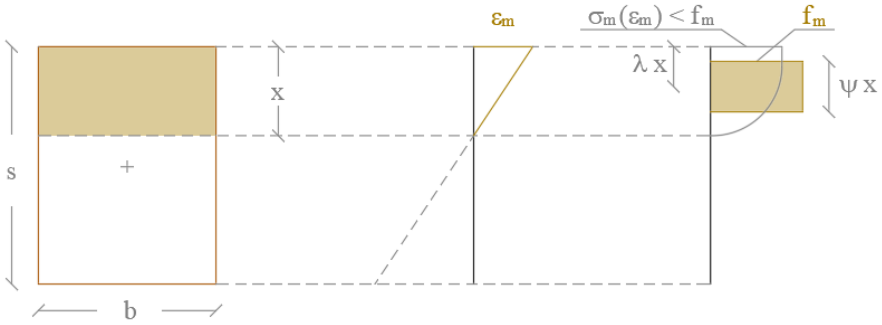


Figure 5.5: Compression parameters ψ and λ

The solutions are provided by the following equations:

$$\text{if } 0 \leq \varepsilon_m \leq \varepsilon_{m0} \rightarrow \begin{cases} \psi_1[\varepsilon_m] = \frac{\varepsilon_m (\varepsilon_m - 3 \varepsilon_{m0})}{3 \varepsilon_{m0}^2} \\ \lambda_1[\varepsilon_m] = \frac{\varepsilon_m - 4 \varepsilon_{m0}}{4 \varepsilon_m - 12 \varepsilon_{m0}} \end{cases}$$

$$\text{if } \varepsilon_{m0} \leq \varepsilon_m \leq \varepsilon_{mu} \rightarrow \begin{cases} \psi_2[\varepsilon_m] = 1 - \frac{\varepsilon_{m0}}{3 \varepsilon_m} \\ \lambda_2[\varepsilon_m] = \frac{1}{4} \left(1 - \frac{\varepsilon_{m0}}{\varepsilon_m} - \frac{3 \varepsilon_m}{\varepsilon_{m0} - 3 \varepsilon_m} \right) \end{cases}$$

The end of parabola strain ε_{m0} and ultimate strain ε_{mu} for masonry are assumed respectively equal to 2‰ and 3.5‰ according to *Eurocode 6 (EC6)*.

Conversely for the tensile behaviour, the stress is neglected due to the basic assumption that the existing masonry is cracked.

5.1.1.2. Strengthening system

Several direct tensile tests (Lignola et al. 2017) have been done to investigate *FRCM* systems behaviour under a tensile loading; from the

resulting diagram, three different stages can be defined: un-cracked, crack development, cracked.

During the first stage, the reinforcement layer is undamaged and its behaviour is linear. Then, the beginning of the second stage is identified by the appearance of the first crack. A stiffness reduction is registered increasing the number of cracks with the increase of the external load. In these first two phases, the behaviour of the composite material is influenced by the mechanical characteristics of the mortar, the textile and the textile/mortar interface from which the stress transfer depends.

At a particular strain, the crack pattern stabilizes and an increase of the tangent stiffness is registered; it is the beginning of the third phase. The failure of the system in the majority of the cases happens because of the textile rupture in tension, in particular, after the first cord breaks, the damage propagates rapidly in all the other cords.

The desired stiffness of the *FRCM* is provided by the appropriate combination of matrix and fibers in terms of individual material properties (modulus of elasticity) and thicknesses.

The most important failure modes registered by the tests are debonding from the substrate, slippage of the textile, tensile rupture of the textile (De Santis et al. 2017).

Therefore, the actual behaviour of composite systems is variable due to the interaction between the fibers and the matrix; also, the type of fibers and matrix influences the final behaviour. Theoretically, the fibers have a linear behaviour while the matrix influences at low strain values with tension stiffening. In the case of organic matrix (*FRP*), the matrix contribution is negligible, therefore the tensile behaviour can be assimilated to the linear behaviour of the fibers. In the following cross section analysis, a linear tensile behaviour is assumed for composite strengthening systems (Figure 5.6), as it is for *CNR-DT 200R1/2013*, or due to the assumptions that the matrix is cracked according to *CNR-DT*

215/2018. In particular, the linear behaviour is defined by an ultimate composite strain ε_{fu} and an elastic modulus E_f .

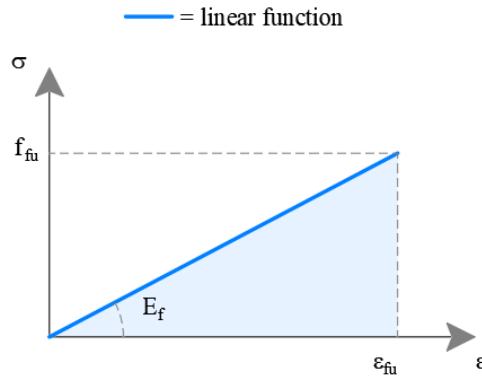


Figure 5.6: Tensile mechanical behaviour of composite strengthening systems

The compressive behaviour is neglected according to Italian guidelines *CNR-DT 200 R1/2013* and *CNR DT 215/2018*.

5.1.2. *P-M interaction diagrams*

P-M interaction diagrams are evaluated in order to clarify the behaviour of masonry walls to horizontal and vertical bending mechanisms and the influence of strengthening systems to the flexural capacity.

The cross section analysis is carried out at the ultimate limit state considering the following basic assumptions according to Italian guidelines *CNR-DT 200 R1/2013* and *CNR DT 215/2018*:

- Conservation of plain sections (linear strain diagrams)
- Masonry is neglected in tension;
- Compression contribution of strengthening system to flexural capacity is zero due to its slenderness;

- Perfect bond between composite system and masonry; strengthening system strain is equal to masonry strain:

$$\varepsilon_m = \varepsilon_f$$

- The ultimate condition of the cross section can be reached by crushing of the compressed masonry or tensile failure of the composite system depending on ultimate composite strain as shown in the following.

Three different failure modes are analysed in order to consider all materials collapse possibilities and the correspondent equilibrium equations are normalized to geometrical and mechanical parameters in order to provide generalizable results that can be used for any masonry wall.

The neutral axis depth x is assumed to be normalized with wall thickness s as basic assumption and the ratio x/s is indicated as ξ .

Assuming the linear strain diagrams, hence considering the conservation of plain sections, it is possible to define dimensionless parameter ξ for balanced collapses that represents the critical ξ corresponding to failure mode changes.

$$\xi_{bal,1} = \frac{\varepsilon_0}{\varepsilon_0 + \varepsilon_{fu}}$$

$$\xi_{bal,2} = \frac{\varepsilon_{mu}}{\varepsilon_{mu} + \varepsilon_{fu}}$$

Furthermore, an additional concentrated load N_s is considered for modelling self-weight and the effect of other storey weights and the moment capacity is obtained by writing a rotation equilibrium around the centroid of the masonry cross section.

In particular, the first failure mode represented by n_1 and m_1 equations, consider that composite strain reaches the ultimate strain

value ε_{fu} and the most compressed masonry fiber has a strain that does not exceed the ε_{m0} strain value (Figure 5.7).

$$if\ 0 \leq \xi < \xi_{bal,1} \rightarrow \begin{cases} n_1 = \frac{N_1}{b s f_m} = \psi_1[\varepsilon_m] \xi - \omega \frac{\varepsilon_{fu}}{\varepsilon_{mu}} \\ m_1 = \frac{M_1}{b s^2 f_m} = \psi_1[\varepsilon_m] \xi (0.5 - \lambda_1[\varepsilon_m] \xi) + 0.5 \omega \frac{\varepsilon_{fu}}{\varepsilon_{mu}} \end{cases}$$

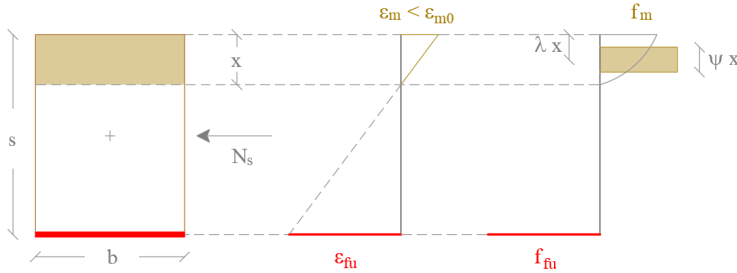


Figure 5.7: Strain and stress diagrams for first failure mode

The second failure mode (n_2 , m_2) assumes that composite strain reaches the ultimate strain value ε_{fu} and the most compressed masonry fiber has a strain that is between ε_{m0} and ε_{mu} (Figure 5.8).

$$if\ \xi_{bal,1} \leq \xi < \xi_{bal,2} \rightarrow \begin{cases} n_2 = \frac{N_2}{b s f_m} = \psi_2[\varepsilon_m] \xi - \omega \frac{\varepsilon_{fu}}{\varepsilon_{mu}} \\ m_2 = \frac{M_2}{b s^2 f_m} = \psi_2[\varepsilon_m] \xi (0.5 - \lambda_2[\varepsilon_m] \xi) + 0.5 \omega \frac{\varepsilon_{fu}}{\varepsilon_{mu}} \end{cases}$$

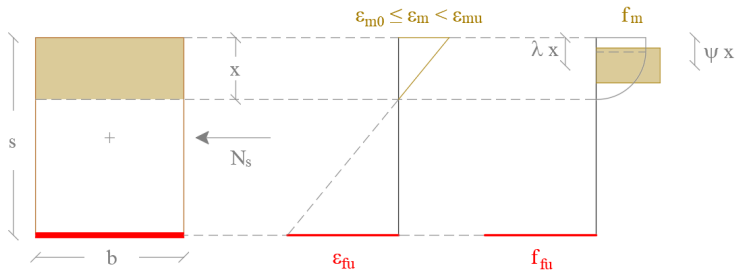


Figure 5.8: Strain and stress diagrams for second failure mode

The last failure mode (n_3, m_3) is characterized by crushing of the compressed masonry (ε_{mu}) and a linear behaviour of the composite before tensile failure (Figure 5.9).

$$if \xi_{bat,2} \leq \xi \leq 1 \rightarrow \begin{cases} n_3 = \frac{N_3}{b s f_m} = \psi_3[\varepsilon_{mu}] \xi - \omega \frac{1 - \xi}{\xi} \\ m_3 = \frac{M_3}{b s^2 f_m} = \psi_3[\varepsilon_{mu}] \xi (0.5 - \lambda_3[\varepsilon_{mu}] \xi) + 0.5 \omega \frac{1 - \xi}{\xi} \end{cases}$$

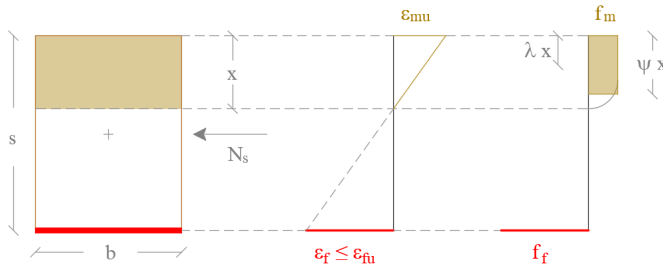


Figure 5.9: Strain and stress diagrams for third failure mode

The composite mechanical percentage is expressed in terms of ratios between masonry and strengthening system stiffnesses. In fact, it is possible to consider the ratio ε_{mu}/f_m like as an elastic modulus because ε_{mu} is a pure number while the compressive strength f_m can be expressed as an elastic modulus according to *Eurocode 6 (EC6)*.

$$E_m = 10^3 f_m$$

$$\omega = \frac{t_f \varepsilon_{mu}}{s f_m} E_f = 10^3 \frac{t_f E_f}{s E_m} \varepsilon_{mu}$$

If ξ is greater than 1, the entire cross section is compressed, the composite system does not carry loads in compression as a basic assumption and the equation degenerates in the classic equilibrium equation considering only the masonry material.

$$\text{if } 1 < \xi \leq 1/\psi_3[\varepsilon_{mu}] \rightarrow \begin{cases} n_4 = \frac{N_4}{b s f_m} = \psi_3[\varepsilon_{mu}] \xi \\ m_4 = \frac{M_4}{b s^2 f_m} = \psi_3[\varepsilon_{mu}] \xi (0.5 - \lambda_3[\varepsilon_{mu}] \xi) \end{cases}$$

In addition, the generic masonry strain is expressed by the following normalized equation:

$$\varepsilon_m = \frac{\xi}{1 - \xi} \varepsilon_{fu}$$

The proposed equations are dependent on three different parameters that are the composite ultimate strain ε_{fu} , the composite mechanical percentage ω and the dimensionless neutral axis depth ξ .

It is important to note that first and second equations are valid only for ω values greater than zero while, in other cases, only the third equation describes the P - M interaction chart.

5.1.3. Parametric analysis

Parametric analyses are performed in order to clarify the effects of composite ultimate strain ε_{fu} and the composite mechanical percentage ω in the P - M interaction diagram. The parameters range are based on materials available on the market and experimental test database.

It is important to specify the meaning of the investigated parameters, the composite mechanical percentage ω is defined as a ratio between composite and masonry stiffnesses while the ultimate strain ε_{fu} is the composite mechanical parameter that influences the contribution of the strengthening system.

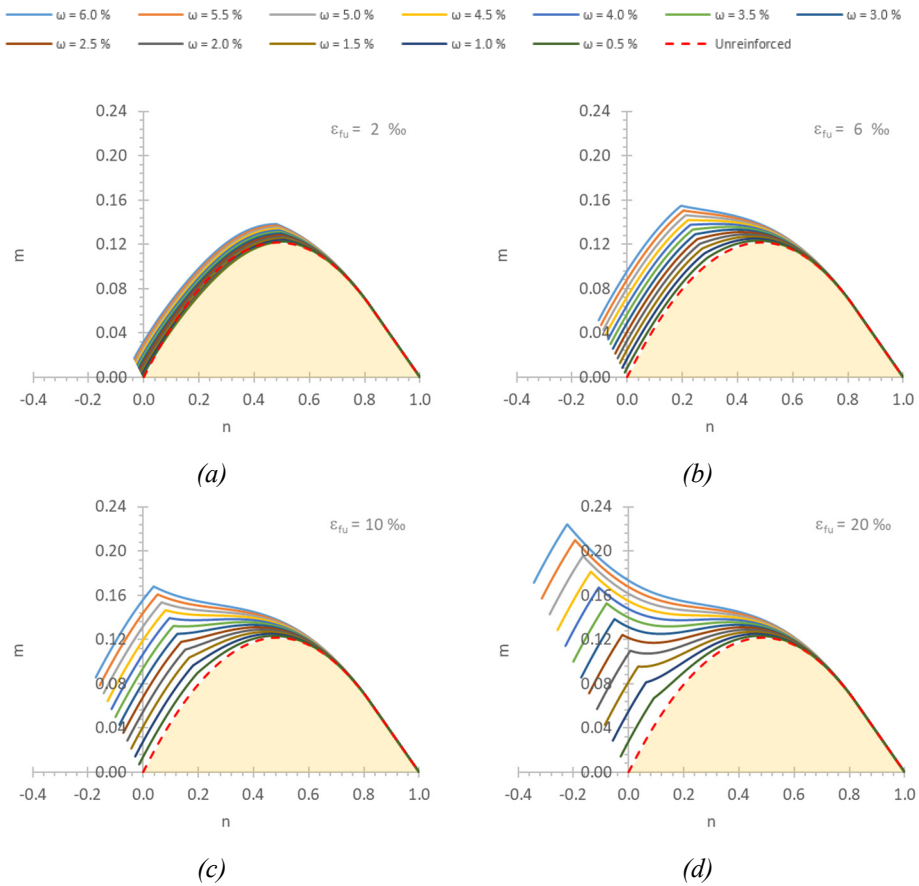


Figure 5.10: P - M interaction diagrams changing the composite mechanical percentage ω and fixed composite ultimate strain ϵ_{fi} equal to 2 ‰ (a), 6 ‰ (b), 10 ‰ (c) and 20 ‰ (d)

In Figure 5.10, P - M interaction diagrams are shown for several composite mechanical percentages ω while the composite ultimate strain ϵ_{fi} is fixed; and it is clear that at low ultimate strains the bending capacity increment depending on ω is negligible. Conversely, at high ultimate strains, small increments of the composite mechanical percentage give significant benefits in terms of bending capacity for the cross section. Angular points represent the failure mode changes.

In addition, it is clear that small increments of composite mechanical ratios provide significant benefits in terms of bending

capacity for the cross section at low axial load levels. In fact, it is assumed that masonry does not carry tractions and the cross section has no bending capacity at zero axial load. Adding a strengthening system to the cross section, that carries tractions, yields to clear benefits at low axial loads in terms of bending capacity.

It is interesting to note that for high axial loads, the benefits of a strengthening system are limited at increasing the composite mechanical ratio. This is due to the higher values of neutral axis depth that yields to a limited strain level in the composite fibers and, consequentially, a limited contribution to the flexural capacity of the cross section.

Furthermore, for high ultimate strains and composite mechanical percentages the maximum bending capacity is reached corresponding to zero axial loads, and it can be defined as a beam behaviour (i.e. pure flexure).

As mentioned above, the upper bound limit of failure mode two could be very important in order to preserve heritage masonry buildings after strengthening design. As shown in Figure 5.10, low ultimate strain values ε_{fu} require high composite mechanical percentages ω to gain significant bending capacity increments.

In Figure 5.11 P - M interaction diagrams are shown for several composite ultimate strains ε_{fu} and at fixed composite mechanical percentages ω ; it is clear how the ultimate strain influences the domain for the third failure mode function and in particular, the lower bound of function decreases while increasing composite ultimate strain due to an higher ultimate curvature of cross section.

It is important to note that in particular cases, the strengthening systems with a low ultimate composite strain and mechanical percentage could not provide benefits in terms of bending capacity. In fact, all curves below the red dashed line (filled in yellow) are characterized by bending moment capacity of cross sections lower than that of a cross

section without any strengthening system. They are representative of cases where the strengthening strategy is ineffectual and the ultimate capacity is certainly governed by the masonry.

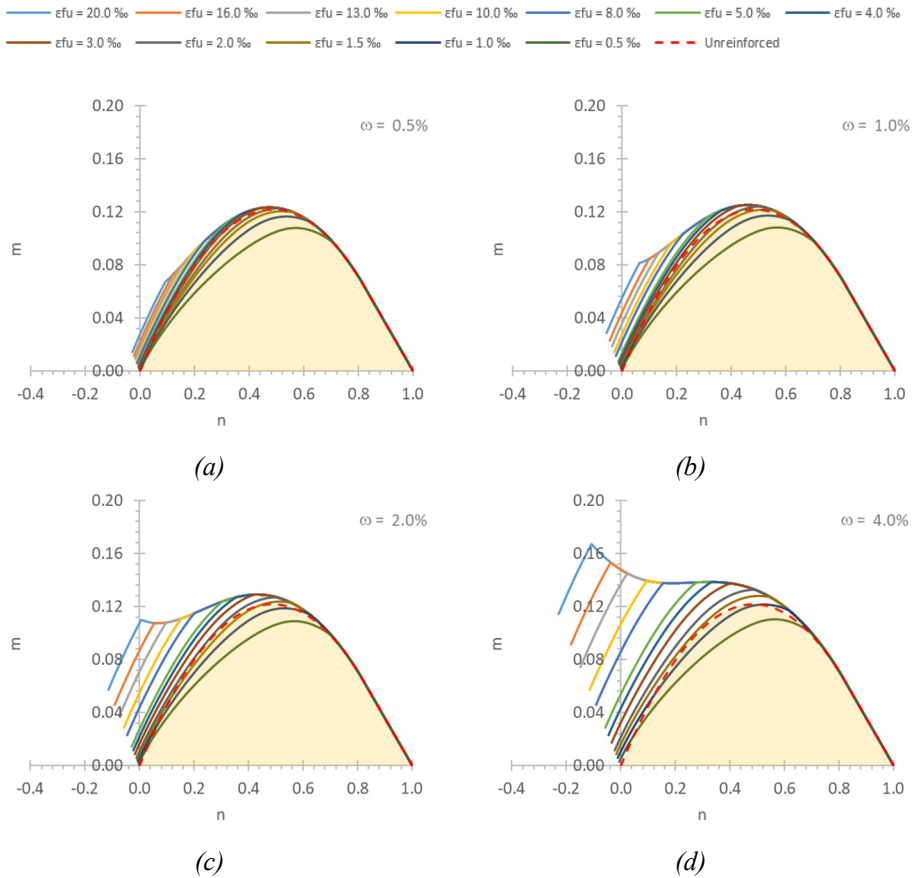


Figure 5.11: *P-M* interaction diagrams while changing composite ultimate strain ϵ_{fu} and at a fixed composite mechanical percentage ω equal to 0.5 % (a), 1.0 % (b), 2.0 % (c) and 4.0 % (d)

Furthermore, in each chart of Figure 5.10 and Figure 5.11 it is possible to observe how the effect of strengthened systems are negligible at high normalized axial load values due to the zero compressive resultant of composite material.

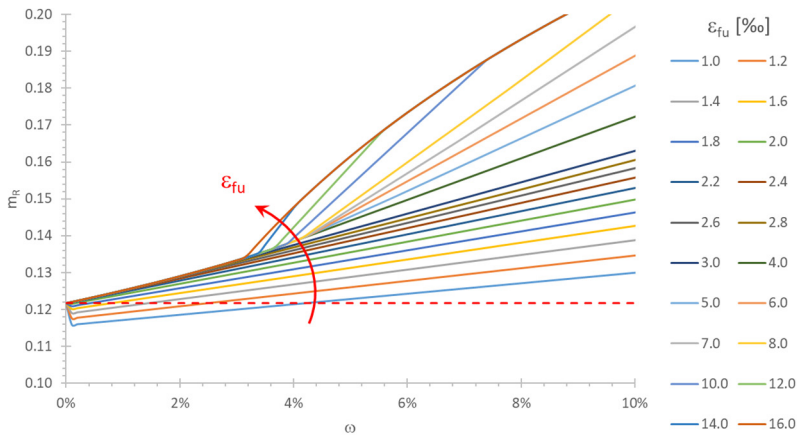


Figure 5.12: Maximum ultimate bending moment m_r – composite mechanical percentage ω diagram while changing the composite ultimate strain ε_{fu}

The red dashed line represents the maximum ultimate bending moment for a cross section without any strengthening system; therefore, for composite mechanical percentages ω equal to zero, it is possible to extrapolate the ultimate bending moment of the cross section without any composite strengthening system.

All curves tend to overlap in one single curve that represents simple bending cases except for the curves characterized by low composite ultimate strain due to the reduced effects on the flexural capacity. For high composite mechanical percentages and ultimate strain values, the maximum bending moment is evaluated at zero axial load (i.e. pure bending) due to negative axial load that characterized bending moment capacity of masonry wall as explained in the following paragraph.

5.1.4. Retrofit system effects on out-of-plane mechanisms

Generally, existing masonry buildings show a high vulnerability to out-of-plane mechanisms activation due to disconnections among walls as reported in post-tsunami event reports and derived fragility curves.

In this paragraph, retrofit system effects on out-of-plane mechanisms (Bellini et al. 2017) are discussed in terms of vertical and horizontal bending mechanisms by means of P - M interaction charts.

5.1.4.1. Vertical bending mechanism

The activation of vertical bending out-of-plane mechanism occurs when maximum external bending moment equals the cross section capacity.

External maximum bending moment trend is evaluated assuming masonry wall modelled as a simply supported beam in order to assess the strengthening system benefits.

Linear analyses are performed considering a mechanical model composed by a simply supported beam with a linear (triangular or trapezoidal) load pattern characterized by a variable inundation depth and a constant slope (equal to the water density) according to the Japanese approach where tsunami loads on structures are described adopting one equivalent hydrostatic load as shown in Chapter 3. The simply supported beam length is equal to the interstorey height H_i .

Furthermore, on the top, an additional concentrated load N_m is considered to model self-weight and the effect of other storey weights. Therefore, a normalised external axial load on the cross section is assumed variable in a range up to about 40% of ultimate axial load capacity of the walls, the corresponding ultimate bending moment is evaluated considering P - M interaction diagrams.

The external bending moment is evaluated according to paragraph §3.4.2.1, where the equations depend on the ratio s/H_i that represents the geometrical vertical slenderness of the masonry wall.

The previous equations have been plotted (Figure 5.13) for different constant values of the geometrical slenderness of the wall s/H_i considering the ratio m_s/k on the y-axis and h/s on the x-axis.

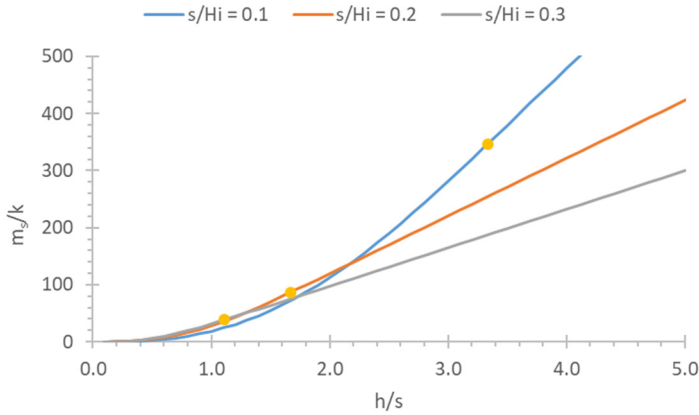


Figure 5.13: Dimensionless critical bending moment

The circular marks represent the points where the triangular load pattern is substituted by the trapezoidal load pattern; these points are evaluated by the simple equality:

$$\eta h = H_i \rightarrow \frac{h}{s} = \frac{1}{\eta \frac{H_i}{s}}$$

The order of magnitude on y-axis is large due to the adimensional constant k value that is usually variable in the range 10^{-4} to 10^{-5} and in particular, it depends mainly on the ratio H_i/f_m because the other parameters can be considered constant in this study.

In addition, in Figure 5.13, the curves overlap due to the influence of wall thickness s despite the external bending moment is independent on the wall thickness.

In order to clarify retrofit system effects, several normalized P - M interaction diagrams are plotted (Figure 5.14) considering different values of the composite mechanical ratio ω , ultimate composite strain ε_{fu} and external normalized axial load values n . Generally, normalized axial loads in real structures range between 0.1 and 0.4.

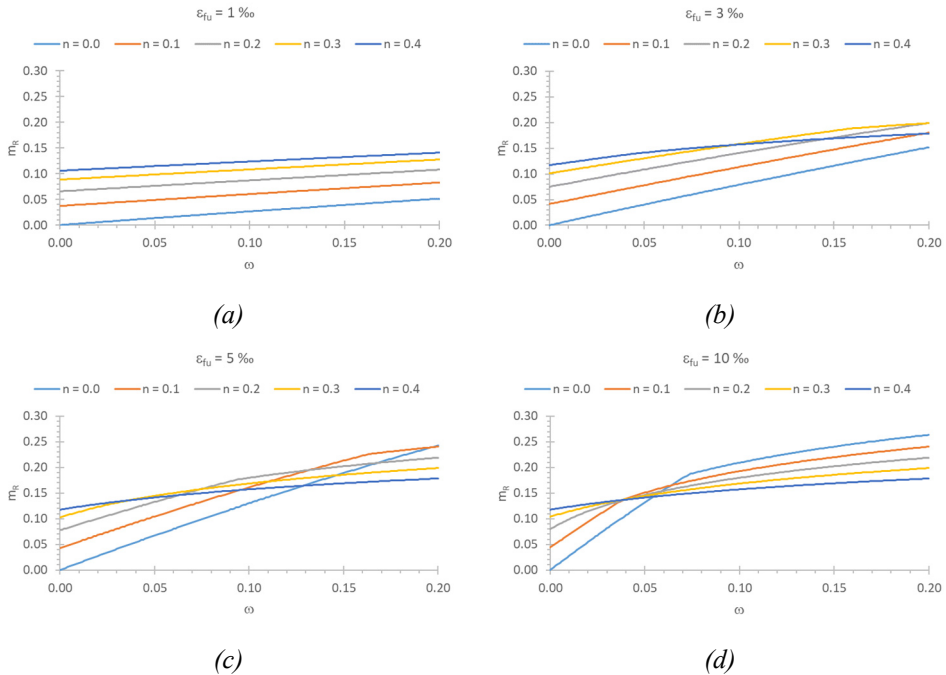


Figure 5.14: Ultimate bending moment diagrams of masonry cross section for different composite properties (1 ‰ (a), 3 ‰ (b), 5 ‰ (c) and 10 ‰ (d)) and fixed external axial loads

For ω equal to zero, it is possible to extrapolate the bending capacity of the cross section without retrofit systems (i.e. unreinforced). In addition, it is clear that small increments of composite mechanical ratios provide significant benefits in terms of bending capacity for the cross section. In fact, it is assumed that masonry does not carry tractions and the cross section has no bending capacity at zero axial load while adding a retrofit system to the cross section that carries only tractions, the benefits at small external axial loads are significant in terms of bending capacity.

It is interesting to note that for high external axial loads, the benefits of a retrofit system are limited by increasing the composite mechanical ratio. This is due to the higher values of neutral axis depth that causes a

limited strain in the composite fibers and, consequentially, a limited fiber contribution.

The proposed diagrams in Figure 5.13 and Figure 5.14 can be useful to design a retrofit system for existing masonry buildings in tsunami prone areas. A numerical example is reported in order to check the potential of the proposed diagrams. In particular, the minimum composite mechanical ratio to guarantee the minimum structural capacity against the activation of vertical bending mechanisms can be easily evaluated by coupling the proposed diagrams, once the expected inundation depth is given.

For example, it is possible to consider a category of walls having an interstorey height H_i of 4.0 meters, an average compressive strength f_m of 6.0 MPa and a normalized external axial load n equal to 0.1. For the composite made of natural fibers, an ultimate strain is assumed equal to 5%. In addition, the following assumptions are made for the constant parameters:

$$\alpha = 0.7;$$

$$\eta = 3;$$

$$g = 9.81 \text{ m/s}^2;$$

$$\rho = 1.1 \text{ ton/m}^3.$$

The density of water ρ assumes that the tsunami flows consist of a mixture of sediment and seawater as reported in *FEMA P-646*.

In this case, the k parameter is equal to $9.32 \cdot 10^{-5}$ and multiplying the external bending moment by k , it is possible to compare the external demand with the capacity of cross section in terms of bending moment (Figure 5.15).

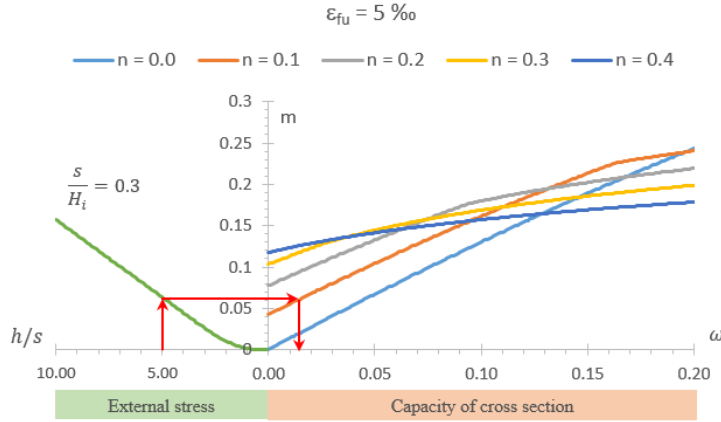


Figure 5.15: Comparison between normalized external bending moment (demand) and bending capacity of cross section

A design chart (Figure 5.16) can be easily obtained by imposing the equality between the external bending moment and the ultimate bending moment of the wall cross section.

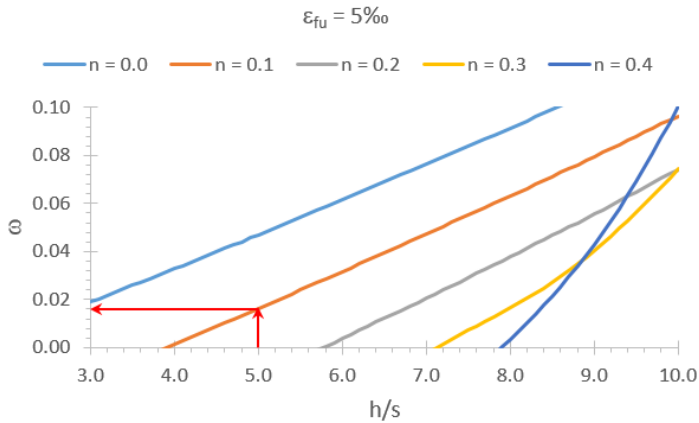


Figure 5.16: Design chart of minimum composite mechanical percentage ω .

Assuming the ratio between the expected inundation depth h and the wall thickness s equal to 5.0, for the considered wall proprieties ($n = 0.1$), a minimum composite mechanical ratio of about 1.6% is required,

yielding to a direct design of a fiber system having $t_f E_f = 32.9 \text{ kN/mm}$. It is evident that at higher axial loads, the increases of composite mechanical percentage ratios become steeper, as the failure is mainly due to masonry.

The proposed design chart represents a fast tool to quantify and design strengthening systems for a masonry wall that shows high vulnerability to vertical bending mechanisms under tsunami loads.

Furthermore, the vertical bending mechanisms are activated when the ultimate bending capacity of the cross section is achieved in a generic section of the masonry wall. The most stressed cross section position is not unique and could be influenced by geometry and mechanical properties of masonry wall and external loads distribution.

The bending moment capacity of masonry wall cross section is assessed with a classical cross section analysis and it is influenced by the external axial loads due to structural components weight and, generally, gravity loads.

In Figure 5.17 the effects of strengthening systems on flexural capacity of cross sections are shown for different composite mechanical percentages ω and composite ultimate strain ε_{fu} values in terms of ratio between ultimate bending moment with and without strengthening system. Furthermore, angular points represent the change of failure mode functions while the red dot line represents the P - M curve of a masonry wall without any strengthening system.

It is important to note that strengthening system application does not change the behaviour of a masonry wall and it gives a significant benefit in terms of flexural capacity of the cross section for typical normalized axial loads n of the masonry walls ranging between 0.05 and 0.30, if properly designed. For zero axial loads, the ratio m_ω/m_0 is mathematically infinite because m_0 is zero, therefore, for low axial load values the strengthening system gives enormous benefits.

In special cases, strengthening systems with a low ultimate composite strain and mechanical percentage could not provide benefits in terms of bending capacity; in fact, all the curves below the dashed line are characterized by a bending moment capacity of the cross section lower than the one of cross section without strengthening system.

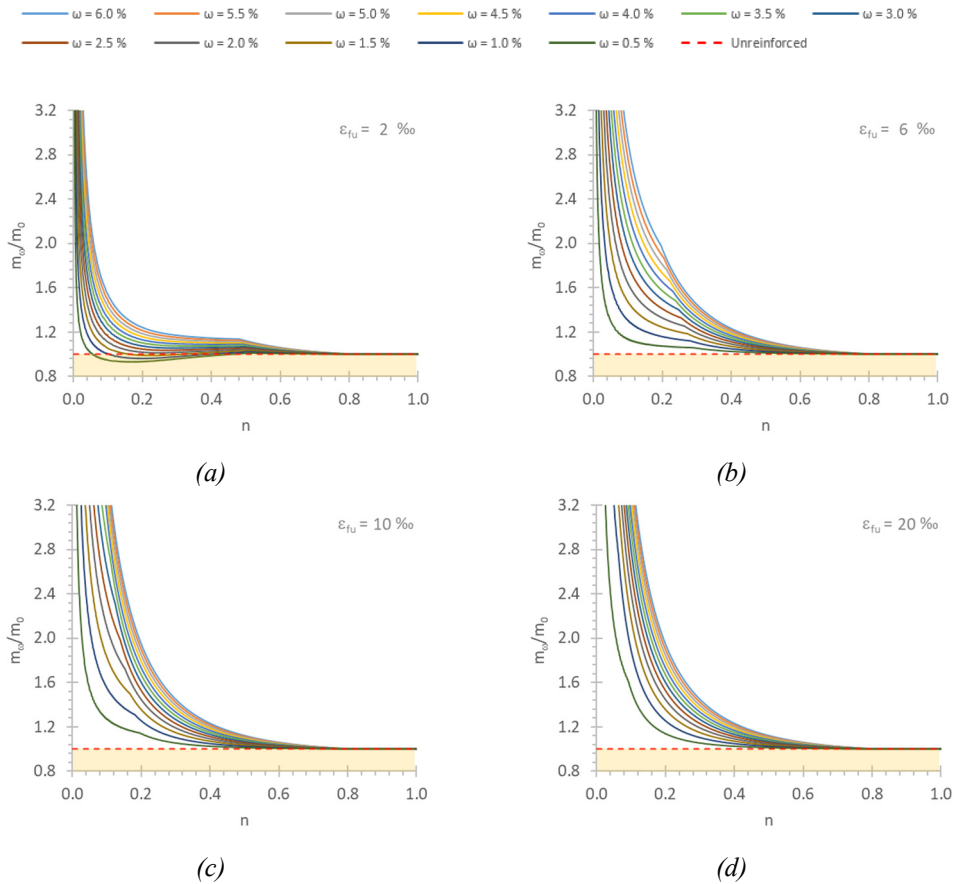


Figure 5.17: Ultimate bending moment increase versus normalized axial load, assuming ϵ_{fu} equal to 2‰ (a), 6‰ (b), 10‰ (c) and 20‰ (d) at different ω values

5.1.4.2. *Horizontal bending mechanism*

The horizontal out-of-plane mechanisms (Guadagnuolo et al. 2008) of masonry walls are highly dependent on connection degree between walls. In fact, unconfined or confined masonry walls show a different out-of-plane behavior in the case of horizontal bending mechanism.

An extremely weak connection promotes a collapse mechanism due to a simple overturning of the masonry walls (Coccia et al. 2016). In this case, the out-of-plane capacity is governed by the rotational equilibrium of a rigid block.

Unconfined masonry walls show a bending capacity due to unit interlock (Vaculik et al. 2017) and they are characterized by rigid block rotation around cylindrical hinges (D. D'Ayala et al. 2003). The inclination and extension of the cylindrical hinges depend on the characteristics of the masonry wall (wall openings and sizes).

The resistance mechanism of confined walls is provided by an arch mechanism. The classic theory is based on plastic analysis assuming the masonry crushing as main failure mode (D. D'Ayala et al. 2003 and De Lorenzis 2008). The limit condition that activates the mechanism is obtained by equating the external load and the capacity of cross section in terms of axial load. If the masonry wall is modelled by the means of an equivalent frame, the compressed isostatic lines depend on restraint conditions. The classic theory provides an optimum mechanical solution in terms of bending moment, assuming an equivalent frame restrained by rotational spring supports. The provided solution is an intermediate case between a simply supported beam and a fixed beam (Figure 5.18) where the bending moment is equal at the mid span and at the ends of the beam. In this case, shear failures are prevented due to the assumption of high friction between masonry walls.

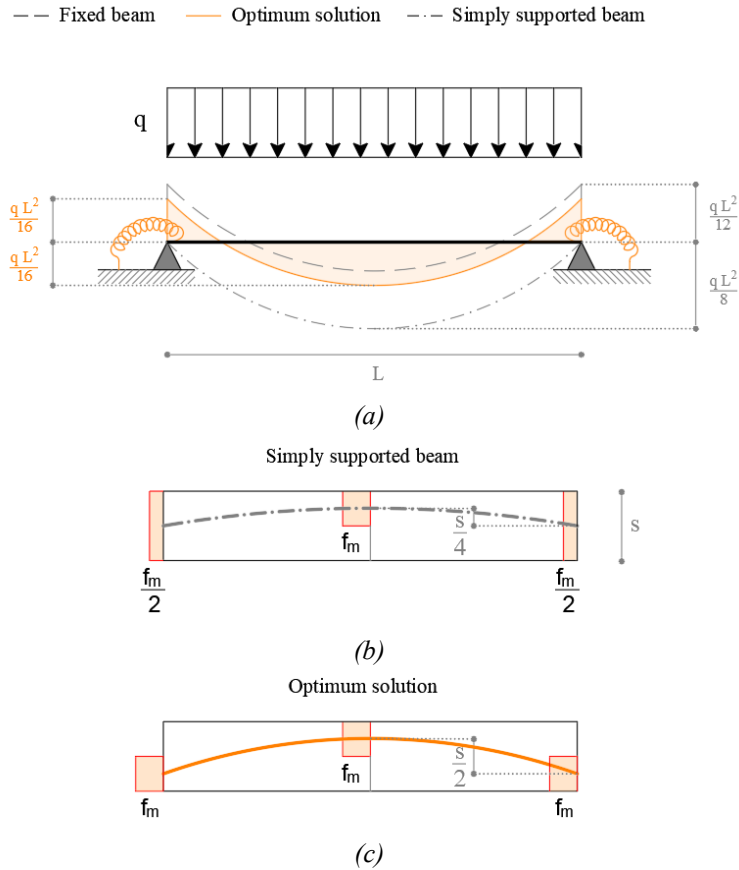


Figure 5.18: Arch mechanism depending on restraint degree: beam stresses (a), arch mechanism for simply supported (b) and for optimum solution (c)

When a strengthening system is applied, the behavior of masonry walls is modified in both unconfined and confined walls. In particular, in the case of unconfined walls, the strengthened masonry wall behavior evolves in a beam mechanism and the ultimate bending moment capacity of the cross section can be evaluated with equations of the paragraph §5.1.2 considering zero axial load. Confined walls with strengthening system show a different behavior due to an internal axial load depending on several parameters as the restraint condition, but it is difficult to estimate. The ultimate bending moment depends on the

external axial load and therefore, more refined analyses are required to properly estimate the axial load inside the masonry wall with strengthening system.

The proposed theory allows to assess the behavior of a strengthened masonry wall, for any external load condition; in Figure 5.18, external loads are represented with a generic uniform load that could be equivalent to a seismic force or a hydrostatic and hydrodynamic load in the case of tsunami loads design (Nistor et al. 2009, Fukuyama et al. 2011).

Furthermore, strengthening of historical heritage buildings (Umar et al. 2015) could be designed considering first or second failure modes to preserve cultural heritage value. As shown in the parametric analyses (Figure 5.10 and Figure 5.11), it is important to balance properly the composite mechanical percentage ω and the ultimate strain ε_{fu} otherwise the strengthening does not improve the cross section flexural capacity.

Chapter 6

Conclusions: results and discussions

Last worldwide tsunami disasters have introduced new issues regarding structural design and retrofit of existing buildings and many studies and researches are in progress.

The Ph.D. thesis debated about the main aspects related to the vulnerability assessment of Italian coastal residential masonry buildings under tsunami loads using a large scale approach. Furthermore, damage scenarios are provided to assess and clarify the effects of a potential tsunami event in the eastern Mediterranean Sea on Italian coastal residential buildings. It represent an important contribution in the tsunami risk assessment (Dall'Osso et al. 2016) and it is the basic step to analyse risk mitigation techniques.

The first step has been represented by a literature research to clarify the physics phenomenon and the actual research progress of the analysed topic. Principal international building codes and guidelines provide different approaches to model tsunami loads on structures and in particular, two different approaches are defined. The first one is provided by U.S. code as *FEMA P-646* and *ASCE 7-16* and it is based on a refined analysis assuming several load distributions to model debris impacts, hydrostatic and hydrodynamic effects. The second approach is provided by Japanese guidelines and it allows to model tsunami loads by an equivalent hydrostatic pressure distribution where the expected inundation depth is increased by a coefficient η in order to take into account both hydrostatics and hydrodynamics effects. The Japanese

approach has been assumed due to the low knowledge level reached in this work at regional large scale.

In addition, comparisons between empirical fragility curves available in literature are performed to clarify the structural behaviour of buildings under tsunami loads and in particular, concrete structures show a better behaviour than masonry buildings. In addition, taller buildings provide a better structural behaviour than low-rise structures as shown in post-tsunami surveys in Tohoku region after “*The 2011 Great East Japan Tsunami*” due to greater cross section geometry. In fact, it is important to note that seismic forces are inertia forces depending on the mass of structure, while tsunami forces are superficial forces that depend on exposed surface of the structure to the tsunami wave.

Fragility curves for Italian coastal residential masonry buildings are derived assuming a large scale approach and they represent an important goal of the research project. Local collapse mechanisms are analysed for a generic building model considering shear and flexural failure for in-plane mechanisms, and horizontal and vertical bending failures for out-of-plane mechanisms.

Several building classes are defined depending on design criteria, number of storeys and age of construction in order to clarify the vulnerability analysis. *Monte Carlo* analyses have been performed in order to simulate the behaviour of Italian masonry buildings based on national census database “*National Institute of Statistics*” (*ISTAT*) and from “*Gruppo Nazionale per la Difesa dai Terremoti*” (*GNDT*) database acquired during post-earthquake surveys by civil protection and other agencies. A large bibliographical research has been done on historical building codes and empirical design equations in order to simulate the design criteria evolution over the years.

Two different structural modelling approaches are adopted to analyse in-plane and out-of-plane mechanisms and in particular, for in-plane mechanisms the behaviour of lateral frames has a huge influence on the structural behaviour of a single panel. Consequently, three different wall models are taken into account to simulate different connection degrees between wall panels depending on age of construction and design criteria. Conversely, out-of-plane behaviour of a masonry wall under tsunami loads is independent from the structural behaviour of the entire building. Therefore, linear analyses are performed considering a mechanical model composed by a simply supported beam with a linear (triangular or trapezoidal) load pattern characterized by a variable inundation depth as reported in the Japanese guidelines.

Several structural analyses have been performed on building models that are representative of Italian coastal buildings with *Mathworks Matlab* in order to define a critical inundation depth that activate a masonry local mechanism in terms of bending and shear failures.

Mechanical fragility curves are derived using least squares regression and a lognormal probability density function based on structural analysis results. Several distributions of η coefficients are assumed in structural analyses in order to provide comparisons with empirical fragility curves and structural behaviour of masonry buildings depending on shields effects and distance of structures from coastline effects. In particular, comparison between empirical and analytical fragility curves show a good match for low damage states while some differences occur at high damage states. As expected, the reasons are related to the empirical fragility curves definition; in fact these curves are strictly related to local building types.

Several sensitivity analyses have been performed in order to obtain important information about the principal geometrical parameters that

influence most the behaviour of masonry walls under tsunami loads; in particular the wall length L has a huge influence on the external demand while the wall thickness s influences mainly the cross section capacity for both horizontal and vertical bending mechanisms. Furthermore, gravitational buildings are more vulnerable to horizontal bending mechanisms while seismic buildings are more sensitive to vertical bending mechanisms.

Damage scenarios are analysed in order to assess and quantify tsunami effects on Italian coastal buildings. A preliminary approach is shown based on specific assumptions coherently with low reached knowledge level. An algorithm is developed based on *GIS* system and *Mathworks MATLAB* scrips to provide a tool to assess Italian high risk tsunami areas. Potentially inundated areas are defined according to New Zealand guidelines *DGL 08-16* and they are divided in grids with spacing 50 meters in urban areas and 100 meters in rural areas.

For each grid, altimetric data are extrapolated from *DTM* with a resolution of 20 meters available on *Italian National Cartographic Portal (PCN) – GEOPORTAL* while information on existing coastal residential buildings are retrieved from census databases of the “*National Institute of Statistics*” (*ISTAT*).

Different inundation simulation approaches are taken into account based on simplified (constant or linear attenuation laws) or refined approaches (*Energy Grade Line analysis*).

It is important to note that the results are strongly dependent on altimetric trend assigned to grid centre; therefore, the influence of digital terrain model *DTM* quality on the results could be not negligible. In fact, the proposed results would only show a preliminary approach that could be used in tsunami multi-hazard analysis. Furthermore, the results are based on a large scale approach and specific basic assumptions due to low achievable knowledge level; more refined simulations are required

to analyse specific buildings in terms of structural and inundation analyses in order to take into account site influence on wave parameters and advanced tsunami load distributions.

The final goal of the research project focuses on main prevention systems available in the case of a tsunami event. In particular, it aims to clarify effects and advantages of retrofit systems against the activation of local mechanisms in a masonry wall under tsunami loads.

Composite retrofit systems are one of the most useful techniques for retrofitting existing buildings due to high durability and fire resistance of materials and sustainability criteria. In fact, the reduced thickness of retrofit system does not influence dynamic characteristics of the structure, as the period of vibration, and the fiber mesh guarantees an improvement of bending moment strength in both principal directions of the retrofitted element.

P - M interaction diagrams are evaluated by means of dimensionless closed form equations considering three different failure modes. Parabolic-constant functions are considered to define compressed masonry behaviour while a linear elastic function is assumed to describe the tensile composite behaviour as basic assumption.

All the results are expressed completely in a dimensionless form in order to provide generalizable results applicable to any masonry cross section and the proposed equations are simply expressed by means of ultimate strain ε_{fu} and the mechanical percentage ω of composite strengthening system. It is important to balance the composite parameters in order to obtain requested performance levels as shown in several parametric analyses. It is important to note that in particular cases, strengthening systems with a low ultimate composite strain and mechanical percentage could not provide benefits in terms of bending capacity.

Several parametric normalized analyses are performed in order to evaluate the benefits of retrofit systems in terms of cross section bending capacity. It is interesting to note that a huge increase of bending capacity is provided at low axial loads due to the tensile behaviour provided by retrofit systems, while for high external axial loads, the benefits of a retrofit system are minor at increasing the composite mechanical percentage. This is due to the high value of neutral axis depth that causes a limited strain in the composite fiber and, consequentially, a limited contribution.

The proposed diagrams depend on normalized parameters in order to evaluate generalizable results applicable to any masonry cross section.

Furthermore, effects of strengthening system on out-of-plane mechanisms (Milano et al. 2006) activation is discussed by analysing P - M interaction diagrams and considering horizontal and vertical bending mechanisms.

In particular, the strengthening system modifies the behaviour of masonry walls both isolated and confined; in particular, isolated walls assume a beam behaviour while confined walls show an arch mechanism with tie-roads. In the case of strengthened confined walls with high mechanical performance, the out-of-plane mechanism evolves in a beam behaviour because the theoretical maximum ultimate bending moment is related to negative axial loads.

Conversely, for vertical bending mechanisms, the strengthening system provides significant benefits in terms of flexural capacity of the cross section for typical normalized axial load levels n of masonry walls between 0.05 and 0.30, if properly designed.

The proposed theory allows to assess the behaviour of a generic strengthened masonry wall, confined or isolated, for any external load condition such as, seismic, tsunami, floods or landslide cases.

It is possible to provide a useful fast tool to design composite retrofit systems for masonry walls in relation to an expected inundation depth depending on the composite mechanical ratio ω comparing external loads and capacity of cross section in terms of bending moment.

The Ph.D. thesis aims to improve the knowledge about the vulnerability of coastal Italian residential masonry buildings under tsunami loads and the prevention systems. Future work could take into account advanced structural analyses based on refined tsunami loads models as shown in *ASCE 7-16* and masonry wall could be modelled as shell elements in order to clarify the masonry wall behaviour. In particular, debris impact loads have a huge influence on the buildings structural behaviour according to empirical fragility curves provided by Reese et al. (2011). An innovative and hard challenge is represented by considering a performance reduction for coastal buildings due to earthquake damages. In this case, the tsunami damages are expected to be greater, the more the earthquake epicentre is close to the coast.

In addition, the structural models depend on several parameters as number of storeys, dimension of panels and masonry quality but many other parameters are neglected according to a large scale approach. Future works could analyse the effects of interlocking among walls, restraint elements and the presence of other common components findable in existing buildings as columns and vaults.

Furthermore, several constitutive relationships can be considered for composites depending on the type of selected composite system (both matrix and fibers) such as bilinear or trilinear behaviour (Triantafillou et al. 2016). In addition, strengthening systems design for in-plane mechanisms represent an innovative research field as future project improvement.

References

Armigliato, A., Pagnoni, G., Paparo, M. A., Tinti, S., Zaniboni, F., Basili, R., Lorito, S., Romano, F., Volpe, M., Belliazzi, S., Lignola, G. P., Di Ludovico, M. and Prota, A. (2019). “A methodology for tsunami hazard-to-damage assessment along the Italian coasts.” *In: Proc., EGU General Assembly 2019, Austria.*

Arnason, H. (2005) “Interactions between and incident bore and a free-standing coastal structure.” *PhD Thesis, University of Washington.*

Asakura, R., Iwase, K., Ikeya, T., Takao, M., Kaneto, T., Fujii, N and Ohmori, M. (2000). “An Experimental Study on Wave Force Acting on On-Shore Structures due to Overflowing Tsunamis.” *Proceedings of Coastal Engineering Japan Society of Civil Engineers: 911-915.*

ASCE/SEI 7-16 (American Society of Civil Engineers). (2017). *Minimum Design Loads for Buildings and Other Structures*, Reston, Virginia.

Augenti, N. (2004) “Il calcolo sismico degli edifici in muratura” *Torino, UTET.* (in Italian)

Augenti, N., Parisi F., and Acconcia, E. (2010). “New tools for non-linear analysis of masonry buildings.” *In Proc., 14th European Conference on Earthquake Engineering, Republic of Macedonia.*

Belliazzi, S., Lignola, G.P., Di Ludovico, M., Prota, A., Di Bucci, D., Dolce, M., Antoncicchi, I., and Terlizze, F. (2017). “Tsunami on existing building stock: preliminary large-scale approach.” *In: Proc.,*

36° GNGTS National Conference (Gruppo Nazionale di Geofisica della Terra Solida), Italy.

Belliazzi, S., Lignola, G. P., and Prota, A. (2018a). “Textile Reinforced Mortars systems: a sustainable way to retrofit structural masonry walls under tsunami loads.” *International journal of Masonry Research and Innovation*. 3 (3): 200-222.

Belliazzi, S., Del Zoppo, M., Lignola, G.P., Di Ludovico, M., Prota, A., Di Bucci, D., Dolce, M., Antoncicchi, I., and Terlizze, F. (2018b). “Tsunami vulnerability of Italian coastal residential areas with a large scale approach.” *In: Proc., 37° GNGTS National Conference (Gruppo Nazionale di Geofisica della Terra Solida), Italy.*

Belliazzi, S., Lignola, G.P., Prota, A., and Fabbrocino, F. (2019a). “Masonry walls retrofitted with natural fibers under tsunami loads”, *In Proc., XXIV Conference of The Italian Association of Theoretical and Applied Mechanics, Italy.*

Belliazzi, S., Lignola, G. P., and Prota, A. (2019b). “Vulnerability of masonry Italian coastal buildings against tsunami loads.” *In Proc., 3rd International Conference on Recent Advances in Nonlinear Design, Resilience and rehabilitation of Structures, Portugal.*

Belliazzi, S., Lignola, G. P., and Cosenza, E. (2019c). “Numerical analysis for rocking response of asymmetric elements.” *In Proc., 3rd International Conference on Recent Advances in Nonlinear Design, Resilience and rehabilitation of Structures, Portugal.*

Bellini, A., Incerti, A., and Mazzotti, C. (2017) “Out-of-plane strengthening of masonry walls with FRCM composite materials.” *Key engineering materials*, 747: 158-165.

Caggegi, C., Carozzi, F. G., De Santis, S., Fabbrocino, F., Focacci, F., Hojdys, L., Lanoye, E. and Zuccarino, L. (2017) “Experimental analysis on tensile and bond properties of PBO and Ara-mid fabric reinforced cementitious matrix for strengthening masonry structures.” *Composites Part-B: Engineering*, 127 (Oct): 175-195.

Caputo, M., and Faita, G. (1987) “Primo catalogo dei maremoti delle coste italiane” *Accademia nazionale dei Lincei*.

Carozzi, F. G., and Poggi, C. (2015) “Mechanical properties and debonding strength of Fabric Reinforced Cementitious Matrix (FRCM) systems for masonry strengthening.” *Composites Part B: Engineering*, 70: 215-230.

Carpentieri, G., Modano, M., Fabbrocino, F., Feo, L. and Fraternali, F. (2017) ‘On the minimal mass reinforcement of masonry structures with arbitrary shapes.’ *Meccanica*, 52 (7): 561-1576.

CEN (European Committee for Standardization). (2006). General Rules for Reinforced and Unreinforced Masonry Structures, part 1.1. Eurocode 6, Brussels, Belgium: CEN.

CNR DT 200R1 (National Research Council). (2013). Guide for the Design and Construction of Externally Bonded FRP Systems for Strengthening Existing Structures, Rome, Italy.

CNR DT 215 (National Research Council). (2018). Guide for the Design and Construction of Externally Bonded Fiber Reinforced Cementitious Matrix systems for Strengthening Existing Structures, Rome, Italy.

Cawley, J. G. (2014). “Review of guidelines for the design of tsunami vertical evacuation buildings.” *Ms Thesis, Oregon State University*.

Chock, G. (2012). “ASCE/JSCE Tohoku Investigation of Structural Damage and Development of the ASCE 7 Tsunami Design Code for Buildings and Other Structures.” American Society of Civil Engineers/Japan Society of Civil Engineers: 184-190.

Circolare LL. PP. n. 21745 - 30.07.1981: Istruzioni per l'applicazione della normativa tecnica per la riparazione ed il rafforzamento degli edifici danneggiati dal sisma, Rome, Italy. (in Italian)

Circolare LL. PP. n. 617 - 02.02.2009: Istruzioni per l'applicazione delle «Nuove norme tecniche per le costruzioni» di cui al decreto ministeriale 14 gennaio 2008, Rome, Italy. (in Italian)

Coccia, S., Di Carlo, F., and Imperatore, S. (2017). “Force reduction factor for out-of-plane simple mechanisms of masonry structures.” *Bulletin of Earthquake Engineering*, 15 (3): 1241–1259.

Cuadra, C., and Ishiyama, S. (2012). “An outline of RC buildings performance under tsunamis triggered by the East Japan Great Earthquake.” *Structures Under Shock and Impact XII*, 126:315-324.

Curioni, G. (1881) “Raccolta di progetti di costruzioni in terra” *Torino, Negro*. (in Italian)

D’Ambra C. (2011) “Vulnerabilità e miglioramento sismico di edifici in aggregato: Il caso studio di Piazza della Prefettura a L’Aquila.” *PhD Thesis, University of Naples Federico II*. (in Italian)

Dall’Osso, F., Dominey-Howes, D., Tarbotton, C., Summerhayes, S., and Withycombe, G. (2016). “Revision and improvement of the PTVA-3 model for assessing tsunami building vulnerability using “international expert judgment”: introducing the PTVA-4 model.” *Natural Hazards*, 83(2): 1229-1256. D’Ayala, D., and Speranza, E.

(2003). "Definition of collapse mechanisms and seismic vulnerability of historic masonry buildings." *Earthquake Spectra*, 19(3): 479-509.

Dames & Moore (1980) "Design and construction standards for residential construction in tsunami-prone areas in Hawaii" Prepared for the Federal Emergency Management Agency, Washington D.C.

De Lorenzis, L. (2008). "Strengthening of masonry structures with fibre-reinforced polymer (FRP) composites." *In Strengthening and Rehabilitation of Civil Infrastructures Using Fibre-Reinforced Polymer (FRP) Composites*. Woodhead Publishing, eds Hollaway LC and Teng JG: 235-266.

De Santis, S., Ceroni, F., de Felice, G., Fagone, M., Ghiassi, B., Kwiecień, A., Lignola, G. P., Morganti, M., Santandrea, M., Valluzzi, M. R. and Viskovic, A. (2017) 'Round Robin Test on tensile and bond behaviour of Steel Reinforced Grout systems.' *Composites Part B-Engineering*, 127 (Oct): 100-120.

DGL 08/16 (Ministry of Civil Defence & Emergency Management). 2016. Tsunami Evacuation Zones, Director's Guideline for Civil Defence Emergency Management Groups, Wellington, New Zealand.

D.M. LL.PP. - 20.11.1987: Norme tecniche per la progettazione, esecuzione e collaudo degli edifici in muratura e per il loro consolidamento, Rome, Italy. (in Italian)

D.M. LL.PP. - 16.01.1996: Norme tecniche per le costruzioni in zone sismiche, Rome, Italy. (in Italian)

D.M. - 14.01.2008: Norme Tecniche per le Costruzioni, Rome, Italy. (in Italian)

FEMA P-646 (Federal Emergency Management Agency). (2012). *Guidelines for Design of Structures for Vertical Evacuation from Tsunamis*, Redwood City, California.

Foytong, P., and Ruangrassamee, A., (2016). “Fragility curves of reinforced-concrete buildings damaged by the 2004 tsunami.” *KKU Engineering Journal*, 43 (S3): 419-423.

Fukuyama, H., Kato, H., Ishihara, T., Tajiri, S., Tani, M., Okuda, Y., Kabeyasawa, T., and Nakano, Y. (2011). “Structural design requirement on the tsunami evacuation buildings.” *Ministry of Land, Infrastructure, Transportation and Tourism MLIT*.

Guadagnuolo, M., and Faella, G. (2008). “The friction in the out-of-plane failure mechanisms of masonry walls.” *In: Proc., 14th International Brick and Block Masonry Conference, Cracow*.

GEOPORTALE Nazionale - Retrieved from:

<http://www.pcn.minambiente.it>

GNDT (Gruppo Nazionale per la Difesa dai Terremoti). (1993). *Manuale per la compilazione della Scheda GNDT/CNR di II livello*. (in Italian)

Hayashi, K., Tamura, S., and Nakashima, M. (2011). “Evaluation of Tsunami Load and Building Damage Mechanism Observation in the 2011 off Pacific Coast of Tohoku Earthquake.” *15th World Conference on Earthquake Engineering, Portugal*.

Ishikawa, N., Beppu, M., Mikami, T., Tatesawa, H., and Asai, M. (2011). “Collapse mechanism of seawalls by impulsive load due to the march 11 tsunami.” *In Proc., 9th International Conference on Shock & Impact Loads on Structures, Republic of Singapore*.

Ismail, N. and Ingham, J.M. (2016) “In-plane and out-of-plane testing of unreinforced masonry walls strengthened using polymer textile reinforced mortar.” *Engineering Structures*, 118: 167-177.

Japanese Cabinet Office. (2005). *Guideline for Tsunami Evacuation Building*, Japan.

Koshimura, S., Oie, T., Yanagisawa, H., and Imamura, F. (2009). “Developing fragility functions for tsunami damage estimation using numerical model and post-tsunami data from Banda Aceh, Indonesia.” *Coastal Engineering Journal*, 51(3): 243-273.

Kouris, L. A. S., and Triantafillou, T. C. (2018) “State-of-the-art on strengthening of masonry structures with textile reinforced mortar (TRM).” *Construction and Building Materials*, 188: 1221-1233.

Levin, B. W., and Nosov, M. (2009). *Physics of tsunamis*, Dordrecht: Springer.

Lignola, G. P., Flora, A., Manfredi, G. (2008). “Simple Method for the Design of Jet Grouted Umbrellas in Tunneling.” *Journal of Geotechnical and Geoenvironmental Engineering*, 134 (12): 1778-1790.

Lignola, G. P., Caggegi, C., Ceroni, F., De Santis, S., Krajewski, P., Lourenço, P. B., Morganti, M., Papanicolaou, C., Pellegrino, C., Prota, A. and Zuccarino, L. (2017) ‘Performance assessment of basalt FRCC for retrofit applications on masonry.’ *Composites Part B-Engineering*, 128 (Nov): 1-188.

Lignos, D. (2011) “Effects of the 2011 Tohoku Japan Earthquake on Steel Structures.” *Earthquake Engineering Research Institute, Team Field Blog*.

Maccarini, H., Vasconcelos, G., Rodrigues, H., Ortega, J., and Lourenço, P. B. (2018) “Out-of-plane behavior of stone masonry walls: Experimental and numerical analysis”. *Construction and Building Materials*, 179: 430-452.

Mallawaarachchi, R. S., and C. Jayasinghe. (2008). “The effects of cyclones, tsunami and earthquakes on built environments and strategies for reduced damage.” *Journal of the National Science Foundation of Sri Lanka*, 36 (1): 3-14.

Marullier, E. (1914) “Guida pratica per la costruzione degli edifizii” *Torino, UTET.* (in Italian)

Mas, E., Koshimura, S., Suppasri, A., Matsuoka, M., Matsuyama, M., Yoshii, T., Jimenez, C., Yamazaki, F., and Imamura, F. (2012). “Developing Tsunami fragility curves using remote sensing and survey data of the 2010 Chilean Tsunami in Dichato.” *Natural Hazards Earth System Sciences*, 12 (8): 2689-2697.

Milani, G.B. (1920) “L’ossatura murale”, *Torino, Crudo.* (in Italian)

Nakano, Y. (2010) “Design load evaluation for tsunami shelters based on damage observations after indian ocean tsunami disaster due to the 2004 Sumatra earthquake.” *Science of Tsunami Hazards*. 29 (1):1-8.

Nakano, Y. (2011) “Structural Design Requirements for Tsunami Evacuation Buildings in Japan.” *SDRTEB, ACI Symposium Publication*, 313:1-12.

Nistor, I., Palermo, D., Nouri, Y., Murty, T., and Saatcioglu, M. (2009) “Tsunami-induced forces on structures.” In *Handbook of coastal and ocean engineering*.

Nouri, Y., Nistor, I., Palermo, D., and Cornett, A. (2010) “Experimental investigation of tsunami impact on free standing structures.” *Coastal Engineering Journal*, 52(1): 43-70.

Okada, T., Sugano, T., Ishikawa, T., Ohgi, T., Takai, S., and Hamabe, C. (2005) “Structural Design Method of Buildings for Tsunami Resistance.” *The Building Letter*, Nov., 2004, *The Building Center of Japan-Building Technology Research Institute*.

O.P.C.M. 3274, 03.05.2005: Primi elementi in materia di criteri generali per la classificazione sismica del territorio nazionale e di normative tecniche per le costruzioni in zona sismica, Rome, Italy. (in Italian)

Pantò, B., Cannizzaro, F., Calì, I. and Lourenço, P.B. (2017). “Numerical and Experimental Validation of a 3D Macro-Model for the In-Plane and Out-Of-Plane Behavior of Unreinforced Masonry Walls.” *International Journal of Architectural Heritage*, 11 (7): 946-964.

Papadopoulos A., and Imamura, F. (2001) “A proposal for a new tsunami intensity scale.” *In Proc., International Tsunami Symposium 2001, USA*: 569-577.

Park, S., van de Lindt, J. W., Cox, D., Gupta, R., and Aguiniga, F. (2012). “Successive Earthquake-Tsunami Analysis to Develop Collapse Fragilities.” *Journal of Earthquake Engineering*, 16 (6): 851-863.

Pelinovsky, E. (2006). Hydrodynamics of tsunami waves. In *Waves in Geophysical Fluids*, Springer, Vienna.

Peiris, N., and Pomonis, A. (2005). “Decembre 26, 2004 Indian Ocean Tsunami: vulnerability functions for loss estimation in Sri Lanka.” *In Proc., Geotechnical Engineering for Disaster Mitigation and Rehabilitation*: 411-416.

Porter, K., Kennedy, R., and Bachman, R., (2007). “Creating fragility functions for performance based earthquake engineering.” *Earthquake Spectra*, 23 (2): 471-489.

Prota, A., Marcari, G., Fabbrocino, G., Manfredi, G., and Aldea, C. (2006). “Experimental In-Plane Behavior of Tuff Masonry Strengthened with Cementitious Matrix–Grid Composites.” *Journal of Composites for Construction*, 10 (3): 223-233.

Reese, S., Bradley, B. A., Bind, J., Smart, G., Power, W., and Sturman, J. (2011). “Empirical building fragilities from observed damage in the 2009 South Pacific tsunamis.” *Earth-Science Reviews*, 107 (1-2): 156-173.

Röbke, B. R., and Vött, A. (2017). The tsunami phenomenon. *Progress in Oceanography*, 159: 296-322.

ROH (Revised Ordinances of the City and County of Honolulu). (1990). City and County of Honolulu Building Code, Honolulu, Hawaii.

Rondelet, J.B. (1802). “Traité Théorique et Pratique de l’Art de Bâtir”, translated by Soresina B. “Trattato Teorico Pratico dell’Arte di Edificare” *Mantova*. (in Italian).

Rondelet, G. (1841) “Trattato teorico e pratico dell’arte di edificare” *Napoli, Del Vecchio*. (in Italian)

Suppasri, A., Koshimura, S., and Imamura, F. (2011). “Developing tsunami fragility curves based on the satellite remote sensing and the numerical modeling of the 2004 Indian Ocean tsunami in Thailand.” *Natural Hazards Earth System Sciences*, 11 (1):173-189.

Suppasri, A., Mas, E., Charvet, I., Gunasekera, R., Imai, K., Fukutani, Y., Abe, Y., and Imamura, F. (2013). “Building damage characteristics based on surveyed data and fragility curves of the 2011

Great East Japan tsunami.” *Natural Hazards Earth System Sciences*, 66 (2): 319-341.

Tinti, S., and Armigliato, A. (2001). Impact of large tsunamis in the Messina Straits, Italy: the case of the 28 December 1908 tsunami. In *Tsunami Research at the End of a Critical Decade*. Springer, Dordrecht.

Tinti, S., and Armigliato, A. (2003). The use of scenarios to evaluate the tsunami impact in southern Italy. *Marine Geology*, 199(3): 221-243.

Tinti, S., Armigliato, A., Tonini, R., Maramai, A., and Graziani, L. (2005). Assessing the hazard related to tsunamis of tectonic origin: a hybrid statistical-deterministic method applied to southern Italy coasts. *ISSET Journal of earthquake technology*, 42(4): 189-201.

Tinti, S. (2007) “I maremoti delle coste italiane” *Geoitalia*.

TSUMAPS-NEAM - Retrieved from: <http://www.tsumaps-neam.eu>

Türkmen, Ö. S., De Vries, B. T., Wijte, S. N. M., and Vermeltfoort, A. T. (2020) “In-plane behaviour of clay brick masonry wallettes retrofitted with single-sided fabric-reinforced cementitious matrix and deep mounted carbon fibre strips.” *Bulletin of Earthquake Engineering*, 18: 725–765.

Umar, M. U., Hanafi, M. H., Latip N. A., and Ahmad, A. G. (2015). “Strengthening of Historic Buildings through Structural Repair Works: Review of the Methods and Process.” *Australian Journal of Basic and Applied Sciences*, 9(7): 358-362.

Vaculik, J., and Griffith, M. C. (2017). “Probabilistic analysis of unreinforced brick masonry walls subjected to horizontal bending.” *ASCE Journal of Engineering Mechanics*, 143(8): 04017056.

Yeh, H., Robertson, I., and Preuss, J. (2005) “Development of Design Guidelines for Structures that Serve as Tsunami Vertical Evacuation Sites.” *Washington Division of Geology and Earth Resources*.

Zecchi, R. (2006). “The tsunamis in the seas of italy.” *Bullettin AIC*, 126-127-128:365-374. (in Italian)

Chapter 7

Appendix A: Fragility Curves

In Appendix A, several mechanical fragility curves are provided based on structural analyses according to Chapter 3. Comparison between fragility curves allows to clarify the structural behaviour of masonry buildings under tsunami loads. Fragility curves assume η coefficient equal to the maximum number in order to simulate the structural behaviour of buildings in front of coastline.

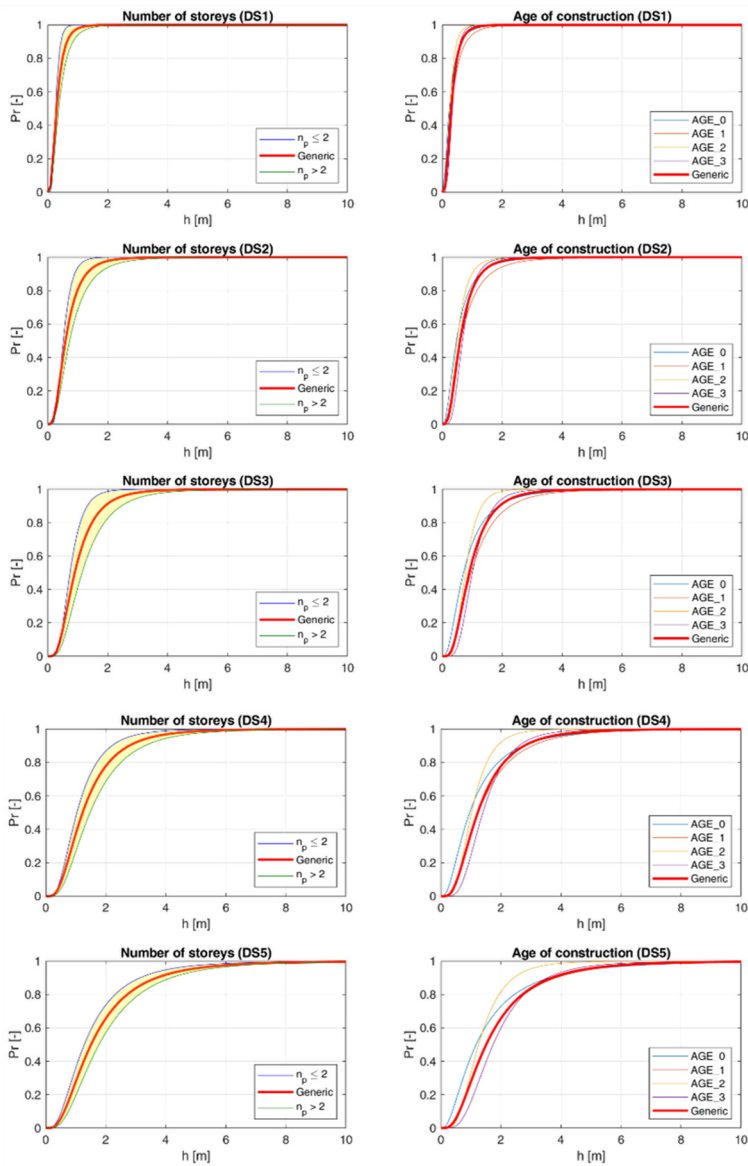


Figure 7.1: Fragility curves summary based on number of storeys and age of construction

In Figure 7.1, fragility curves summary is shown and it is possible to appreciate that low damage states are not strongly influenced by number of storeys and age of construction. High rise buildings show a better structural behaviour than low rise buildings as expected.

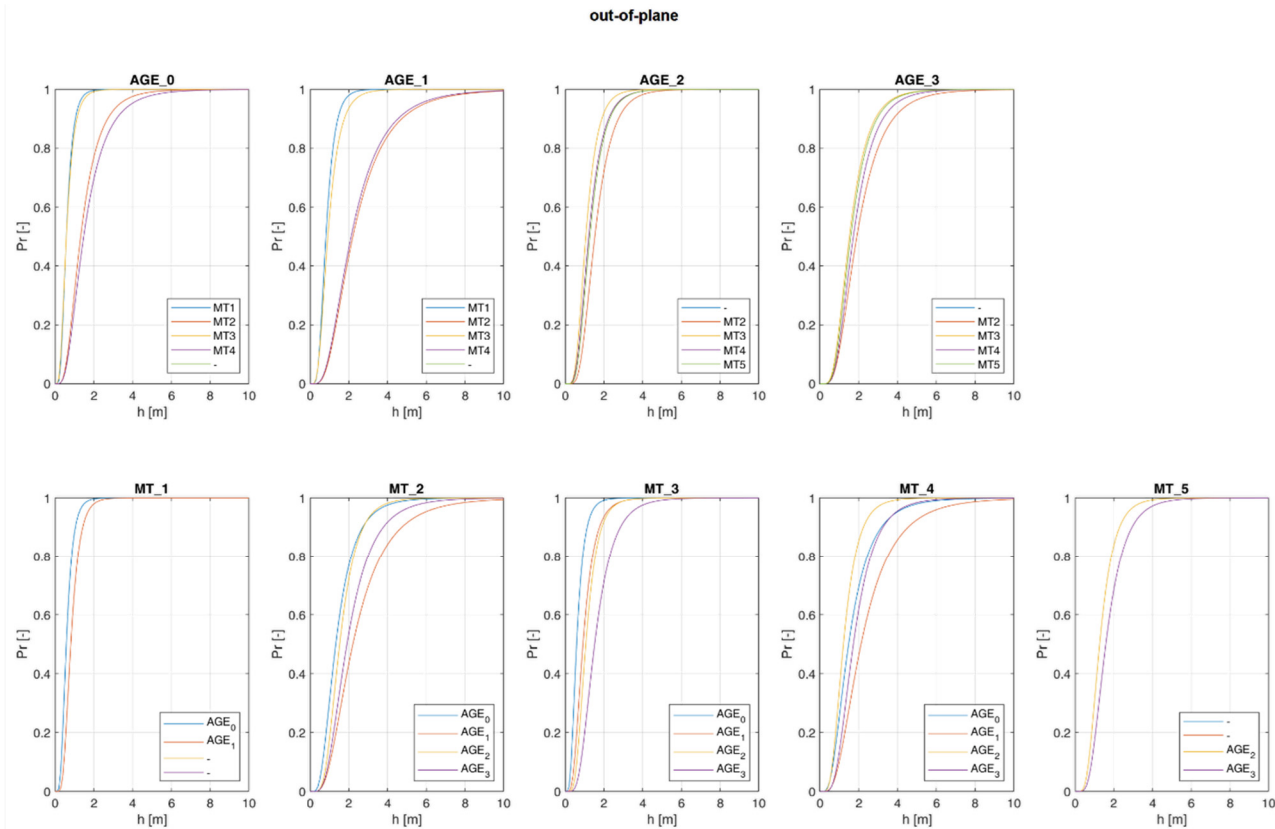


Figure 7.2: Fragility curves related to out-of-plane mechanisms activation and damage state DSs depending on age of construction (AGE) and masonry types (MT): poor stone, tuff stone, hollow clay bricks, clay brick and full clay brick.

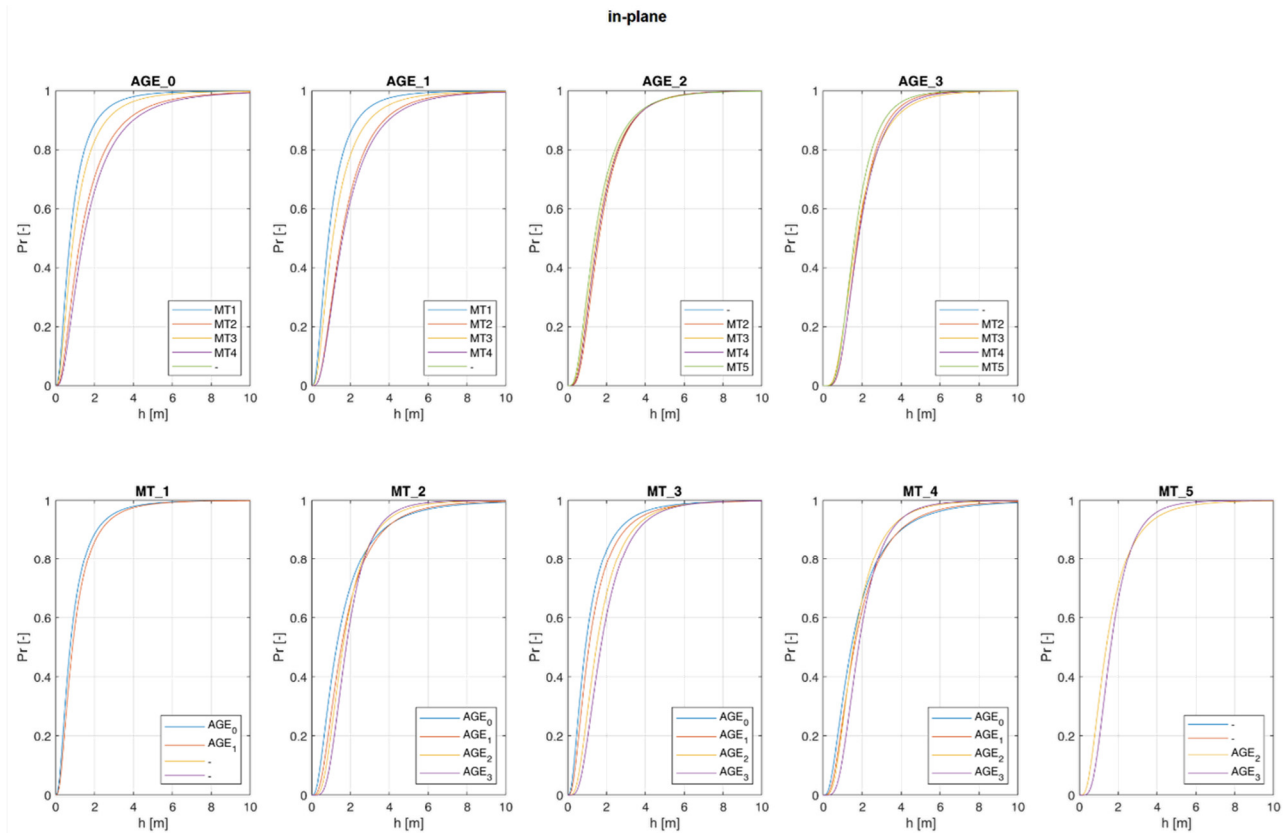


Figure 7.3: Fragility curves related to in-plane mechanisms activation and damage state DSs depending on age of construction (AGE) and masonry types (MT): poor stone, tuff stone, hollow clay bricks, clay brick and full clay brick.

Figure 7.2 and Figure 7.3 allow to analyse the influence of ages of construction and masonry type on local mechanisms activation. In-plane mechanisms activation show huge influence related to age of construction in *AGE_0* and *AGE_1* due to the wall model *I* and *II* while in *AGE_2* and *AGE_3* a large part of masonry buildings frame are modelled according shear-type assumption. Similarly, out-of-plane mechanisms activation are influenced by age of constructions due to wall length limits introduced by seismic design approaches; in fact, wall length is strictly related to tsunami loads.

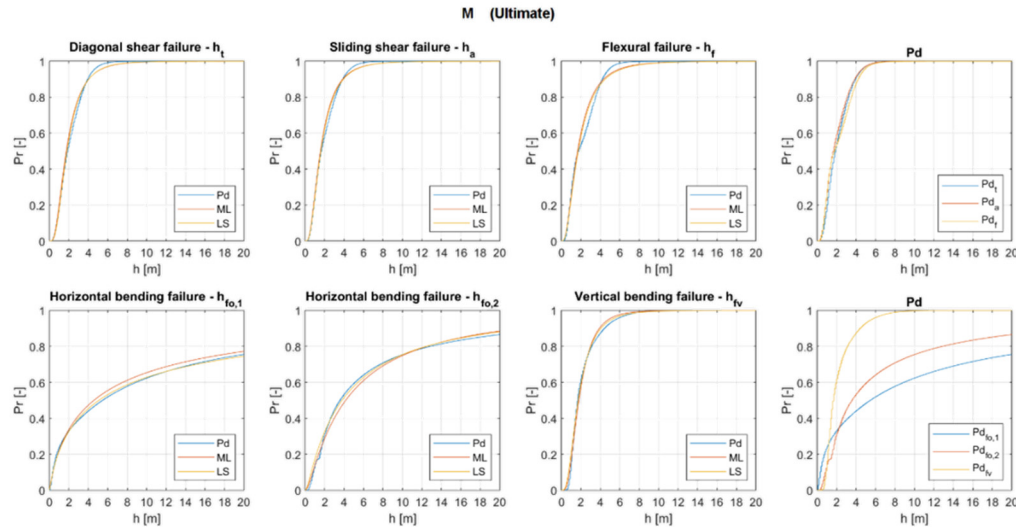


Figure 7.4: Fragility curves comparison based on generic masonry buildings between in-plane and out-of-plane failure modes depending on ultimate limit state

Appendix A

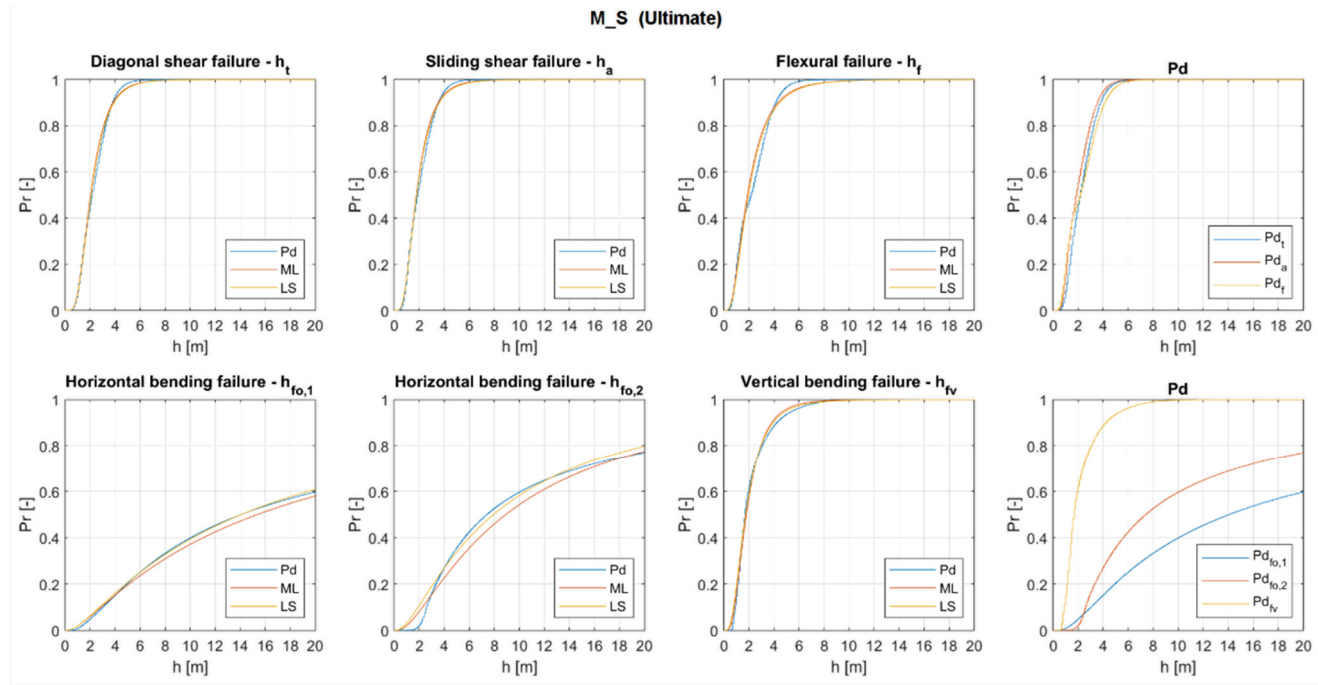


Figure 7.5: Fragility curves comparison based on seismic masonry buildings between in-plane and out-of-plane failure modes depending on ultimate limit state

Appendix A

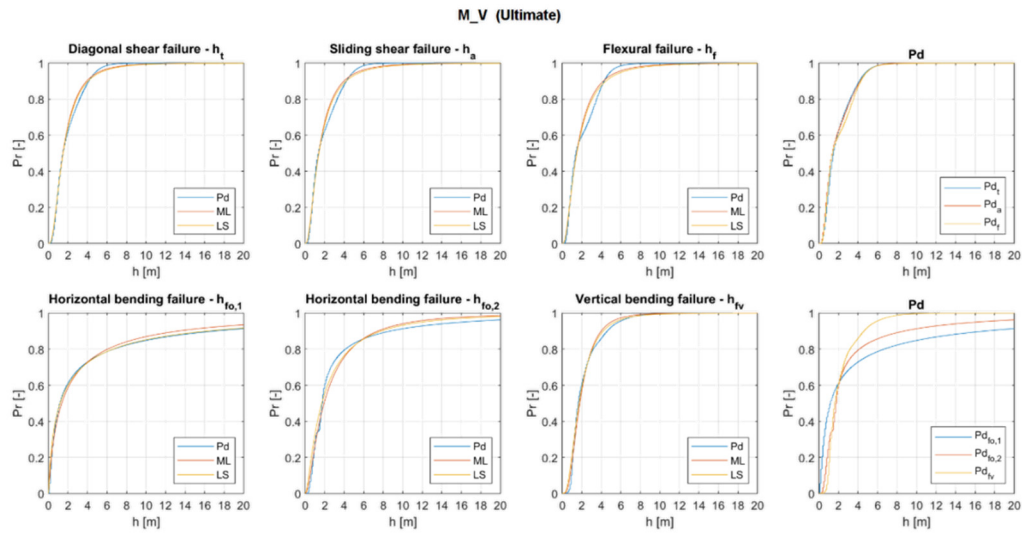


Figure 7.6: Fragility curves comparison based on gravitational masonry buildings between in-plane and out-of-plane failure modes depending on ultimate limit state

Where h_t , h_a and h_f represent critical inundation depths that activate respectively the diagonal shear, sliding and flexural failure modes, while $h_{fo,1}$, $h_{fo,2}$ and h_{fv} are related to respectively the horizontal and vertical bending mechanisms activation. P_d represent the discretised probability of exceedance function while ML and LS represent two different approaches to derive fragility curves, the Maximum Likelihood estimation and Least Square estimation method.

Appendix A

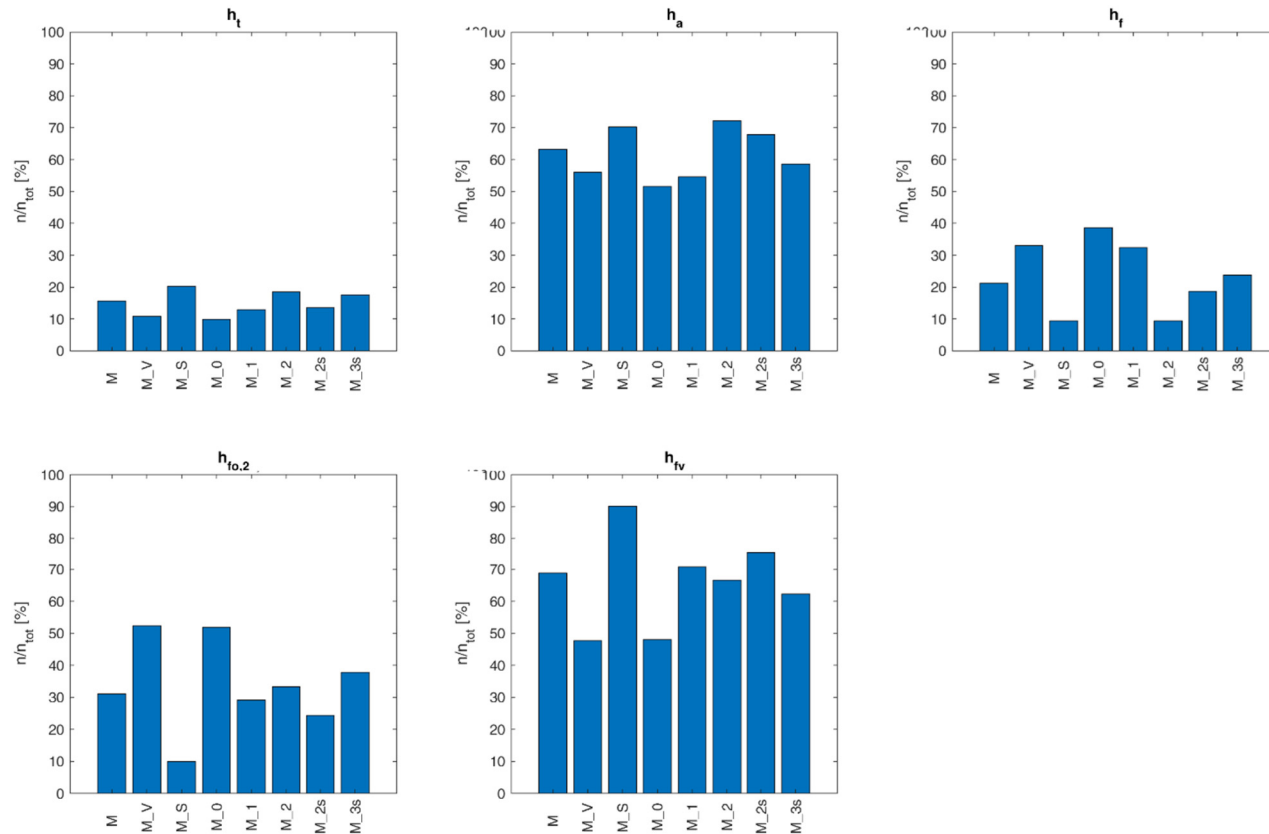


Figure 7.7: Number of buildings ratio related to different failure modes and building classes groups.

Where M represent generic masonry building, $M_V - M_S$ are related to gravitational and seismic masonry buildings, $M_0 - M_1 - M_2 - M_3$ are based on age of constructions, $M_{2s} - M_{3s}$ are related to respectively low and high rise buildings. Each group of buildings is based on the sum of the buildings depending on the building classes defined in Figure 3.5. In Table 7.1, a summary of the number of building of each group is shown.

ID	Number of buildings
M	$10 \cdot 10^6$
M_V	$6 \cdot 10^6$
M_S	$4 \cdot 10^6$
M_0	$2 \cdot 10^6$
M_1	$4 \cdot 10^6$
M_2	$4 \cdot 10^6$
M_{2s}	$5 \cdot 10^6$
M_{3s}	$5 \cdot 10^6$

Table 7.1: Number of buildings for each buildings group

Figure 7.4, Figure 7.5, Figure 7.6 and Figure 7.7 permit to assess the vulnerability to a specific local mechanisms, both in-plane and out-of-plane mechanisms, depending on several buildings groups in order to clarify the influence of design approaches, ages of construction and number of storeys.

In-plane critical inundation depth are similar and the sliding failure modes is the more vulnerable local mechanisms while, out-of-plane mechanisms show high vulnerability to vertical bending mechanisms activation.

Chapter 8

Appendix B: Application example

The proposed research project aims to provide damage scenario analysis in the case of a tsunami event in terms of number of damaged buildings, reconstruction costs and potential casualties. An algorithm is developed based on *GIS* system and *Mathwork MATLAB* scripts as shown in paragraph §4.2 and the results are stored in "*shapefile ESRI*" files in order to provide geo-referenced data. In addition, damage scenario results are shown by thematic maps considering different representation scales (grid, municipality, province and region).

Extended and detailed application examples are fully described in this Appendix B assuming the following statements:

- a constant inundation depth distribution along the coastline of 2, 5 and 10 meters based on *TSUMAPS-NEAM* project results on specific points of interest of Calabria coasts. In particular, the inundation depth of 2 and 5 meters are related to a return periods of 2475 years while the inundation depth of 10 meters is related to a return periods of 9975 years;
- inundation simulations are performed assuming a constant inland attenuation law;
- building damages are based on empirical fragility curves provided by Suppasri et al. (2013) related to "*The 2011 Great East Japan Tsunami*" due to the large amount of empirical data collected in post-tsunami surveys, for both masonry and concrete residential structures.

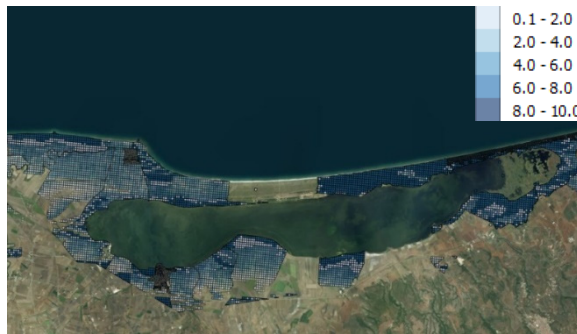
Inundation simulation maps are shown for different constant inundation depth distributions along the coastline in Figure 8.1 and Figure 8.2.



(a)



(b)



(c)

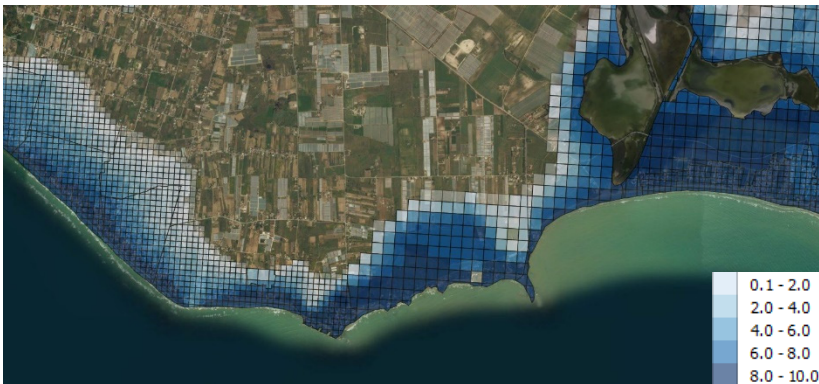
Figure 8.1: Inundation maps in Lesina city (Foggia, Puglia) assuming 2 (a), 5 (b) and 10 (c) meters of inundation depth along the coastline



(a)



(b)



(c)

Figure 8.2: Inundation maps in Ispica city (Ragusa, Sicilia) assuming 2 (a), 5 (b) and 10 (c) meters of inundation depth along the coastline

In Figure 8.1 and Figure 8.2, it is possible to note the progressive increasing of inundated areas increasing the inundation depth along the coastline.

Furthermore, in Figure 8.2, there are compatible-inundated areas neglected due to the absence of residential buildings and therefore, they are not interesting for the goal of the project. In addition, this allows to manage less grids and the algorithm performances are increased.

Number of buildings damaged is shown by means of histograms depending on damage states for different constant inundation depth distribution along the coastline according to municipality scale (Figure 8.3).

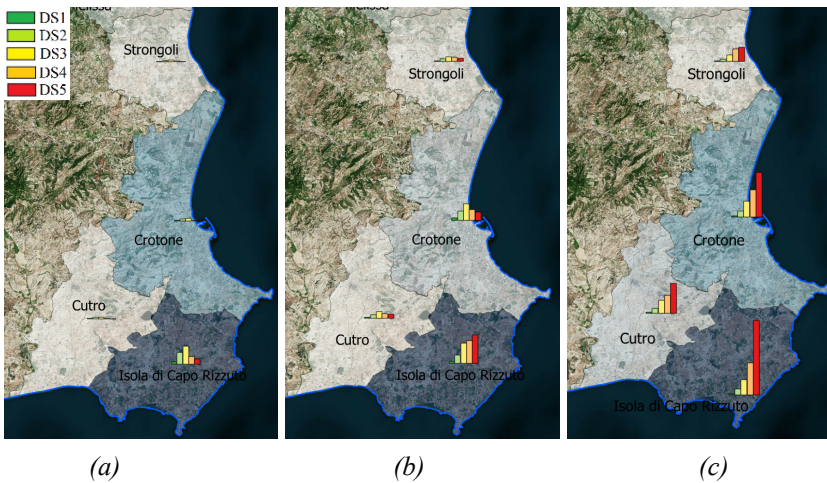


Figure 8.3: Number of buildings damaged for several Cities in Calabria assuming 2 (a), 5 (b) and 10 (c) meters of inundation depth along the coastline

As expected, the number of buildings is strictly dependent on the inundation depth along the coastline and in particular, a higher number of buildings attains high damage states increasing the inundation depth.

Reconstruction costs are shown in Figure 8.4, Figure 8.5 and Figure 8.6 depending on DS_2 and DS_5 for different constant inundation depth distributions along the coastline according to municipality scale.

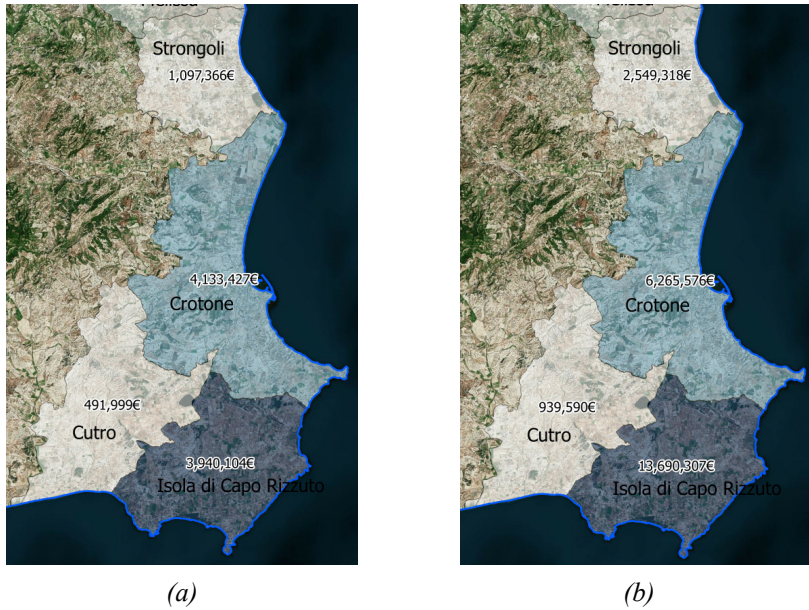


Figure 8.4: Reconstruction costs for several Cities in Calabria assuming 2 meters of inundation depth along the coastline based on DS₂ (a) and DS₅ (b)

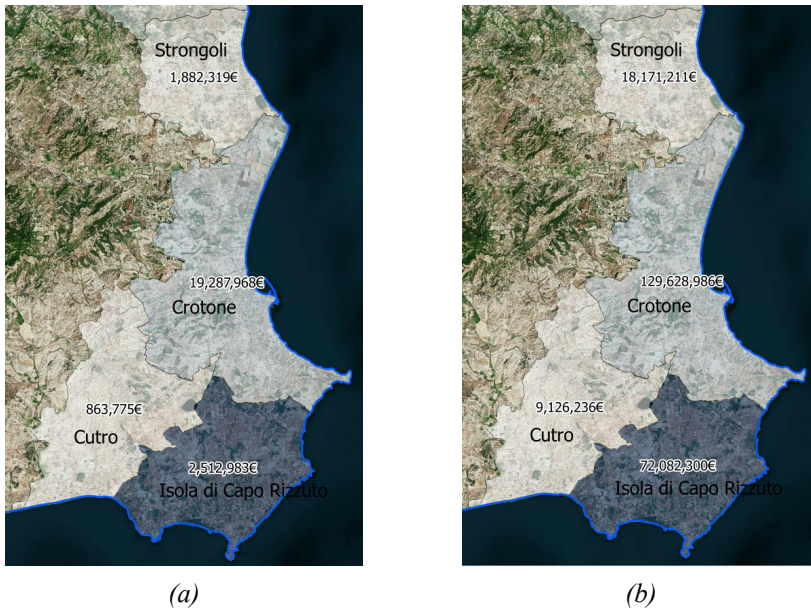


Figure 8.5: Reconstruction costs for several Cities in Calabria assuming 5 meters of inundation depth along the coastline based on DS₂ (a) and DS₅ (b)

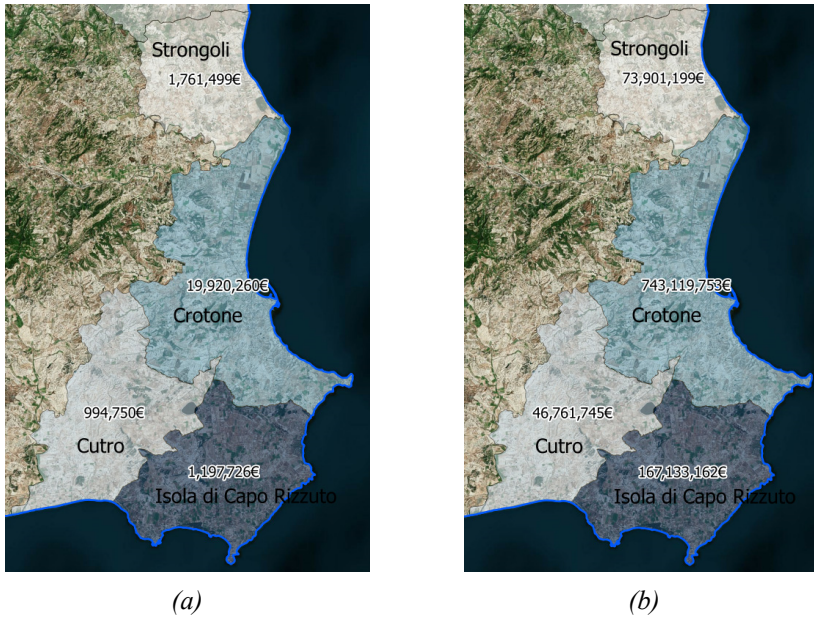


Figure 8.6: Reconstruction costs for several Cities in Calabria assuming 10 meters of inundation depth along the coastline based on DS₂ (a) and DS₅ (b)

Reconstruction costs depend on number of buildings related to a specific damage state; higher inundation depths correspond to several structural damages, higher damage state activation and consequentially, higher reconstruction costs. In addition, it is clear that reconstruction costs are influenced by buildings density comparing Crotone and Isola di Capo Rizzuto costs as shown in Figure 8.4, Figure 8.5 and Figure 8.6.

Same analyses are repeated assuming a province scale considering several south of Italy regions in terms of number of damaged buildings (Figure 8.7) and reconstruction costs (Figure 8.8, Figure 8.9 and Figure 8.10).



(a)



(b)



(c)

Figure 8.7: Number of damaged buildings in Sicilian provinces assuming 2 (a), 5 (b) and 10 (c) meters of inundation depth along the coastline



(a)



(b)

Figure 8.8: Reconstruction costs in Sicily provinces assuming 2 meters of inundation depth along the coastline based on DS₂ (a) and DS₅ (b)



(a)



(b)

Figure 8.9: Reconstruction costs in Sicily provinces assuming 5 meters of inundation depth along the coastline based on DS_2 (a) and DS_5 (b)



(a)



(b)

Figure 8.10: Reconstruction costs in Sicily provinces assuming 10 meters of inundation depth along the coastline based on DS_2 (a) and DS_5 (b)

Similarly, same analyses are repeated in Calabria, Basilicata and Puglia provinces in terms of number of damaged buildings (Figure 8.11) and reconstruction costs (Figure 8.12).



(a)



(b)

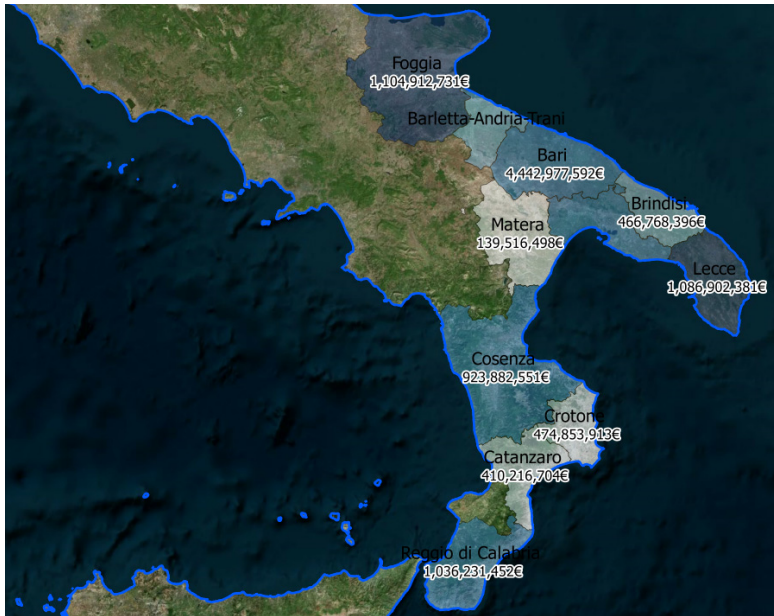


(c)

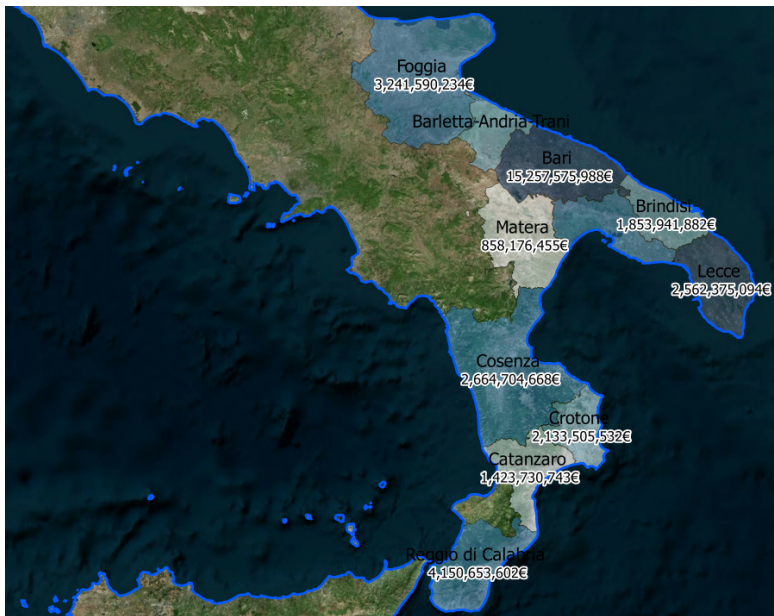
Figure 8.11: Number of damaged buildings in Calabria, Puglia and Basilicata provinces assuming 2 (a), 5 (b) and 10 (c) meters of inundation depth along the coastline



(a)



(b)



(c)

Figure 8.12: Reconstruction costs in Calabria, Puglia and Basilicata provinces assuming 2 (a), 5 (b) and 10 (c) meters of inundation depth along the coastline based on DS₅

Furthermore, results summary is provided considering several Italian regions in terms of number of damaged buildings (Figure 8.13) and reconstruction costs (Figure 8.14, Figure 8.15 and Figure 8.16).



(a)



(b)



(c)

Figure 8.13: Number of damaged buildings in Italy regions assuming 2 (a), 5 (b) and 10 (c) meters of inundation depth along the coastline



(a)



(b)

Figure 8.14: Reconstruction costs in Italy regions assuming 2 meters of inundation depth along the coastline based on DS2 (a) and DS5 (b)



(a)



(b)

Figure 8.15: Reconstruction costs in Italy regions assuming 5 meters of inundation depth along the coastline based on DS2 (a) and DS5 (b)



(a)



(b)

Figure 8.16: Reconstruction costs in Italy regions assuming 10 meters of inundation depth along the coastline based on DS2 (a) and DS5 (b)

Similar to municipal and provincial results, reconstruction costs depend on number of buildings, size of the involved areas, and flat areas where inundated grids number is greater than hilly areas.

It is important to note that the results are strongly dependent on altimetric trend assigned to grid centres and minimum distance lines between grid centre and coastline; consequentially, the influence of assumed digital terrain model *DTM* quality on the results could be not negligible. In fact, the proposed results follow a preliminary approach that could be used in tsunami multi-hazard analysis. Furthermore, the results are based on a large scale approach and specific basic assumptions due to low achievable knowledge level; more refined simulations are required to analyse specific buildings in terms of structural and inundation analyses in order to take into account site influence on wave parameters and advanced tsunami load distributions.